

2420 37th St
Sacramento, CA USA 95817

Department of Biomechanical Engineering
Delft University of Technology
Delft, Netherlands

Dear Search Committee:

I am writing to apply for the “Assistant/Associate Professor (tenure track) in Dynamics of Multibody systems” in the Department of Biomechanical Engineering at TU Delft. For the last 15 years, I have developed unique research expertise in the dynamics and control of bicycles as well as other topics that align with your department’s research areas, making me a highly qualified candidate for this position. I have authored or co-authored 21 journal and conference articles on the subject of bicycles and my doctoral work focused almost exclusively on the topic, resulting in a dissertation entitled “Human Control of a Bicycle” which is well cited. I have published 8 other articles, many of which were ancillary to the bicycle dynamics and control research. These works and my active role in the associated academic communities make me one of the handful of people in the world with the expertise needed to take the TU Delft Bicycle Dynamics and Control lab into the future.

I am currently an Assistant Professor of Teaching in the Mechanical and Aerospace Engineering Department at the University of California, Davis. My position is an academic senate tenure-track position primarily focused on advancing undergraduate engineering education. I spend approximately 70% of my time on teaching and learning, 20% on professional achievements and activities, and 10% on academic and public service. I have been in this position for over four years and my accomplishments over those years align mostly with this position’s teaching focus. I have also maintained a research program centered on human mobility in transportation, sports, and assistive technologies with much of the work advancing engineering in the dynamics and control of bicycles. Prior to this position, I was a postdoctoral researcher in the field of human motion and control with applications in powered lower limb exoskeletons. Before that, I was a graduate student with research in bicycle dynamics, control, and handling in a sport biomechanics lab. Through these experiences, I have developed strong applied computational and experimental vehicle dynamics and biomechanics experience.

My current research trajectory is focused on developing human-machine synergistic controllers for powered exoskeletons, powered prostheses, and personal mobility vehicles, particularly single track vehicles. These assistive devices will play a significant role in how abled and disabled individuals get around in the future.

I am well versed in the various funding opportunities in the USA and have a strong record of obtaining competitive funding even though it is not a requirement for my current position. As a graduate student, I initiated and co-authored an awarded US National Science Foundation grant to study the control of bicycles. This effort was unique given both the student initiative and the fact that we were able to make the case for obtaining resources for a research area that is often more challenging to fund. As a student, I was also awarded a very competitive Fulbright Scholarship to the Netherlands, where I spent a productive year in the bicycle dynamics lab at TU Delft. Most recently, I was co-PI on a successful \$5 million grant from the US Department of Education. Over the last four years I have also been awarded several internal grants for education activities. I am looking forward to learning about the funding systems that support faculty research in the Netherlands so that I can continue my successful trajectory. At TU Delft, I plan to fund my future work through grants and industry partnerships in the Netherlands, European Union, and internationally.

My extensive teaching record in dynamics and design includes courses in the topics of mechanical design, mechanical vibrations, system dynamics, multibody dynamics, and vehicle dynamics at the undergraduate (BSc) and graduate (MSc, PhD) levels. I make use of many education research backed practices in my teaching and I am constantly improving the courses using these practices. I have taught courses of up to 120 students and managed up to four teaching assistants per class. I am also a leader in the use and promotion of computational thinking for learning, recently co-authoring a book entitled “Teaching and Learning with Jupyter” which provides an introduction to the related methods and tools. I look forward to expanding this for the large courses at TU Delft.

Over the past four years, I have also mentored nearly 500 BSc and MSc students in over 100 engineering projects. As these projects involved external project sponsors, I developed relationships with a diverse set of research, non-profit, and industry organizations. Several of these projects are also with international groups in Kenya, Nicaragua, Cambodia, and Sweden. I am especially proud of the mechanical design exchange program I have developed with Meijo University in Japan. As my native language is English, I will be able to teach MSc classes immediately at TU Delft, but I also have a beginner understanding of Dutch and am eager to become fluent so I can teach BSc courses.

Lastly, I have a strong service record. I serve on my department's undergraduate curriculum committee where we are modernizing our course offerings. I serve on the scientific and planning committees of the Bicycle and Motorcycle Dynamics conference series and recently hosted the International Cycling Safety Conference at UC Davis for the first offering outside of Europe. On the education front, I am a topic editor of the innovative Journal of Open Source Education, now in its second year of publishing.

If at TU Delft, I see numerous opportunities for collaboration within the university. It is exciting that so many authors of papers I have read are at this institution. In the Biomechanical Engineering department, Prof. van der Helm and Prof. Harlaar's expertise in upper and lower limb biomechanics will provide insight for bicycling biomechanics. Prof. Vallery's work in biomechatronics and teaching dynamics can align nicely with this position's efforts. I have interacted with Prof. Seth when he was at Stanford and his foundational work and expertise in musculoskeletal simulation are a strong interest of mine. I have studied and cited Prof. van der Kooij's control identification work and would be excited to learn directly from him. Dr. Geijtenbeek's predictive simulation methods and tools are leading this research area and his connections to Motek Medical would be helpful for my experimental work. I have co-authored a paper with Prof. Happee in the Department of Transport and Planning and will seek collaborations related to vehicle engineering. The Control and Simulation group has strong expertise in manual control theory and identification that I have leveraged in the past. For example, I have worked with Prof. van Paassen on the Python control software and could expand that effort and Prof. Mulder's work in manual control has benefited my applications to single track vehicles. Lastly, I am excited to develop collaborations with Dutch bicycle companies being that the country leads the world in innovative utility bicycle designs.

The best career fit for me is to be a faculty member at a university department that is mission focused, works together forwarding this common mission, and strives for continuous change all while deeply valuing engineering education through teaching and research mentorship.

I have included my research plan that centers around human mobility and a teaching statement that outlines my pedagogical practices in addition to how I think I would fit into your department.

Thank you for your consideration.

Sincerely,

Jason K. Moore

Research Statement

Jason K. Moore

Introduction

My primary research efforts have centered on understanding and improving human mobility by developing biomimetic controllers derived from data collected on human motion during unassisted activities (e.g. standing, walking) and activities in which the human is operating a vehicle (e.g. bicycling, skateboarding) or interacting with a machine or implement (e.g. leg prostheses, sporting equipment). I am most interested in developing human control compatible machine designs and human-in-the-loop control systems that augment a person's experience for improved control, safe operation, and performance enhancement. The fundamental question that I am currently focused on is:

Can dynamically human-similar or human-coupled machines and their controllers be designed to move as well as or better than a human controller would move, if provided neurally-limited control inputs?

To answer this question, my current research has three primary foci:

1. Identifying how humans balance and locomote through data intensive computational estimation, learning, and identification.
2. Applying biomimetic control algorithms and design enhancements derived from identified controllers to assistive devices such as bicycles, exoskeletons, powered prostheses, personal mobility vehicles, and humanoid robots.
3. Developing next generation open and collaborative computational tools to back efforts in the first two items.

My prior research combines knowledge and methods derived from multibody dynamics, sports biomechanics, human motion and control, transportation, and computational engineering. I consider myself an applied computational and experimental dynamics and control engineer; equally comfortable at the whiteboard, on the computer, and in the lab. Much of my work utilizes single track vehicles as a platform for studying multibody dynamics and manual control.

My Past Work in Human Motion and Control

Much of my prior research has focused on the problem of control identification in human balance where I have attempted to answer this question:

Given the simultaneous measurements of the kinematics of human motion and optionally human/environment interface and internal system forces, what is the causal relationship from sensing to actuation in human motion?

My graduate work focused on understanding the control mechanisms humans use while balancing on a bicycle. Because the bicycle is a dynamically complex vehicle [1, 15, 36, 18] that acts as an intermediary between the human and the environment, it is an ideal vehicle platform for understanding balance and manual control.

My early graduate work focused on applying principal component analysis to a large collection of motion capture data during steady state bicycling on a treadmill, which identified dominant motion patterns and exposed subtle leg motions used for balance at low speeds [17, 35]. We further confirmed this low speed behavior with video analysis of more natural bicycling behavior around a city and on a treadmill [13]. This work has since been widely cited in the motion studies literature.

Following those initial experiments, I designed and fabricated a uniquely instrumented bicycle, capable of accurately measuring the full dynamic state of the rider-vehicle system [21, 32], including the most

accurate steer torque measurements to date. With this instrument, I collected copious amounts of data during responses to lateral perturbations in path tracking tasks. Then, starting with our theoretic manual control model [11], I applied data driven parameter estimation techniques to arrive at a set of controllers that explained the rider's dominant linear response behavior to the perturbations [21]. I showed that this control model was able to mimic human behavior for a broader set of control tasks and could be used to estimate the handling qualities of different bicycle designs. This work also supported other theoretic controller structures for bicycling [45, 47, 46] and was also applied to aircraft control identification [12].

The work on bicycle control identification lead into postdoctoral work focused on developing controllers for lower extremity exoskeletons designed to assist paraplegic individuals in walking. We partnered with Parker Hannifin Corp. and targeted their Indego Exoskeleton. My research was led by the goal to provide natural gait and unassisted balance for these devices, something that is still lacking today. Utilizing an actuated treadmill coupled with full body kinematic tracking, I collected large quantities of walking data from both normal walking and longitudinally perturbed walking. I published the data as one of the first data papers in the field [30] and demonstrated the effectiveness of the treadmill belt perturbation method. The data has been used in a variety of other control studies (e.g. [42, 49, 51]), as well as inspiring more data papers [43, 8, 7, 44].

I used the perturbed walking data with a direct gait cycle gain scheduled feedback identification technique to identify possible closed loop controllers [38, 28, 29]. The technique proved to be very computationally efficient and the identified controllers exhibited repeatable feedback patterns in the gait cycle across the walkers.

Difficulties in utility of the prior work led to the development of an indirect identification technique based on parameter estimation with direct collocation to enable simulated validation of the controllers [40, 41]. We demonstrated the computational efficiency and ability to accurately identify control from kinematic data in simulated perturbed human standing. I further codified this technique in a general purpose software library that efficiently constructs the optimization or identification problem from a high level problem description [39, 37].

My Current Work in Human Motion and Control

Since moving into a teaching focused position at UC Davis, I have mentored and led a number of sensing, instrumentation, software, and robotics projects with various local companies and undergraduate students that build on my prior research. We have developed an adaptive mouth-based control for an electric tricycle which is quadriplegic friendly with Outrider USA and Disability Reports and developed a powered cable driven hand prostheses for partial upper body paralysis with Ekso Bionics. With SRE Engineering we developed a wireless boot for measuring ground reaction forces for horse trotting in non-laboratory settings that I would like to develop for human walking. I also mentored a group that developed a robot to tie a shoe [3], one of the more complex tasks human hands perform.

I have further developed our single track vehicle handling quality metric proposed in [11] and utilized it in discovering a variety of bicycle designs with theoretically optimal handling [19, 34]. To validate this theory, we have developed experimental methods with preliminary results indicating a likely relationship in the handling quality metric and rider subjective ratings [14]. And most recently, we have begun constructing the optimal bicycles [10] and evaluating them in terms of their handling.

I have also led two projects in sports engineering in the past couple of years: 1) development of a web application for designing and analyzing ski jumps for improving jumper safety [33, 5] and 2) the implementation of real-time algorithms that improve estimation of competitive rowing performance metrics from smartphone inertial measurement unit data [4].

All of my research relies heavily on open source computational data analysis and simulation tools, many of which I have developed and published. Most notably, I am a core developer of the computer aided algebra system, SymPy [48], and the lead maintainer of the associated classical mechanics package [9]. Our 2017 paper [16] on the now 13 year old software has over 250 citations, along with thousands of users and hundreds of contributors making it one of the most popular packages in the scientific Python ecosystem. Additionally, I have developed a suite of bicycle dynamics and control software packages [22, 23, 24, 20], general purpose dynamics and control packages [39, 25], and biomechanics packages [6, 25, 26, 27].

More about my research projects can be viewed on my lab website: <http://mechmotum.github.io>.

My Bicycle Research Plans

Over the last two decades, the use of bicycles has increased in many countries where its use as a mode of transportation has been historically low. This positive change is the result of many factors, including advances in bicycle related technologies such as electrification and public use designs. In the near future, I foresee bicycles connected into the smart city, far greater use of electric bicycles, growing use of cargo bicycles in urban centers, and growth in both older and younger riders. Yet, despite the increase in ridership, bicyclists will still remain vulnerable road users. More political and technological solutions will be needed to increase safety for bicyclists. As a mechanical engineer, I plan to play an integral role in increasing bicycle safety and use around the world through technological advances.

The lab I envision will support all types of bicycle technologies. Collaborations with other TU Delft researchers will help us make advances in tire material properties, evaluation of electric bicycle transmissions, power augmentation control in pedal assist bicycles, ergonomics, and performance improvements.

As a professor focusing on bicycle dynamics and control, I will have several parallel and intertwined avenues of research that will support this broader social vision:

- Data driven vehicle and biomechanical modeling of the bicycle-rider system
- Data driven manual control characterization and identification in bicycle balance and navigation
- Design and augmented/autonomous control for improvements in bicycling safety and handling
- Development of the next generation of bicycle designs for improvements to transportation
- Application of vehicle dynamics to influence transportation infrastructure design
- Performance and safety improvements in the sport of cycling

I will initiate these research avenues by focusing on several low hanging fruit among the current state of the art, my prior work, and the TU Delft Bicycle and Control Laboratory's prior work. The following paragraphs detail the initial projects I have in mind.

The most popular open loop bicycle vehicle dynamics model fails to make accurate predictions of the vehicle's motion resulting from prescribed input forces acting on the handlebars [31]. Using data collected during closed-loop riding (via robotic and/or human control) I want to identify the missing first principles. I also plan to develop a simple rider biomechanical model that captures the most important degrees of freedom and actuation methods based on [25]. These two aspects will advance the state of the art vehicle-rider system models.

Identification of the controller in a closed-loop feedback and feed-forward system is not a simple task [50]. I want to expand on the robustness of my earlier efforts by collecting data during a broad set of events more rich in frequency content while also collecting additional physiological measures to capture signals related to the human's internal sensing system. This identification will use optimal control, parameter identification, and physics-informed machine learning methods. This will result in general validated human control models for single track vehicles.

To succeed at the above initiatives, I want to design and construct a new force sensing treadmill for single track vehicle experimentation. Measuring the ground reaction forces and moments at each individual tire while performing maneuvers on a treadmill in a simulated environment will provide the next level of fidelity in understanding the vehicle and rider dynamics. This treadmill will be unique to the world and combined with simulation environments developed at TU Delft will offer a capable experimental platform that will be attractive for many industry interests.

Using both a robotic bicycle (currently on loan to TU Delft from UC Davis) and TU Delft's steer-by-wire bicycle, I plan to explore how vehicle and controller design can effectively assist the rider's control, i.e. to take over when the human's deficiencies are present and to maximize the performance in safety critical maneuvering. These efforts will provide essential elements to having autonomous single track vehicles in the future and safety enhancements that go far beyond simple traction control.

I want my research to have direct impact on transportation mode share and safety for bicycling. I have preliminary work on using bicycle simulations for evaluating bicycle transportation infrastructure and creating standards for infrastructure [2]. There is also an opportunity to apply bicycle balance and control theory to the design of cargo bicycles and other non-traditional bicycles. Both of which will connect my work to practice.

Finally, I have long had a dream of being part of a team that could attain the world human powered speed record. TU Delft has done so in the past and I intend to help them do so again. I would like to apply both my work in trajectory optimization for speed improvements and lateral control to relieve the rider so they can focus fully on power generation.

References

- [1] Karl J. Åström, Richard E. Klein, and Anders Lennartsson. Bicycle dynamics and control: Adapted bicycles for education and research. *IEEE Control Systems Magazine*, 25(4):26–47, August 2005.
- [2] Theodore Buehler and Jason K. Moore. Time and Energy Penalties of Squiggly Bike Routes, June 2012.
- [3] Andrew Choi, Stephanie Thai, Jacklyn Tran, Gabriela Gomes, and Joel Humes. Shoe Tying Robot. <https://www.youtube.com/watch?v=erNi07dH5pw>, 2018.
- [4] Bryn Cloud, Britt Tarien, Ada Liu, Thomas Shedd, Xinfan Lin, Mont Hubbard, R. Paul Crawford, and Jason K. Moore. Adaptive smartphone-based sensor fusion for estimating competitive rowing kinematic metrics. *PLoS ONE*, 2019. Under review.
- [5] Bryn Cloud, Britt Tarien, Jason K. Moore, and Mont Hubbard. Accessible, Open-source Computational Analysis and Design of Terrain Park Ski Jumps. In *23rd International Congress on Snow Sports Trauma and Safety*, Squaw Valley, California, USA, April 2019. Abstract.
- [6] Christopher Dembia, Jason K. Moore, Stefen Yin, and Oliver Lee. Yeadon: A Python Library For Human Inertia Estimation. <https://github.com/chrisdembia/yeadon>, June 2011.
- [7] Claudiane A. Fukuchi, Reginaldo K. Fukuchi, and Marcos Duarte. A public dataset of overground and treadmill walking kinematics and kinetics in healthy individuals. *PeerJ*, 6:e4640, April 2018.
- [8] Reginaldo K. Fukuchi, Claudiane A. Fukuchi, and Marcos Duarte. A public dataset of running biomechanics and the effects of running speed on lower extremity kinematics and kinetics. *PeerJ*, 5:e3298, May 2017.
- [9] Gilbert Gede, Dale L. Peterson, Angadh S. Nanjangud, Jason K. Moore, and Mont Hubbard. Constrained Multibody Dynamics With Python: From Symbolic Equation Generation to Publication. In *Volume 7B: 9th International Conference on Multibody Systems, Nonlinear Dynamics, and Control*, Portland, Oregon, USA, August 2013. DETC2013-13470.
- [10] Roy Gilboa, Anastasia Kubicki, Anthony Toribio, Mont Hubbard, and Jason K. Moore. Practical Realization of a Theoretical Optimal-Handling Bicycle. In *Bicycle and Motorcycle Dynamics: Symposium on Dynamics and Control of Single Track Vehicles*, page 11, 2019.
- [11] Ronald Hess, Jason K. Moore, and Mont Hubbard. Modeling the Manually Controlled Bicycle. *IEEE Transactions on Systems, Man, and Cybernetics - Part A: Systems and Humans*, 42(3):545–557, February 2012.
- [12] Ronald A. Hess and Jason K. Moore. Estimating Parameters of the Structural Pilot Model Using Simulation Tracking Data. In *AIAA Guidance, Navigation, and Control Conference*, August 2013.
- [13] J. D. G. Kooijman, A. L. Schwab, and Jason K. Moore. Some Observations on Human Control of a Bicycle. In *Proceedings of the ASME 2009 International Design and Engineering Technical Conferences & Computers and Information in Engineering Conference*. ASME, August 2009.
- [14] Scott W. Kresie, Jason K. Moore, Mont Hubbard, and Ronald A. Hess. Experimental Validation of Bicycle Handling Prediction. In *Proceedings of the 6th Annual International Cycling Safety Conference*, Davis, CA, USA, September 2017.
- [15] J. P. Meijaard, Jim M. Papadopoulos, Andy Ruina, and A. L. Schwab. Linearized dynamics equations for the balance and steer of a bicycle: A benchmark and review. *Proceedings of the Royal Society A: Mathematical, Physical and Engineering Sciences*, 463(2084):1955–1982, August 2007.
- [16] Aaron Meurer, Christopher P. Smith, Mateusz Paprocki, Ondřej Čertík, Sergey B. Kirpichev, Matthew Rocklin, AMiT Kumar, Sergiu Ivanov, Jason K. Moore, Sartaj Singh, Thilina Rathnayake, Sean Vig, Brian E. Granger, Richard P. Muller, Francesco Bonazzi, Harsh Gupta, Shivam Vats, Fredrik Johansson, Fabian Pedregosa, Matthew J. Curry, Andy R. Terrel, Štěpán Roučka, Ashutosh Saboo, Isuru Fernando, Sumith Kulal, Robert Cimrman, and Anthony Scopatz. SymPy: Symbolic computing in Python. *PeerJ Computer Science*, 3(e103), January 2017.

- [17] J. K. Moore, J. D. G. Kooijman, and A. L. Schwab. Rider motion identification during normal bicycling by means of principal component analysis. In K. Arczewski, J. Frączek, and M. Wojtyra, editors, *Proceedings of Multibody Dynamics 2009, ECCOMAS Thematic Conference*, Warsaw, Poland, June 2009.
- [18] Jason Moore and Mont Hubbard. Parametric Study of Bicycle Stability. In Margaret Estivalet and Pierre Brisson, editors, *The Engineering of Sport 7*, volume 2. Springer, 2008.
- [19] Jason Moore, Mont Hubbard, and Ronald A. Hess. An Optimal Handling Bicycle. In *Proceedings of the 2016 Bicycle and Motorcycle Dynamics Conference*. Figshare, September 2016.
- [20] Jason K. Moore. HumanControl: Human control of a bicycle. University of California, Davis, May 2011. <https://github.com/moorepants/HumanControl>.
- [21] Jason K. Moore. *Human Control of a Bicycle*. Doctor of Philosophy, University of California, Davis, CA, August 2012. <http://moorepants.github.io/dissertation>.
- [22] Jason K. Moore, P. D. L. de Lange, and Yumiko Henneberry. BicycleDAQ: Data aquisition application for an instrumented bicycle. University of California, Davis, October 2010. <http://github.com/moorepants/BicycleDAQ>.
- [23] Jason K. Moore, P. D. L. de Lange, and Stefen Yin. BicycleDataProcessor: Data storage and processing library for an instrumented bicycle. University of California, Davis, February 2011. <https://github.com/moorepants/BicycleDataProcessor>.
- [24] Jason K. Moore, Chris Dembia, and Oliver Lee. BicycleParameters: A Python library for bicycle parameter estimation and analysis. <https://github.com/moorepants/BicycleParameters>, April 2011.
- [25] Jason K. Moore, Chris Dembia, and Oliver Lee. DynamicistToolKit: A Python library for dynamcis and controls. <https://github.com/moorepants/DynamicistToolKit>, June 2011.
- [26] Jason K. Moore, Tarun Gaba, Oliver Lee, Sahil Shekhawat, Dale L. Peterson, Chris Dembia, Yashu Seth, Nikhil Pappu, Gilbert Gede, James Crist, Brandon James Milam, Frédéric Bastien, Pranjal Mittal, Robert McMurry, Varun Joshi, Ivan Angelov, and Nikolay Mayorov. PyDy: A multi-body dynamics analysis package written in Python. PyDy, October 2011. <http://pydy.org>.
- [27] Jason K. Moore, Sandra K. Hnat, Obinna Nwanna, Michael Overmeyer, and Antonie J. van den Bogert. GaitAnalysisToolKit: A Python Library for Gait Analysis. <https://github.com/csu-hmc/GaitAnalysisToolKit>, December 2013.
- [28] Jason K. Moore, Sandra K. Hnat, and Antonie J. van den Bogert. Identification of human control during perturbed walking. In *Midwest American Society of Biomechanics Regional Meeting*, Akron, Ohio, USA, March 2014. <https://github.com/moorepants/MASB2014>.
- [29] Jason K. Moore, Sandra K. Hnat, and Antonie J. van den Bogert. Identification of human control during perturbed walking. In *Dynamic Walking*, Zurich, Switzerland, June 2014. <https://github.com/moorepants/DW2014>.
- [30] Jason K. Moore, Sandra K. Hnat, and Antonie J. van den Bogert. An elaborate data set on human gait and the effect of mechanical perturbations. *PeerJ*, 3(e918), April 2015.
- [31] Jason K. Moore and Mont Hubbard. Identification of open loop dynamics of a manually controlled bicycle-rider system. In *Proceedings of Bicycle and Motorcycle Dynamics: Symposium on the Dynamics and Control of Single Track Vehicles*, Narashino, Chiba, Japan, November 2013.
- [32] Jason K. Moore and Mont Hubbard. Methods for elimination of crosstalk and inertial effects in bicycle and motorcycle steer torque estimation. In *Proceedings of Bicycle and Motorcycle Dynamics: Symposium on the Dynamics and Control of Single Track Vehicles*, Narashino, Chiba, Japan, November 2013.
- [33] Jason K. Moore and Mont Hubbard. Skijumpdesign: A Ski Jump Design Tool for Specified Equivalent Fall Height. *The Journal of Open Source Software*, 3(28):818, August 2018.

- [34] Jason K Moore and Mont Hubbard. Expanded Optimization for Discovering Optimal Lateral Handling Bicycles. In *Bicycle and Motorcycle Dynamics 2019: Symposium for Dynamics and Control of Single Track Vehicles*, page 12, Padua, Italy, 2019. Figshare.
- [35] Jason K. Moore, J. D. G. Kooijman, A. L. Schwab, and Mont Hubbard. Rider motion identification during normal bicycling by means of principal component analysis. *Multibody System Dynamics*, 25(2):225–244, February 2011.
- [36] Jason K. Moore, Dale L. Peterson, and Mont Hubbard. Influence of rider dynamics on the Whipple bicycle model. In *Proceedings of the 11th International Symposium on Computer Simulation in Biomechanics*, Tainan, Taiwan, June 2007. https://www.researchgate.net/publication/216750976_Influence_of_rider_dynamics_on_the_Whipple_bicycle_model.
- [37] Jason K. Moore and Antonie van den Bogert. Opty: Software for trajectory optimization and parameter identification using direct collocation. *Journal of Open Source Software*, 3(21):300, January 2018.
- [38] Jason K. Moore and Antonie J. van den Bogert. Direct Identification of Human Gait Control. <https://github.com/csu-hmc/gait-control-direct-id-paper>, August 2013.
- [39] Jason K. Moore and Antonie J. van den Bogert. Opty: A library for using direct collocation in the optimization and identification of dynamic systems. Cleveland State University, May 2014. <https://github.com/csu-hmc/opty>.
- [40] Jason K. Moore and Antonie J. van den Bogert. Perturbed Standing Controller Parameter Identification: A comparison of Methods. <https://github.com/csu-hmc/inverted-pendulum-sys-id-paper>, August 2014.
- [41] Jason K. Moore and Antonie J. van den Bogert. Quiet Standing Control Parameter Identification with Direct Collocation. In *XV International Symposium on Computer Simulation in Biomechanics*, Edinburgh, UK, July 2015. <https://github.com/csu-hmc/ISBTGCS2015>.
- [42] Farbod Rohani, Hanz Richter, and Antonie J. van den Bogert. Optimal design and control of an electromechanical transfemoral prosthesis with energy regeneration. *PLOS ONE*, 12(11):e0188266, November 2017.
- [43] Damiana A. Santos and Marcos Duarte. A public data set of human balance evaluations. *PeerJ*, 4:e2648, November 2016.
- [44] Alessandro Santuz, Antonis Ekizos, Lars Janshen, Falk Mersmann, Sebastian Bohm, Vasilios Baltzopoulos, and Adamantios Arampatzis. Modular Control of Human Movement During Running: An Open Access Data Set. *Frontiers in Physiology*, 9, October 2018.
- [45] A. L. Schwab, P. D. L. de Lange, R. Happee, and Jason K. Moore. Rider control identification in bicycling, parameter estimation of a linear model using lateral force perturbation tests. In *Proceedings of the IMSD2012 - The 2nd Joint International Conference on Multibody System Dynamics*, Stuttgart, Germany., May 2012.
- [46] A. L. Schwab, P. D. L. de Lange, R. Happee, and Jason K. Moore. Rider control identification in bicycling using lateral force perturbation tests. *Proceedings of the Institution of Mechanical Engineers, Part K: Journal of Multi-body Dynamics*, 227(4):390–406, August 2013. 2013 SAGE Best Paper Award.
- [47] Arend Schwab, Peter de Lange, and Jason K. Moore. Rider Optimal Control Identification in Bicycling. In *Proceedings of the 5th Annual Dynamic Systems and Control Conference and 11th Annual Motion and Vibration Conference*, Fort Lauderdale, Florida, USA, October 2012. ASME. <http://bicycle.tudelft.nl/schwab/Publications/schwab2012riderB.pdf>.
- [48] SymPy Development Team. SymPy: Python library for symbolic mathematics. <http://www.sympy.org>, 2006.
- [49] Nitish Thatte, Helei Duan, and Hartmut Geyer. A Method for Online Optimization of Lower Limb Assistive Devices with High Dimensional Parameter Spaces. In *2018 IEEE International Conference on Robotics and Automation (ICRA)*, pages 5380–5385, May 2018.

- [50] Herman van der Kooij, Edwin van Asseldonk, and Frans C.T. van der Helm. Comparison of different methods to identify and quantify balance control. *Journal of Neuroscience Methods*, 145(1-2):175–203, June 2005.
- [51] Amit Kumar Vimal, Piyush Swami, Sneh Anand, Upinderpal Singh, Shubhendu Bhasin, and Deepak Joshi. Search algorithm for optimal damping parameters of transfemoral prosthetic limb. *Applied Mathematical Modelling*, 72:356–368, August 2019.

Teaching Statement

Jason K. Moore

My interest in mechanical engineering began during my childhood where I spent many hours making, tinkering, and discovering how the built environment functioned. These hands-on experiences allowed me to develop a desire to discover the connection to mathematics, physics, and science in order to improve my projects. Once that realization occurred, any barriers I had towards learning the engineering fundamentals were lifted. I hope to bring similar kinds of experiences and motivation to the students I teach.

Teaching Philosophy

Traditional engineering pedagogy focuses heavily on lecture-based theoretical courses paired with few hands-on laboratory courses. The aspects of creativity, team work, realistic constraints, and an infinite possibility of problem solutions are too often absent. These aspects are needed to develop the practical side of engineering that students will require in their future careers. Often, only the students who participate in extracurricular projects, internships, or research positions make the connection from theory to practice early on in the curriculum. Thus, the traditional structure may not be the best way to maximize student understanding of engineering principles and instill the agile problem solving methods they will need in the future.

Although there are variety of motivational reasons students pursue engineering, I believe introducing the applied engineering practices early in education will build passion and interest. Once this door is open, it is much easier to weave in the skills the students need to become stronger engineers in their future careers. I would like to see a curriculum that mimics the actual practice of engineering through an iterative pattern of posing realistic problems followed by a search for the necessary fundamentals, culminating in the application of new knowledge to arrive at a solution. Like my childhood experiences, this model provides interesting realistic problems that allow students to discover the engineering fundamentals as opposed to presenting all of the fundamentals before the interesting problems arrive.

Engineering students are capable of creating and solving problems when they enter college. We should enrich their entire experience (especially in the first year!) with challenges from real-world problems that leave them begging for the knowledge and tools that they typically have to slog through during their first years of school. Richard Miller, President of Olin College, often draws an analogy between engineering students and violin students: “Can you imagine not playing the violin until your fourth year of study? Violinists start making sounds with their instrument the first day of lessons.” An engineering curriculum could allow our students to draw the engineering bow across the strings the minute they step into the classroom. For these early project-based courses to be effective, however, the latest pedagogical developments must be utilized to maximize learning potential.

Practical Classroom Examples

In my courses, I try to provide students with open-ended problems that lead into larger projects instead of problems designed for rote learning and traditional exams. This approach more closely mimics the practice of engineering. I combine this approach with rubric based assessments that set the bar for mastery for improving student outcomes and effective assessment. I attempt to have a good mixture of group and individual work, leaning more heavily toward the former so students are prepared for the needs of industry. I also have been working to orient my classrooms towards active learning. My best example is the utilization of “computational thinking” that makes use of live coding in class. I have setup a [JupyterHub server](#) that students log into via laptops, tablets, and phones during class that provides an interactive engineering computational environment. This allows access to my interactive textbook that students use as a reading guide while I provide examples paired with short computing exercises to periodically assess learning. I have developed a related workshop for other practitioners with my colleague

Allen Downey from Olin College of Engineering which has been successful. I use exam reflections surveys to provide self-guided preparation for subsequent exams. Lastly, another very important method that I make use of is rapid in-class assessment; at every break, each student provides me with anonymous quick feedback: one line comments that share what they didn't understand and what was effective. This allows me to adjust my teaching after the break based on the feedback. I tie this in with collected feedback before, during, and after the course to have data to back my teaching decisions.

All of these methods are backed by evidence from education research. To keep up-to-date on topics like these, I follow the education research literature, especially the summary literature aimed at practicing educators and attend “teach the teachers” style workshops as much as possible. I have worked closely with the UCD Center for Educational Effectiveness and the UCD Engineering Education Learning Community these past four years to improve student learning in my courses and for my department.

Prior Experience and Future Interests

A teacher is often at their best when they know their material well. I spent most of my graduate school years in the UCD MAE department and now four years on the faculty making me intimately familiar with their undergraduate and graduate curriculum. I have taught a number of the available courses as a teaching assistant, lecturer, and professor. At the undergraduate level I have strong experience with the dynamics and controls courses along with mechanics and machine design curriculum. I have taught “[Engineering Graphics and Design](#)”, “[Manufacturing Processes](#)”, “[Introduction to Mechanical Vibrations](#)”, “[Mechanical Design](#)”, “[Mechanical Systems Design Project](#)”, “[Vehicle Stability](#)”, and “[Analysis, Simulation and Design of Mechatronic Systems](#)”. I have also taught “[Multibody Dynamics](#)” at the graduate level. I believe my prior experience makes me quite versatile and able to teach a broad variety of courses.

In evidence based practices and innovations in the classroom. Some highlights from the last four years are:

- developed a design competition and exchange program with Meijo University (Nagoya, Japan) on the cultural influences of robot and machine design
- flipped a mechanical vibrations class by utilizing “computational thinking” and project oriented learning with a custom designed interactive textbook and deployment through a JupyterHub server
- created a design studio classroom space that facilities active learning for our design courses
- created extensive rubric based assessment for written and oral communication in the capstone design course
- created a set of twenty Jupyter notebooks on multibody dynamics for in-class use and accompanying publicly available videos
- developed a transit bus bicycle rack design project which included reverse engineering, concept generation, and lightweight prototyping
- solicitation and mentoring of over 90 industry, government, and non-profit supported design projects spanning the mechanical engineering discipline
- co-awarded a \$5M Department of Education grant to create interactive OER engineering textbooks as part of the LibreTexts project
- co-wrote a book on teaching with Jupyter
- co-developed a workshop designed to teach STEM educators effective methods to teach with computation

There are at least four undergraduate courses that I would like to co-develop in the future that are influenced by my research endeavors: 1) a first year problem solving with data, simulation, and engineering computation, 2) an upper level applied robotics and controls course centered around hands on work with robotic vehicles, 3) an upper level elective focusing on project based assistive device design, and 4) an introduction to computational optimization.

At the graduate level, I am also well prepared to teach many courses in dynamics, control theory, biomechanics, optimization, software engineering, and vehicle dynamics. I would like to continue to teach advanced multibody dynamics from computational perspective. Additional ideas include developing a course focusing on the design, simulation, and optimization of legged biomechatronics that aligned closely with my post doctoral research. Students will learn about neuromuscular modeling, mammalian gait, and

get exposed to the latest tools in the field (OpenSim, Biomechanical ToolKit, ROS/Gazebo, IPOPT, etc). Lastly, I would very much an experimental biomechanics oriented course would also nicely complement the computational oriented one to prepare students for applied work in the field.

My course topic strengths are not entirely based on UCD MAE offerings. I have spent time at Delft University of Technology, Old Dominion University, Cleveland State University, Stanford University, and with the Software Carpentry non-profit where I have gleaned both new course ideas and methodologies to provide stronger connections to industry. I have experience in teaching computational methods for data science. I have given numerous workshops and tutorials to scientists and engineers on simulation, optimization, and data analysis. I have been trained by the Software Carpentry organization in pedagogical methods and teach two-day workshops around the world to introduce scientists and engineers to the best practices and methods in scientific computing. The mechanical engineer of the future will be additionally tasked with data driven engineering. The engineering curriculum will need to adapt to bring data science into many of the core courses for our students to stay competitive in the job market, which I am ready to do.

Contact Information For References

Jason K. Moore

Here I provide a list of references that are most familiar with my research and teaching efforts. Additional, references are listed on the last page of the C.V.

Research References

- Dr. Antonie J. van den Bogert, *Post Doctoral Supervisor*, Professor, Cleveland State University, Mechanical Engineering Department, 1960 E. 24th St., SH 232, Cleveland, Ohio 44115, +01-216-687-5329, a.vandenbogert@csuohio.edu
- Dr. Mont Hubbard, *MSc and PhD advisor*, Professor Emeritus, University of California, Davis, Mechanical and Aerospace Engineering Department, One Shields Avenue, Davis, CA 95616, +01-530-752-6450, mhubbard@ucdavis.edu
- Dr. Ronald Hess, *PhD advisor*, Professor Emeritus, University of California, Davis, Mechanical and Aerospace Engineering Department, One Shields Avenue, Davis, CA 95616, +01-530-752-1513, rahess@ucdavis.edu

Teaching References

- Dr. Allen Downey, *Educational Collaborator*, Professor, Olin College, Needham, MA, USA, allen.downey@olin.edu
- Dr. Petros Abraha, *Engineering Education Collaborator*, Professor, Meijo University, Nagoya, Japan, petros@meijo-u.ac.jp
- Dr. Susan Handy, *COSMOS Lead Instructor*, Professor, University of California, Davis, Davis, CA, slhandy@ucdavis.edu

Jason K. Moore

CONTACT INFORMATION	Sacramento, CA, USA moorepants@gmail.com +01-530-601-9791	Personal Website: moorepants.info Lab Website: mechmotum.github.io G-Scholar: tinyurl.com/jkm-gscholar Github: github.com/moorepants Linkedin: tinyurl.com/jkm-link Twitter: @moorepants
CITIZENSHIP	United States of America	
LANGUAGE	English [US] (mother tongue), Spanish [GU] (beginner), Dutch [NL] (beginner)	
RESEARCH INTERESTS	Multibody dynamics, bicycle dynamics, human biomechanics, human operator control, gait control identification, exoskeleton control, vehicle handling qualities, vehicle dynamics, control systems, aircraft control, aircraft dynamics, appropriate technology, human powered machines, system identification, software engineering, wind tunnel experimentation, computational reproducibility, open science, optimal control, machine design, computer aided algebra	
ACADEMIC POSITIONS	Assistant Professor of Teaching <i>Mechanical and Aerospace Engineering Department, University of California, Davis</i> (Chairs: C. P. van Dam [2015-2016], Stephen K. Robinson [2016-2019], Cristina E. Davis [2019-Present])	September 2015 to present
	Postdoctoral Research Associate <i>Human Motion and Control Laboratory, Cleveland State University</i> (PI: Antonie J. van den Bogert)	July 2013 to August 2015
	Visiting NCSRR Scholar <i>Neuromuscular Biomechanics Laboratory, Stanford University</i> (PI: Scott L. Delp)	August 2014
	Postdoctoral Research Programmer <i>Institute for Transportation Studies, University of California, Davis</i> (PI: Tai Stillwater)	January 2013 to June 2013
	Lecturer (Unit 18) <i>Mechanical and Aerospace Engineering Department, University of California, Davis</i> (Chair: C.P. van Dam)	September 2012 to December 2012
	Graduate Student Researcher <i>Sports Biomechanics Laboratory, University of California, Davis</i> (PIs: Mont Hubbard, Ronald Hess)	September 2009 to August 2012
	Visiting Fulbright Scholar <i>Bicycle Dynamics Laboratory, Delft University of Technology</i> (PI: A.L. Schwab)	August 2008 to August 2009
	Teaching Assistant <i>Mechanical and Aerospace Engineering Department, University of California, Davis</i> (Instructors: Jim Schaaf, Rida Farouki)	March 2006 to June 2007

EDUCATION**University of California at Davis**, Davis, California USA

Ph.D., Mechanical and Aerospace Engineering, August 2012

- Dissertation: Human Control of A Bicycle
- Dissertation Topic: Bicycle dynamics, control, and handling qualities
- Areas of Study: Multibody dynamics, control systems, biomechanics, and system identification
- Advisors: Mont Hubbard, Ron A. Hess, Arend L. Schwab
- Lab: UCD Sports Biomechanics Lab, TU Delft Bicycle Dynamics Lab

M.Sc., Mechanical and Aeronautical Engineering, June 2007

- Advisor: Mont Hubbard
- Area of Study: Multibody dynamics, control systems, and machine design
- Lab: Sports Biomechanics Lab

Old Dominion University, Norfolk, Virginia USA

B.Sc., Mechanical Engineering, December 2004

- *Magna cum Laude*
- Machine Design Specialization
- Minor in Mathematics
- Minor in Philosophy and Religious Studies

Tunstall High School, Dry Fork, Virginia USA

Advanced Diploma, May 2000

- Graduated with Honors

PROFESSIONAL ACCREDITATION

Passed the Fundamentals of Engineering Exam in Virginia

RESEARCH EXPERIENCE**University of California at Davis**, Davis, California USA**Faculty****September 2015 to Present**

- Created and led the **Laboratorium of Marvelous Mechanical Motum**
- Safe ski jump design: mentored one undergraduate in developing methods for designing, measuring, and analyzing ski jumps for minimal impact velocity using interactive web applications and accurate GPS measures, see [skijumpdesign.info](#).
- Smartphone rowing data backed coaching: Worked with local startup and six undergraduates in a data science and dynamics project to predict rowing motions from smartphone data
- Optimal bicycle design: mentored one post-graduate and six undergraduates students in an experimental study on bicycle handling, developed and optimization algorithm to discover optimal handling bicycle designs
- Design of an efficient human powered irrigation pump: mentored one graduate student and two undergraduate students in this research/design effort, partnered with World Bicycle Relief and Buffalo Bikes
- Identification of human standing control: mentored ten undergraduates in the design of a double pendulum balancing robot for balance control studies
- Member of 4 MSc committees
- Mentored 4 graduate students, 20+ undergraduates

Postdoctoral Researcher and Programmer**February 2013 to June 2013**

- Developed a cross platform smart phone/tablet application for real-time automobile driver fuel economy feedback. This application was used to conduct an experiment with 200 drivers in San Francisco on driver behavior: SmartDrive

- Won \$2K in the first Phase of the White House's Apps for Vehicles Challenge with simpler version of SmartDrive for consumer use, Drive5
- Designed statistical Kalman filter based fuel economy prediction algorithms based on smart phone sensor data.

Graduate Student Researcher

September 2005 to August 2012

- Graduate Student Researcher at the Sports Biomechanics Lab.
- Member of UC Davis's Institute for Transportation Studies.
- Co-wrote and co-managed a three year National Science Foundation grant.
- Developed a custom instrumented bicycle and performed control experiments to characterize the human control system in the bicycling balancing and tracking task.
- Developed numerous open source software packages.
- Mentored five graduate students during summer internships in experimental, theoretical, and computational dynamics.
- Mentored approximately ten undergraduate student interns in a lab setting.
- Mentored four undergraduates in their senior design project.
- Led multiple tours of the Sport Biomechanics Lab.
- Involved in the graduate student recruitment week.
- Designed and administered the lab website.
- Co-founded Davis Open Science.
- Co-wrote and awarded two Google Summer of Code grants (2011, 2012).
- Organized weekly lab meetings.
- Refereed an article for Vehicle System Dynamics.
- Organized and co-chaired both an invited and special session at the 2012 ASME DSCC conference.
- Featured in "Science of Balancing a Bike" by the UC Office of the President.
- Featured in "Science of Riding a Bicycle" video by KQED Quest.

Biomedical Research Engineer

August 2007 to August 2009

- Designed and supervised the fabrication of a cell shearing device for the UCD Biomedical Passerini Lab.

Cleveland State University, Cleveland, Ohio USA

Post Doctoral Research Associate

July 2013 to August 2015

- PI: Ton van den Bogert
- Lab: Human Motion and Control Lab
- Identified control schemes for exoskeletons in human walking using data driven approaches.
- Developed and ran multi-subject gait experiments with a modern gait lab.
- Developed software for gait data analysis and simulation.
- Developed human walking computational models.
- Mentored several undergraduate and graduate students in research projects.
- Mentored undergraduate students in their senior design projects.
- System administrator for the lab web site.
- Developed an open data paper for a very large gait dataset.

Delft University of Technology, Delft, Zuid-Holland Netherlands

Fulbright Visiting Scholar and Researcher

August 2008 to August 2009

- Ph.D. researcher at the Bicycle Dynamics Laboratory.
- Co-developed an instrumented bicycle with video logging and accompanying software.

- Used the instrumented bicycle in various experiments on and off the treadmill resulting in two conference papers.
- Participated in canceled gyro, negative trail bicycle experiments that eventually resulted a Science publication.
- Lead motion capture study on bicycle/rider kinematics resulting in two conference papers and one peer reviewed journal article.
- Developed a systematic method of measuring the physical properties of a bicycle and rider resulting in two conference papers.
- Gave a colloquium talk on the year's research.
- Researched the bicycle transportation system in the Netherlands, kept an informal blog, attended the Velo-City Brussels conference, and gave a talk on the subject at the UCD Institute of Transportation Studies.

**GRADUATE
COMMITTEE
MEMBERSHIPS**

University of California, Davis

- Scott Kresie, MSc, 2019
- Abraham McKay, MSc, 2018 [Chair]
- Farhad Ghadamli, MSc, 2017
- Sui Nam Chan, MSc, 2017

**TEACHING
EXPERIENCE**

University of California at Davis, Davis, California USA

Assistant Professor of Teaching MAE

September 2015 to Present

- Taught "Analysis, Simulation and Design of Mechatronic Systems", Winter/Fall 2019 & Winter 2020, 40-60 students, upper level elective, 1 teaching assistant, developed new simulation guide, integrated active learning problems during class, created Segway control module, redesigned computational lab assignments
- Taught "Vehicle Dynamics", Fall 2018 & Spring 2020, 15-40 students, upper level elective, 1 teaching assistant, integrated new objective based assessment for homeworks and enhanced the single track vehicle lectures
- Taught "Introduction to Mechanical Vibrations", Fall 2016/2017 & Winter 2020, 20-40 students, upper level elective, 1 teaching assistant, redesigned entire course second time teaching it to focus on active learning and computational thinking, developed an interactive open access textbook
- Taught Multibody Dynamics, Fall 2017/2019, 10-20 students, graduate course, custom software, PyDy, developed and used in the course
- Co-taught Mechanical Systems Design Project, Winter/Spring 2016/2017/2018/2019, 140-160 students, 4 teaching assistants, capstone design course, mentored 90+ projects for industry clients, developed exchange program with Meijo University in Japan
- Taught Mechanical and Aerospace Engineering Graduate Seminar, Spring 2017, invited 10 guest speakers for 1 hour seminars
- Taught Mechanical Design, Fall 2015/2016, required upper level course, 20-35 students, introduced new design project, active learning
- Taught modules in the high school summer program COSMOS in the transportation track, Summer 2018/2019
- Participated in the Engineering Education Learning Community
- Mentored 10 teaching assistants.

Lecturer

August 2012 to December 2012

- Taught "Engineering Graphics in Design", 120 students, 4 Teaching Assistants
- Topics: Design, Sketching, Drawing, Drafting, Solid Modeling, CAD

<i>Graduate Student Researcher</i>	September 2005 to August 2012
<ul style="list-style-type: none"> Mentored five graduate students during summer internships in experimental, theoretical, and computational dynamics. Mentored approximately ten undergraduate student interns in a lab setting. Mentored four undergraduates in their senior design project. Led multiple tours of the Sport Biomechanics Lab. 	
<i>Machine Shop Supervisor</i>	January 2007 to June 2008
<ul style="list-style-type: none"> Supervised the College of Engineering student machine shop. Helped students with machining and fabrication projects. Taught the shop safety class. Fabricated various doodads and gizmos for the shop. Organized the shop. Worked on design projects for various campus research groups. 	
<i>Teaching Assistant</i>	March 2006 to June 2007
<ul style="list-style-type: none"> EME 150B, Mechanical Design (Spring 2006): Worked with student groups during the discussion period on their design projects, graded homework assignments, and held weekly office hours. EME 50, Manufacturing Processes (Fall 2006 and Winter 2007): Taught hands-on machining and fabrication during weekly lab sections, graded homework assignments and tests, and organized the end of quarter party. ENG 4, Engineering Graphics (Spring 2007): Led lab sections with lectures in sketching and 2D/3D computer aided design with modern CAD software. 	
<i>Davis Open Science Co-founder</i>	February 2010 to June 2013
<ul style="list-style-type: none"> Co-founded the graduate student group. Co-hosted several seminars and panels with prominent speakers in Open Science. Worked with various faculty and staff on open science projects. Led workshops on open science topics. 	
<i>Action Research Team Facilitator</i>	March 2007 to December 2007
<ul style="list-style-type: none"> Led group of students in the design and construction of a pedal powered desk laptop charging station. Competed in Google and Specialized's Innovate or Die Contest. The project was featured in many articles and news broadcasts. Featured in the book <u>Human Powered Home</u> by Tamara Dean. 	
<i>Assistant Action Research Team Facilitator</i>	March 2006 to June 2006
<ul style="list-style-type: none"> Co-led a group of students through the process of starting a mock non-profit group. 	
<i>Reader</i>	September 2006 to December 2006
<ul style="list-style-type: none"> Graded mechanical design assignments (EME 150B). 	
Software Carpentry , Everywhere, Planet Earth	
<i>Volunteer Instructor</i>	January 2015 to now
<ul style="list-style-type: none"> Lead multiple workshops on computation for scientists and engineers. Developed lesson plans. Passed the instructor certification. 	

Cleveland State University, Cleveland, Ohio USA

Post Doctoral Research Associate

July 2013 to December 2014

- Mentored graduate students.
- Mentored undergraduate students in their senior design projects.
- Led “Open Source Code Nights” workshops with the undergraduate IEEE group.
- Gave tutorials on multibody dynamics and control to graduate and undergraduate students.

Delft University of Technology, Delft, Zuid-Holland Netherlands

Fulbright Visiting Scholar and Researcher

August 2008 to August 2009

- Mentored undergraduate students in their senior design projects.

GRANTS AND AWARDS

United States Department of Education

- Expanding the LibreTexts Project into the Next-Generation Hub for Construction, Dissemination, and Usage of Open Educational Resource Textbooks, September 2018-September 2021, CO-PI, \$5M.

UC Davis Global Affairs

- Influence of Culture in Mechanical Design , PI, 2018-2019, \$24k.

Center for Educational Effectiveness

- Development of an Interactive Textbook Backed by Cloud Infrastructure to Pilot Active Computational Learning in an Upper Level Mechanical Vibrations Engineering Course , PI, 2017-2018, \$22k.

National Center of Simulation in Rehabilitation Research, Stanford University

- 2014 NCSRR Visiting Scholarship, \$8k.

SAGE Publishing

- 2013 Best Paper Award, Journal of Multibody Dynamics, \$400.

U.S. General Services Administration

- White House Apps for Vehicles Challenge: Phase 1, 2013, \$2k.

2012 Dynamic Systems and Control Conference

- Best paper in the Single Track Vehicle Dynamics and Control Session, 2012.

National Science Foundation

- NSF Standard Grant: Human Control of Bicycle Dynamics with Experimental Validation and Implications for Bike Handling and Design, Co-Author, 2009-2012, \$300k.

U.S. Department of State

- Fulbright Grant to the Netherlands, 2008-2009, \$10k.

University of California, Davis

- Summer Graduate Student Researcher Award, 2010
- Campus Sustainability Grant (Human Powered Utility Vehicle Pilot Program), 2008
- Campus Sustainability Grant (Davis Bike Church Physical Space Renovation), 2008
- Graduate Student Association Travel Award, 2008
- Institute for Transportation Studies Travel Award, 2008
- Campus Sustainability Grant (Pedal Powered Charging Table), 2007
- Joseph Beggs Fellowship for Kinematics, 2006–2007

- MAE Department Fellowship, UC Davis, 2005–2006

Old Dominion University

- Governor's Technology Scholarship, Full Tuition, \$16k, 2000–2004.

PROPOSALS UNDER REVIEW

REJECTED PROPOSALS

None at present

National Science Foundation

- Collaborative Research: Dissemination of the LibreTexts Libraries through Expansion and Training in Digital Interfaces to Enhance Science Education across the Nation, CO-PI, 2018-2022, \$3M.
- Collaborative Research: SI2-SSI: Infrastructure for Cross-Disciplinary Scientific Computation Through Optimized Symbolic Code Generation with SymPy, CO-PI, 2017-2019, \$3M.

JOURNAL PUBLICATIONS

- [1] Xiaodong Qian, Jason K. Moore, and Deb Niemeier. “Predicting Bicycle Pavement Ride Quality: A Sensor-Based Statistical Model”. In: *Journal of Infrastructure Systems* (2019). Under review.
- [2] Bryn Cloud et al. “Adaptive Smartphone-Based Sensor Fusion for Estimating Competitive Rowing Kinematic Metrics”. en. In: *PLOS ONE* 14.12 (Dec. 2019), e0225690. ISSN: 1932-6203. DOI: [10.1371/journal.pone.0225690](https://doi.org/10.1371/journal.pone.0225690).
- [3] Jason K. Moore and Mont Hubbard. “Skijumpdesign: A Ski Jump Design Tool for Specified Equivalent Fall Height”. In: *The Journal of Open Source Software* 3.28 (Aug. 2018), p. 818. DOI: [10.21105/joss.00818](https://doi.org/10.21105/joss.00818).
- [4] Jason K. Moore and Antonie van den Bogert. “Opty: Software for Trajectory Optimization and Parameter Identification Using Direct Collocation”. In: *Journal of Open Source Software* 3.21 (Jan. 2018), p. 300. DOI: [10.21105/joss.00300](https://doi.org/10.21105/joss.00300).
- [5] Aaron Meurer et al. “SymPy: Symbolic Computing in Python”. In: *PeerJ Computer Science* 3.e103 (Jan. 2017). ISSN: 2376-5992. DOI: [10.7717/peerj-cs.103](https://doi.org/10.7717/peerj-cs.103).
- [6] Jason K. Moore, Sandra K. Hnat, and Antonie J. van den Bogert. “An Elaborate Data Set on Human Gait and the Effect of Mechanical Perturbations”. In: *PeerJ* 3.e918 (Apr. 2015). ISSN: 2167-8359. DOI: [10.7717/peerj.918](https://doi.org/10.7717/peerj.918).
- [7] Chris Dembia, Jason K. Moore, and Mont Hubbard. “An Object Oriented Implementation of the Yeadon Human Inertia Model”. In: *F1000Research* 3.233 (Apr. 2015). DOI: [10.12688/f1000research.5292.2](https://doi.org/10.12688/f1000research.5292.2).
- [8] A. L. Schwab et al. “Rider Control Identification in Bicycling Using Lateral Force Perturbation Tests”. In: *Proceedings of the Institution of Mechanical Engineers, Part K: Journal of Multi-body Dynamics* 227.4 (Aug. 2013). 2013 SAGE Best Paper Award, pp. 390–406. ISSN: 1464-4193, 2041-3068. DOI: [10.1177/1464419313492317](https://doi.org/10.1177/1464419313492317).
- [9] Ronald Hess, Jason K. Moore, and Mont Hubbard. “Modeling the Manually Controlled Bicycle”. In: *IEEE Transactions on Systems, Man, and Cybernetics - Part A: Systems and Humans* 42.3 (Feb. 2012), pp. 545–557. ISSN: 1083-4427, 1558-2426. DOI: [10.1109/TSMCA.2011.2164244](https://doi.org/10.1109/TSMCA.2011.2164244).
- [10] Jason K. Moore et al. “Rider Motion Identification during Normal Bicycling by Means of Principal Component Analysis”. en. In: *Multibody System Dynamics* 25.2 (Feb. 2011), pp. 225–244. ISSN: 1384-5640, 1573-272X. DOI: [10.1007/s11044-010-9225-8](https://doi.org/10.1007/s11044-010-9225-8).

BOOKS & THESES

- [1] Lorena A. Barba et al. *Teaching and Learning with Jupyter*. <https://jupyter4edu.github.io/jupyter-edu-book/>. Nov. 2018.
- [2] Jason K. Moore and Kenneth Lyons. *Resonance: Learning Mechanical Vibration Engineering Through Computation*. <https://moorepants.github.io/resonance/>. Dec. 2017.
- [3] Jason K. Moore. "Human Control of a Bicycle". <http://moorepants.github.io/dissertation>. Doctor of Philosophy. Davis, CA: University of California, Aug. 2012.

CONFERENCE PAPERS

- [1] Jason K Moore and Mont Hubbard. "Expanded Optimization for Discovering Optimal Lateral Handling Bicycles". en. In: *Bicycle and Motorcycle Dynamics 2019: Symposium for Dynamics and Control of Single Track Vehicles*. Padua, Italy: Figshare, 2019, p. 12. DOI: [10.6084/m9.figshare.9942938.v1](https://doi.org/10.6084/m9.figshare.9942938.v1).
- [2] Trevor Z. Metz and Jason K. Moore. "Design of an Electric Bicycle Speed Controller". In: *Bicycle and Motorcycle Dynamics 2019: Symposium on the Dynamics and Control of Single Track Vehicles*. Padua, Italy: Figshare, 2019. DOI: [10.6084/m9.figshare.9937091.v1](https://doi.org/10.6084/m9.figshare.9937091.v1).
- [3] Roy Gilboa et al. "Practical Realization of a Theoretical Optimal-Handling Bicycle". en. In: *Bicycle and Motorcycle Dynamics: Symposium on Dynamics and Control of Single Track Vehicles*. 2019, p. 11. DOI: [10.6084/m9.figshare.9883328.v1](https://doi.org/10.6084/m9.figshare.9883328.v1).
- [4] Jason K. Moore, Mont Hubbard, and Ronald A. Hess. "Optimal Bicycle Design to Maximize Handling and Safety". In: *Proceedings of the 6th Annual International Cycling Safety Conference*. Davis, CA, USA, Sept. 2017. DOI: [10.6084/m9.figshare.5405242.v1](https://doi.org/10.6084/m9.figshare.5405242.v1).
- [5] Scott W. Kresie et al. "Experimental Validation of Bicycle Handling Prediction". In: *Proceedings of the 6th Annual International Cycling Safety Conference*. Davis, CA, USA, Sept. 2017. DOI: [10.6084/m9.figshare.5405233.v1](https://doi.org/10.6084/m9.figshare.5405233.v1).
- [6] Jason Moore, Mont Hubbard, and Ronald A. Hess. "An Optimal Handling Bicycle". In: *Proceedings of the 2016 Bicycle and Motorcycle Dynamics Conference*. Figshare, Sept. 2016. DOI: [10.6084/m9.figshare.3806310.v1](https://doi.org/10.6084/m9.figshare.3806310.v1).
- [7] Jason K. Moore and Mont Hubbard. "Methods for Elimination of Crosstalk and Inertial Effects in Bicycle and Motorcycle Steer Torque Estimation". In: *Proceedings of Bicycle and Motorcycle Dynamics: Symposium on the Dynamics and Control of Single Track Vehicles*. Narashino, Chiba, Japan, Nov. 2013.
- [8] Jason K. Moore and Mont Hubbard. "Identification of Open Loop Dynamics of a Manually Controlled Bicycle-Rider System". In: *Proceedings of Bicycle and Motorcycle Dynamics: Symposium on the Dynamics and Control of Single Track Vehicles*. Narashino, Chiba, Japan, Nov. 2013.
- [9] Ronald A. Hess and Jason K. Moore. "Estimating Parameters of the Structural Pilot Model Using Simulation Tracking Data". In: *AIAA Guidance, Navigation, and Control Conference*. Aug. 2013.
- [10] Gilbert Gede et al. "Constrained Multibody Dynamics With Python: From Symbolic Equation Generation to Publication". In: *Volume 7B: 9th International Conference on Multibody Systems, Nonlinear Dynamics, and Control*. DETC2013-13470. Portland, Oregon, USA, Aug. 2013. ISBN: 978-0-7918-5597-3. DOI: [10.1115/DETC2013-13470](https://doi.org/10.1115/DETC2013-13470).

- [11] Arend Schwab, Peter de Lange, and Jason K. Moore. "Rider Optimal Control Identification in Bicycling". In: *Proceedings of the 5th Annual Dynamic Systems and Control Conference and 11th Annual Motion and Vibration Conference*. <http://bicycle.tudelft.nl/schwab/Publications/schwab2012riderB.pdf>. Fort Lauderdale, Florida, USA: ASME, Oct. 2012.
- [12] A. L. Schwab et al. "Rider Control Identification in Bicycling, Parameter Estimation of a Linear Model Using Lateral Force Perturbation Tests". In: *Proceedings of the IMSD2012 - The 2nd Joint International Conference on Multibody System Dynamics*. Stuttgart, Germany., May 2012.
- [13] Jason K. Moore et al. "An Accurate Method of Measuring and Comparing a Bicycle's Physical Parameters". In: *Proceedings of Bicycle and Motorcycle Dynamics: Symposium on the Dynamics and Control of Single Track Vehicles*. Delft, Netherlands, Oct. 2010.
- [14] Dale L. Peterson et al. "Low-Power, Modular, Wireless Dynamic Measurement of Bicycle Motion". In: *Procedia Engineering*. Vol. 2. The Engineering of Sport 8 - Engineering Emotion. July 2010, pp. 2949–2954. DOI: [10.1016/j.proeng.2010.04.093](https://doi.org/10.1016/j.proeng.2010.04.093).
- [15] Jason K. Moore et al. "Statistics of Bicycle Rider Motion". In: *The Engineering of Sport 8 - Engineering Emotion*. Vol. 2. The Engineering of Sport 8 - Engineering Emotion. July 2010, pp. 2937–2942. DOI: [10.1016/j.proeng.2010.04.091](https://doi.org/10.1016/j.proeng.2010.04.091).
- [16] Jason K. Moore et al. "A Method for Estimating Physical Properties of a Combined Bicycle and Rider". In: *Proceedings of the ASME 2009 International Design Engineering Technical Conferences & Computers and Information in Engineering Conference, IDETC/CIE 2009*. San Diego, CA, USA: ASME, Aug. 2009. DOI: [10.1115/DETC2009-86947](https://doi.org/10.1115/DETC2009-86947).
- [17] J. D. G. Kooijman, A. L. Schwab, and Jason K. Moore. "Some Observations on Human Control of a Bicycle". In: *Proceedings of the ASME 2009 International Design and Engineering Technical Conferences & Computers and Information in Engineering Conference*. ASME, Aug. 2009. DOI: [10.1115/DETC2009-86959](https://doi.org/10.1115/DETC2009-86959).
- [18] J. K. Moore, J. D. G. Kooijman, and A. L. Schwab. "Rider Motion Identification during Normal Bicycling by Means of Principal Component Analysis". In: *Proceedings of Multibody Dynamics 2009, ECCOMAS Thematic Conference*. Ed. by K. Arczewski, J. Frączek, and M. Wojtyra. Warsaw, Poland, June 2009.
- [19] Jason Moore and Mont Hubbard. "Parametric Study of Bicycle Stability". In: *The Engineering of Sport 7*. Ed. by Margaret Estivalet and Pierre Brisson. Vol. 2. Springer, 2008. DOI: [10.1007/978-2-287-99056-4_39](https://doi.org/10.1007/978-2-287-99056-4_39).

PREPRINTS

- [1] Bryn Cloud et al. "Adaptive Smartphone-Based Sensor Fusion for Estimating Competitive Rowing Kinematic Metrics". In: (Dec. 2018). Preprint, Version 1. DOI: [10.31224/osf.io/nykuh](https://doi.org/10.31224/osf.io/nykuh).
- [2] Jason K Moore, Sandra K. Hnat, and Antonie J. van den Bogert. "An Elaborate Data Set on Human Gait and the Effect of Mechanical Perturbations". In: *PeerJ PrePrints* 3.e700v4 (Apr. 2015). Preprint. ISSN: 2167-9843. DOI: [10.7287/peerj.preprints.700v2](https://doi.org/10.7287/peerj.preprints.700v2).
- [3] Jason K. Moore and Mont Hubbard. "Kinetic and Kinematic Measurements from an Instrumented Bicycle during Different Maneuvers on and off the Treadmill". <https://github.com/moorepants/bicycle-data-paper>. Aug. 2014.

CONFERENCE
ABSTRACTS

- [4] Jason K. Moore and Antonie J. van den Bogert. "Perturbed Standing Controller Parameter Identification: A Comparison of Methods". <https://github.com/csu-hmc/inverted-pendulum-sys-id-paper>. Aug. 2014.
- [5] Jason K. Moore and Antonie J. van den Bogert. "Direct Identification of Human Gait Control". <https://github.com/csu-hmc/gait-control-direct-id-paper>. Aug. 2013.

- [1] Petros Abraha, Jason K. Moore, and Shigemichi Ohshima. "Design Without Borders: Influence of Cultural Exchange on Machine Design and Engineering Careers". In: *ASEE Pacific Southwest 2020*. Under review. Davis, CA, USA, 2020.
- [2] Xiaodong Qian, Wei Ma, and Jason K. Moore. "Analysis of Adoption of Intelligent Transportation Technologies to Improve Cyclist Safety". In: *8th Annual International Cycling Safety Conference*. Abstract, Retracted. Brisbane, Australia, Nov. 2019.
- [3] Bryn Cloud et al. "Accessible, Open-Source Computational Analysis and Design of Terrain Park Ski Jumps". In: *23rd International Congress on Snow Sports Trauma and Safety*. Abstract. Squaw Valley, California, USA, Apr. 2019.
- [4] Jason K. Moore, Mont Hubbard, and Ronald A. Hess. "Expanded Optimization for Discovering Optimal Lateral Handling Bicycles". en. In: *Bicycle and Motorcycle Dynamics 2019*. Abstract. 2019, p. 2.
- [5] Trevor Metz and Jason K. Moore. "Design of an Electric Bicycle Speed Controller". en. In: *Bicycle and Motorcycle Dynamics 2019*. Abstract. Padova, Italy, 2019, p. 2.
- [6] Roy Gilboa et al. "Practical Realization of a Theoretical Optimal-Handling Bicycle". en. In: *Bicycle and Motorcycle Dynamics 2019*. Abstract. 2019, p. 2.
- [7] Bryn Cloud et al. "Adaptive Smartphone-Based Sensor Fusion for Estimating Competitive Rowing Kinematic Metrics". In: *XXVII Congress of the International Society of Biomechanics & 43rd Annual Meeting of the American Society of Biomechanics*. Abstract, Retracted. Calgary, Canada, 2019.
- [8] Jason K. Moore and Antonie J. van den Bogert. "Quiet Standing Control Parameter Identification with Direct Collocation". In: *XV International Symposium on Computer Simulation in Biomechanics*. <https://github.com/csu-hmc/ISBTGCS2015>. Edinburgh, UK, July 2015.
- [9] Jason K. Moore, Sandra K. Hnat, and Antonie J. van den Bogert. "Identification of Human Control during Perturbed Walking". In: *Dynamic Walking*. <https://github.com/moorepants/DW2014>. Zurich, Switzerland, June 2014.
- [10] Jason K. Moore, Sandra K. Hnat, and Antonie J. van den Bogert. "Identification of Human Control during Perturbed Walking". In: *Midwest American Society of Biomechanics Regional Meeting*. <https://github.com/moorepants/MASB2014>. Akron, Ohio, USA, Mar. 2014.
- [11] Mont Hubbard et al. "Human Control of Bicycle Dynamics with Experimental Validation and Implications for Bike Handling and Design". In: *Proceedings of 2011 NSF Engineering Research and Innovation Conference*. Jan. 2011.
- [12] Jason K. Moore, Dale L. Peterson, and Mont Hubbard. "Influence of Rider Dynamics on the Whipple Bicycle Model". In: *Proceedings of the 11th International Symposium on Computer Simulation in Biomechanics*. https://www.researchgate.net/publication/216750976_Influence_of_rider_dynamics_on_the_Whipple_bicycle_model. Tainan, Taiwan, June 2007.

BLOG POSTS

- [1] Jason K. Moore and Kenneth Lyons. *Using Computational Thinking to Teach Mechanical Vibrations*. <http://engineering.ucdavis.edu/eelc/using-computational-thinking-to-teach-mechanical-vibrations/>. Apr. 2018.
- [2] Jason K. Moore. *Learning Mechanical Design Through Lightweight Prototyping*. <http://engineering.ucdavis.edu/eelc/learning-mechanical-design-through-lightweight-prototyping/>. Feb. 2017.

SOFTWARE

- [1] Jason K. Moore, Mont Hubbard, and Bryn Cloud. *SkiJumpDesign: A Ski Jump Design Tool for Equivalent Fall Height*. <https://gitlab.com/moorepants/skijumpdesign>. Dec. 2017.
- [2] Jason K. Moore and Kenneth Lyons. *Resonance: A Python Package for Mechanical Vibration Analysis*. University of California, Davis. <https://github.com/moorepants/resonance/>. July 2017.
- [3] Ian Kyle, Jason K. Moore, and Maegen Simmonds. *Agricultural Field Statistics Package*. <https://github.com/ucd-ipd/agroft>. 2016.
- [4] Jason K. Moore and Antonie J. van den Bogert. *Opty: A Library for Using Direct Collocation in the Optimization and Identification of Dynamic Systems*. Cleveland State University. <https://github.com/csu-hmc/opty>. May 2014.
- [5] Jason K. Moore et al. *GaitAnalysisToolKit: A Python Library for Gait Analysis*. <https://github.com/csu-hmc/GaitAnalysisToolKit>. Cleveland State University, Dec. 2013.
- [6] Jason K. Moore et al. *PyDy: A Multi-Body Dynamics Analysis Package Written in Python*. PyDy. <http://pydy.org>. Oct. 2011.
- [7] Jason K. Moore, Chris Dembia, and Oliver Lee. *DynamicistToolKit: A Python Library for Dynamics and Controls*. <https://github.com/moorepants/DynamicistToolKit>. June 2011.
- [8] Christopher Dembia et al. *Yeadon: A Python Library For Human Inertia Estimation*. <https://github.com/chrisdembia/yeadon>. June 2011.
- [9] Jason K. Moore. *HumanControl: Human Control of a Bicycle*. University of California, Davis. <https://github.com/moorepants/HumanControl>. May 2011.
- [10] Jason K. Moore, Chris Dembia, and Oliver Lee. *BicycleParameters: A Python Library for Bicycle Parameter Estimation and Analysis*. <https://github.com/moorepants/BicycleParameters>. Apr. 2011.
- [11] Jason K. Moore, P. D. L. de Lange, and Stefen Yin. *BicycleDataProcessor: Data Storage and Processing Library for an Instrumented Bicycle*. University of California, Davis. <https://github.com/moorepants/BicycleDataProcessor>. Feb. 2011.
- [12] Jason K. Moore, P. D. L. de Lange, and Yumiko Henneberry. *BicycleDAQ: Data Acquisition Application for an Instrumented Bicycle*. University of California, Davis. <http://github.com/moorepants/BicycleDAQ>. Oct. 2010.
- [13] SymPy Development Team. *SymPy: Python Library for Symbolic Mathematics*. <http://www.sympy.org>. 2006.

ACADEMIC
SERVICE

- Board Member of the Engrxiv: Preprint Server (April 2019-present)
- Co-Editor of the Journal of Open Source Education
- Co-Editor of the Journal of Open Engineering
- UCD MAE Undergraduate Committee (January 2017-Present)
- UCD MAE Website Committee (2017-2019)
- Lead organizer of the 6th Annual International Cycling Safety Conference in Davis, CA, USA, September 20-23, 2017. (January 2016-September 2017)
- Served on the organizing committees, publishing chair, for the 2016 Bicycle and Motorcycle Dynamics Conference in Milwaukee, Wisconsin.
- Served on the scientific committee for the 2013, 2016, and 2019 Bicycle and Motorcycle Dynamics Conferences.
- Volunteer instructor for Software Carpentry.
- Co-organizer of Cleveland's "North Coast Biomechanics and Brew" group (2014).
- Organized and mentored for Google Summer of Code under the Python Software Foundation, SymPy, and PyDy (2009-2018)
- Organized and co-chaired both an invited and special session on single track vehicle dynamics at the 2012 ASME DSCC conference.

ARTICLE AND
ABSTRACT
REVIEWS

- Reviewed 54 abstracts for the 2019 Bicycle and Motorcycle Dynamics Conference.
- Reviewed SciPy 2018 tutorial proposals.
- Reviewed 10 SciPy 2017 tutorial proposals.
- Reviewed "A data set with kinematic and ground reaction forces of human balance" for PeerJ, 2017.
- Reviewed "Motion analysis of a device including a disk and two slender bars with a design change for full disk revolution" for The Journal of Open Engineering, 2017.
- Reviewed "The effect of tyre and rider properties on the stability of a bicycle" by Bulsink, Vera, et. al, for Advances in Mechanical Engineering, 2015.
- Reviewed "Changing the bicycle seat height: Effects on rider control." for the European Journal of Sports Sciences, 2015.
- Reviewed "Gyro device for bicycle handling assessment: A reliability study" by Fonda, Borut, et. al for the Journal of Applied Biomechanics, 2015.
- Reviewed "Self-driving Lego Mindstorms Robot" for SciPy 2014 Proceedings, 2014.
- Reviewed "On the influence of tyre and rider properties on the stability of a bicycle." by Vera Bulsink, et. al, for Vehicle System Dynamics, 2014.
- Reviewed "Are subject-specific musculoskeletal models robust to the uncertainties in parameter identification?" by Giordano Valente, et. al for PLoS One, 2014.
- Reviewed four papers for the Bicycle and Motorcycle Dynamics Conference 2013 proceedings, July 2013.
- Reviewed "Experimental and Numerical Analysis of Rider Motion in Weave Conditions" Doria, Alberto, et. al for Vehicle System Dynamics, 2011.

INVITED TALKS

University of Wisconsin-Stout, Menomonie, WI, USA

Estimating Rowing Kinematic Metrics: An Undergraduate Sports Biomechanics Research Project April
12, 2019

JupyterCon, New York, NY

The Future of Jupyter in Education Panel

August 23, 2018

Meijo University, Nagoya, Japan

The Trail Towards An Optimally Handling Bicycle

June 21, 2018

UC Davis Education Graduate Group, Davis, CA

Computational Thinking in the Engineering Curriculum: A Case Study in Mechanical Vibrations

March 11, 2018

TU Delft, Delft, Netherlands

Identification of human control during walking

June 6, 2014

U.S. Bicycling Hall of Fame, Davis, CA

How We Ride Bikes with Luke Peterson, Mont Hubbard, and Ron Hess

October 19, 2011

UCD Tahoe Environmental Research Center, Lake Tahoe, NV

How We Ride Bikes with Luke Peterson and Mont Hubbard

May 12, 2011

Fulbright FAST Conference, San Francisco, CA

Bicycling in the Netherlands and Europe, policies and practices: What can America learn from them.

March 12, 2010

UC Davis D-Lab, Davis, CA

Use of Human Power in the Developing World

January 31, 2013

January 31, 2012, January 25, 2011, January 26, 2010

TU Delft Mechanics Colloquium, Delft, Netherlands

A First Look at Rider Biomechanics while Controlling a Bicycle

June 4, 2009

TUTORIALS AND
WORKSHOPS

KEEN National Conference 2019, Dallas, TX, USA

Eight Ways to Use Computation to Teach Everything Else (with Allen Downey)

January 5, 2019

COSMOS 2018, Davis, CA, USA

Squiggly Bicycle Routes: Physics Based Design Evaluation

July 10, 2017

UCD CEE and DSI, Davis, CA, USA

Computational Thinking in the Engineering Curriculum (123 views)

January 10, 2017

SCIPY 2017, Austin, Texas, USA

Automatic Code Generation With SymPy (7,500 views)

July 10, 2017

Delta Stewardship Council Sacramento, California, USA

Software Carpentry Workshop

May 18–19, 2017

UCD Center for Education Excellence Davis, California, USA

Software Carpentry Workshop

August 25, 2016

iHub Nairobi, Kenya

Software Carpentry Workshop

June 17–18, 2016

UCI Data Science Initiative Irvine, California, USA

Software Carpentry Workshop

February 21–22, 2015

SCIPY 2016, Austin, Texas, USA

Simulating Robot, Vehicle, Spacecraft, and Animal Motion (9,051 views) **July 14, 2016**

SCIPY 2015, Austin, Texas, USA

Multibody Dynamics and Control with Python (6,902 views)

July 18, 2015

SCIPY 2014, Austin, Texas, USA

Multibody Dynamics and Control with Python (4,809 views)

July 6, 2014

PYCON 2014, Montreal, Quebec, Canada

Dynamics and Control with Python (2,918 views)

April 9, 2014

MASB 2014, Akron, Ohio, USA

Simulation and Control of Biomechanical Systems with Python

March 9, 2014

TALKS

SacPy, Sacramento, California, USA

What to do when chicks go bad in your flock: JupyterHub on Bare Metal with Kubernetes **November 14, 2019**

First Year Bicycle Engineering Seminar Guest Lecture, Davis, California, USA

What the Bicycle Can Tell Us About Human Control

2018

UCD CoE Decision Day, Davis, California, USA

Introduction to UCD Mechanical and Aerospace Engineering

2018,2019

SCIPY 2018, Austin, Texas, USA

Resonance: Learning Mechanical Vibrations Through Computational Thinking Prepared by me, presented by Kenneth Lyons (414 views) **July 10, 2017**

EME 1 Guest Lecture, Davis, California, USA

What the Bicycle Can Tell Us About Human Control

2018

SacPy, Sacramento, California, USA

Resonance: An Interactive Textbook and Software Library for Learning About Mechanical Vibrations **November 9, 2017**

EME 1 Guest Lecture, Davis, California, USA

What the Bicycle Can Tell Us About Human Control

November 28, 2016

BMD 2016, Milwaukee, Wisconsin, USA

An Optimal Handling Bicycle

September 21, 2016

SciPy 2015, Austin, Texas, USA

Optimal Control and Parameter Identification of Dynamical Systems with Direct Collocation using SymPy (1,279 views)

July 8, 2015

Cleveland State University Human Motion and Control Seminar, Cleveland, Ohio, USA

Reproducible Scientific Computing with Open Software and Open Data **September 17, 2014**

2014 NCSSR Visiting Scholar Kickoff, Stanford, California, USA

Indirect identification of human control during walking

July 15, 2014

Dynamic Walking 2014, Zurich, Switzerland

Identification of human control during walking

June 10, 2014

MASB 2014, Akron, Ohio, USA

Identification of human control during walking

November 13, 2013

BMD 2013, Narashino, Chiba, Japan

Methods for Elimination of Crosstalk and Inertial Effects in Bicycle and Motorcycle Steer Torque Estimation

November 13, 2013

BMD 2013, Narashino, Chiba, Japan

Identification of Open Loop Dynamics of a Manually Controlled Bicycle-Rider System

November 11, 2013

SciPy 2013, Austin, Texas, USA

Estimating and Visualizing the Inertia of the Human Body with Python (2,438 views)

June 27, 2013

SciPy 2013, Austin, Texas, USA

Dynamics with SymPy Mechanics

June 27, 2013

ASME DSCC 2012, Fort Lauderdale, Florida, USA

The Future of Bicycle and Motorcycle Dynamics

October 18, 2012

Velo-city Global 2012, Vancouver, British Columbia, Canada

Time and Energy Penalties of Squiggly Bike Routes with Ted Buehler **June 28, 2012**

MAE Exit Seminar, Davis, CA, USA

Human Control of a Bicycle

May 15, 2012

UCD ITS Seminar, Davis, CA

Bicycling in the Netherlands and Europe, policies and practices: What can America learn from them. with Eva Heinen

October 23, 2009

UCD MAE Seminar, Davis, CA

A First Look at Rider Biomechanics while Controlling a Bicycle **October 29, 2009**

UCD MAE Qualifying Exam, Davis, CA

Human Control of a Bicycle

October 9, 2009

ASME IDETC/CIE 2009, San Diego, CA

A Method for Estimating the Physical Properties of a Combined Bicycle and Rider
August 31, 2009

Mulitbody Dynamics 2009, Warsaw, Poland

Rider Motion Identification During Normal Bicycling By Means of Principal Component Analysis
July 1, 2009

Fulbright Mid Year Presentation, Amsterdam, Netherlands

Jason Moore, In The Netherlands...

February 5, 2009

ISEA 2008, Biarritz, France

Parametric Study of Bicycle Stability

June 6, 2008

PROFESSIONAL
EXPERIENCE

UC Davis, Davis, CA, USA USA

Consultant

June-August 2015

- Co-developed a R Shiny web application for Agricultural Field Trial Statistics (Agroft). github.com/ucd-ipb/agroft

Plotly, Montreal, Quebec, Canada USA

Consultant

July 2015

- Developed a Jupyter notebook demonstrating the use of Plotly tools in control engineering.

Old Dominion University, Norfolk, Virginia USA

Langley Full Scale Tunnel Design Engineer

June 2004 to August 2005

- Extensive design, modeling and drafting with Autodesk Inventor.
- Designed a portable floor system for a car balance.
- Designed a six degree of freedom full scale car balance.
- Wrote stress analysis reports for NASA specifications.
- Test-model design, fabrication and repair.
- Support in daily activities (test preparation, taking data, etc.).

Maglev Tram Design Engineer **May 2004 to January 2005**

- Created a reference CAD model of a full-scale magnetic levitation train car using AutoCAD Mechanical Desktop.

ODU HPV Team Project Lead **September 2003 to January 2005**

- Lead and managed a mechanical engineering senior design project.
- Designed and constructed a human powered land vehicle.
- Focused on bicycle frame, controls, stability, and drive train design
- Received 6th place out of 20 as a rookie team at the ASME Human Powered Vehicle Challenge.
- Website designer and maintainer.

ODU SAE Formula Team Design Engineer **2001 to 2002**

- Helped design and fabricate a scaled formula race car.
- Extensive design, modeling and drafting with AutoCAD Mechanical Desktop.
- Designed and fabricated the drive train and composite body.
- Website designer.

Bauer Compressors, Norfolk, Virginia USA

Mechanical Design Engineer Intern **June 2003 to December 2003**

- Extensive 3D modeling with Autodesk Inventor: modeled complex air compressor systems.
- Sheet metal design and fabrication.
- V-belt drive designs.
- Oil filtration system design.
- Designed parts and prepared drawings for fabrication.

Area Access, Norfolk, Virginia USA

Elevator Mechanic Assistant **May 2002 to August 2002**

- Installed and repaired elevators and various accessibility machines.
- Exposed to various electrical and mechanical systems.
- Forced to listen to Rush Limbaugh every morning during the truck ride.

Danville Community College, Danville, Virginia USA

CNC Mill Operator **June 2001 to August 2001**

- Learned G-code/Manual Programming.
- Learned FeatureCam 3D CAD/CAM software.
- Programmed and operated a HAAS 3-axis mill.

Mark D. Moore Construction Company, Danville, Virginia USA

Carpenter **1995 to 2001**

- Residential house construction and remodeling
- Framing, finishing, painting, drywall, hardwood floors, masonry

VOLUNTEER
SERVICE

Across the Causeway Transit Collective, Davis & Sacramento, CA, USA

Member, Organizer, and Facilitator **July 2019 to June 2020**

- Transit advocacy for a better city-to-city commuter route.

Davis Bike Collective, Davis, CA USA

Bicycle Mechanic, Teacher and Organizer **September 2005 to June 2013**

- Volunteered bi-weekly as a teaching mechanic.
- Co-founded a consensus based non-profit.
- Co-wrote bylaws and setup the legal non-profit.
- Raised thousands of dollars in donations and grants.
- Organized conferences, parties, fundraisers, bike rides, work parties, outreach events.
- Organized two 1500+ attendee beer tasting and movie events with New Belgium Brewery.
- Web site maintenance, shift scheduling, handled distributor orders, managed email listservs.
- Lead the workshop series “Open Bike Night” for one year.

Davis Bicycles!, Davis, CA USA

Volunteer **September 2009 to June 2013**

- Administer the organization’s websites [1] and [2].
- Lobby city council for bicycle amenities.
- Worked directly with city staff on various projects.

Maya Pedal, San Andres Itzapa, Guatemala

Volunteer Engineer **Summer 2007**

- Constructed pedal powered machines (i.e. blender, corn dekerneler/grinder, etc).
- Design work on a macadamia nut sheller.
- Repaired bicycles.
- Shop organization: tool boards, bike graveyard.

Whirlwind Wheelchair International, Lusaka, Zambia

Volunteer Engineer **Summer 2006**

- Worked at the Disacare Wheelchair Center.
- Worked on the design and fabrication team for a bicycle ambulance trailer.
- Fixture design and training.

Virginia Beach Public Schools, Virginia Beach, VA

Volunteer Mentor **2004**

- Assisted high schools students with an engineering design competition.

UC Davis Institute for Transportation Engineers, Davis, CA

Tour Leader **December 2006**

- Organized a group bicycle ride and museum tour.

ODU College of Engineering, Norfolk, VA

Tour Guide **February 2004**

- Led open house tours for middle school children.

Davis Bicycle Commission, Davis, CA

Bicycle Counter

- Participated in bicycle usage data collection.

FABRICATION SKILLS

Extensive machining and fabrication experience: milling, turning, welding (MIG, TIG, ARC, Torch, Brazing), wood working, sheet metal work

SOFTWARE PROFICIENCIES

Extensive drafting, solid modeling, CAD, CAM, and FEA experience. Proficient in: CADKEY, AutoCAD, AutoCAD Mechanical Desktop, Autodesk Inventor, FeatureCAM 3D, IntelliCAD, PATRAN/NASTRAN, PRO-Engineer/PRO-Mechanica, GMAX, CNC/G-code, OnShape

Programming Languages (in approximate order of proficiency): Python, MATLAB, R, BASH, C, Javascript, C++, Lua

Web development: HTML, CSS, Javascript, Pelican, Hyde, Sphinx, Flask, Amazon Web Services, Ubuntu Server, Apache, NGinx, Plone, Wordpress, Joomla, Homesite, Microsoft Front Page, Macromedia Dreamweaver

Websites that I currently administer: moorepants.info [Hyde], Sports Biomechanics Lab [Plone 3], moorepants [HTML]. 2017 ICSC [Wordpress], PyDy [Sphinx]

Websites that I developed but no longer administer: hmc.csuohio.edu [Plone 4], N Street Cohousing [Plone 4], Davis Bike Collective [Joomla & Wordpress], BikeDavis.info [Wordpress], smartdrive.ucdavis.edu, drive5.us [Flask], clevelandwiki.org [Django], ODU HPV [HTML],

Dynamics and Simulation: SymPy Mechanics, SciPy, MATLAB/Simulink, Working Model, Autolev, Axl/CampG, Opensim, Simbody

Computational: SciPy, NumPy, Uncertainties, Pandas, Cython, IPOPT, CMA-ES, SymPy, MATLAB, MathCAD

Instrumentation: National Instruments products including LabVIEW, MatLab DAQ Toolbox, Serial Protocols

Data: HDF5, PyTables, MySQL, MariaDB, SQLite, MongoDB

Graphics: Matplotlib, R, MATLAB, GIMP, Inkscape, Paint Shop Pro, Macromedia Fireworks, Blender, GMAX

Operating Systems: Linux (Ubuntu 8.04-17.10 and other distros), Microsoft Windows (3.1-7), DOS

Utilities: FTP, Version Control (Git/Mercurial/Subversion), SSH, BASH

Reference management: BIBTeX, JabRef, Zotero, Mendeley, Endnote

Word processing: Vim, L^AT_EX, Google Docs, LibreOffice Writer, TeXnic Center, Microsoft Word

REFERENCES

Academic Research

- Dr. Mont Hubbard, *MSc and PhD advisor*, Professor, University of California, Davis, Mechanical and Aerospace Engineering Department, One Shields Avenue, Davis, CA 95616, +01-530-752-6450, mhubbard@ucdavis.edu
- Dr. Arend Schwab, *Fulbright and PhD advisor*, Professor, Delft University of Technology, Mekelweg 2, NL 2628 CD Delft, The Netherlands, +31 15 27 82701, a.l.schwab@tudelft.nl
- Dr. Antonie J. van den Bogert *Post Doctoral Supervisor* Professor, Cleveland State University, Mechanical Engineering Department, 1960 E. 24th St., SH 232 Cleveland, Ohio 44115, +01-216-687-5329, a.vandenbogert@csuohio.edu
- Dr. Ronald Hess, *PhD advisor*, Professor, University of California, Davis, Mechanical and Aerospace Engineering Department, One Shields Avenue, Davis, CA 95616, +01-530-752-1513, rahess@ucdavis.edu
- Dr. Xinfan Lin, *Research Collaborator*, Assistant Professor, University of California, Davis, Mechanical and Aerospace Engineering Department, One Shields Avenue, Davis, CA 95616, lxflin@ucdavis.edu
- Dr. R. Paul Crawford, *Research Collaborator*, CEO, Hegemony Technologies, Davis, CA, paul.crawford@hegemonytechnologies.com
- Dr. Luke Peterson, *Collaborator at UCD*, dlpeterson@ucdavis.edu
- Dr. Jodi Kooijman, *Collaborator at TU Delft*, jodikooijman@gmail.com

Teaching and Education

- Dr. Petros Abraha *Educational Collaborator*, Professor, Meijo University, Department of Mechanical Engineering, 1-501 Shiogamaguchi Tenpaku-ku Nagoya 468-8502 Japan, petros@meijo-u.ac.jp
- Dr. Allen Downey *Educational Collaborator*, Professor, Olin College, Needham, MA, USA, Allen.Downey@olin.edu
- Dr. Steven Velinsky *Capstone Design Co-Instructor*, Distinguished Professor, University of California, Davis, Mechanical and Aerospace Engineering Department, One Shields Avenue, Davis, CA 95616,
- Dr. Susan Handy, *COSMOS Lead Instructor*, Professor, University of California, Davis, Davis, CA, slhandy@ucdavis.edu
- Dr. Jim Schaaaf, *TA and Lecturer supervisor*, Continuing Lecturer, University of California, Davis, Mechanical and Aerospace Engineering Department, One Shields Avenue, Davis, CA 95616, +01-530-752-5548, jas@ucdavis.edu
- Dr. Rida Farouki, *TA supervisor*, Professor, University of California, Davis, Mechanical and Aerospace Engineering Department, One Shields Avenue, Davis, CA 95616, +01-530-752-1779, farouki@ucdavis.edu

Engineering

- Dr. Tai Stillwater, *SmartDrive and Pedal Desk*, Postdoctoral Researcher, Institute of Transportation Studies, University of California, Davis, 2028 Academic Surge, One Shields Avenue, Davis, CA, 95616, tstillwater@ucdavis.edu
- Matthew Seitzler, P.E. *Colleague*, Professional Engineer, at Davis Energy Group, Davis, CA, matt@sre-engineering.com
- Dr. Drew Landman, *LFST supervisor and undergraduate mentor*, Professor, Old Dominion University, Mechanical and Aerospace Engineering, 1311 Engr and Comp Sci Bldg, Norfolk, VA 23529, +01-757-683-6008, dlandman@odu.edu
- Dr. Anthony Passerini, *Cell shearing project supervisor*, Assistant Professor, University of California, Davis, Biomedical Engineering Department, One Shields Avenue, Davis, CA 95616, +01-530-754-6715, agpasserini@ucdavis.edu
- John Dwyer, *Bauer Compressors supervisor*, Engineer Department Manager, john.dwyer@bauercomp.com

Academic and Community Service

- Dr. Debbie Niemeier, *ICSC 2017 Co-Organizer*, Professor, University of California, Davis, National Academy of Engineering, Davis, CA, dniemeier@ucdavis.edu
- Dr. Robb Davis, *Past Mayor of Davis, CA*, Davis, CA, rdavis@cityofdavis.org
- Dr. Sarah McCullough, *Colleague at the Davis Bike Collective*, UC San Diego, smcc@ucdavis.edu
- Dr. Susan Handy, *ICSC 2017 Co-Organizer*, Professor, University of California, Davis, Davis, CA, slhandy@ucdavis.edu

Sample Papers

Jason K. Moore

I have attached three sample papers that demonstrate my research and writing. The first paper is my highest cited first author journal article that was published in Multibody System Dynamics as a graduate student [3]. The second paper is another first author paper published in PeerJ [2] during my postdoc. And the third paper is a preprint of my lab's most recent work in which I mentored the student authors and was the primary author of the text. It has been accepted for publication in PLOS ONE [1].

References

- [1] Bryn Cloud, Britt Tarien, Ada Liu, Thomas Shedd, Xinfan Lin, Mont Hubbard, R. Paul Crawford, and Jason K. Moore. Adaptive smartphone-based sensor fusion for estimating competitive rowing kinematic metrics. *PLoS ONE*, 2019. Under review.
- [2] Jason K. Moore, Sandra K. Hnat, and Antonie J. van den Bogert. An elaborate data set on human gait and the effect of mechanical perturbations. *PeerJ*, 3(e918), April 2015.
- [3] Jason K. Moore, J. D. G. Kooijman, A. L. Schwab, and Mont Hubbard. Rider motion identification during normal bicycling by means of principal component analysis. *Multibody System Dynamics*, 25(2):225–244, February 2011.

Rider motion identification during normal bicycling by means of principal component analysis

Jason K. Moore · J.D.G. Kooijman · A.L. Schwab ·
Mont Hubbard

Received: 18 December 2009 / Accepted: 9 September 2010 / Published online: 9 October 2010
© The Author(s) 2010. This article is published with open access at Springerlink.com

Abstract Recent observations of a bicyclist riding through town and on a treadmill show that the rider uses the upper body very little when performing normal maneuvers and that the bicyclist may, in fact, primarily use steering input for control. The observations also revealed that other motions such as lateral movement of the knees were used in low speed stabilization. In order to validate the hypothesis that there is little upper body motion during casual cycling, an in-depth motion capture analysis was performed on the bicycle and rider system.

We used motion capture technology to record the motion of three similar young adult male riders riding two different city bicycles on a treadmill. Each rider rode each bicycle while performing stability trials at speeds ranging from 2 km/h to 30 km/h: stabilizing while pedaling normally, stabilizing without pedaling, line tracking while pedaling, and stabilizing with no-hands. These tasks were chosen with the intent of examining differences in the kinematics at various speeds, the effects of pedaling on the system, upper body control motions and the differences in tracking and stabilization.

Principal component analysis was used to transform the data into a manageable set organized by the variance associated with the principal components. In this paper, these principal components were used to characterize various distinct kinematic motions that occur during

J.K. Moore (✉) · M. Hubbard
Mechanical and Aerospace Engineering, University of California, Davis, One Shields Avenue, Davis, CA 95616-5294, USA
e-mail: jkmoor@ucdavis.edu

M. Hubbard
e-mail: mhubbard@ucdavis.edu

J.D.G. Kooijman · A.L. Schwab
Laboratory for Engineering Mechanics, Delft University of Technology, Mekelweg 2, 2628 CD Delft, The Netherlands

J.D.G. Kooijman
e-mail: jodikooijman@gmail.com

A.L. Schwab
e-mail: a.l.schwab@tudelft.nl

stabilization with and without pedaling. These motions were grouped on the basis of correlation and conclusions were drawn about which motions are candidates for stabilization-related control actions.

Keywords Bicycle · Principal component analysis · Motion capture · Human control

1 Introduction

Much progress has been made in understanding the rigid body dynamics of an uncontrolled bicycle [1, 2] and various control schemes have been explored for tracking purposes [3–5], but little is understood about how a bicyclist stabilizes a bicycle during normal riding. A bicycle and rider system is unique among vehicles in that the rider is 80 to 90% of the total mass of the system, the system is laterally unstable, and the rider is flexibly coupled to the bicycle in such a way that many body motions can be used as control inputs. Previous research into realistic bicycle control has focused on both steering and rider lean as control inputs, but there has been no experimental verification of which motions a rider actually uses for control. Recent observations of a bicyclist riding through town and on a treadmill [6] show that the rider moves the upper body very little when performing normal maneuvers and that the bicyclist may, in fact, primarily use steering input for control. This corresponds well with the fact that control by leaning requires high gains compared to the gains required for steering when employing an optimal control strategy on a model [3–5]. The observations also revealed that the rider may use other control inputs such as drastic knee movements at low speeds. These conclusions were drawn by visually reviewing video data, so a more rigorous objective method of characterizing the dominant movements of the bicyclist while stabilizing a bicycle was needed. In order to validate the hypothesis that there is little upper body motion during normal cycling, motion capture techniques were used on the bicycle and rider system with the intent to employ principal component analysis to identify the major motion patterns.

Principal component analysis has successfully been used with data collected from motion capture techniques to identify the dominant modes of motion of a person walking on a treadmill [7] and to characterize different types of walking. We use similar methods for steady, normal bicycle riding on a treadmill. Cyclic motions, such as pedaling, are easily identified and separated from the other less cyclic control actions. Identifying the patterns of movement gives insight into which body movements are primarily used and are candidates for control inputs. This will be valuable for our overall research goals that include the design of a realistic biomechanical-based control system of a bicycle rider, among other things.

2 Experiments

To test our hypotheses, three riders performed a set of stability tasks in a controlled environment while the motion of the bicycle and rider were collected with a motion capture system. The tasks were performed on a 3×5 meter treadmill Fig. 1 capable of belt speeds up to 35 km/h. The treadmill was chosen because the envelope of space was suitable for the motion capture system and it eliminated any disturbances such as wind, rough ground, and obstacles. We chose three male riders of similar age [31, 23, 26 years], build [height (1.76, 1.84, 1.83 m) and mass (72, 74, 72 kg)]. We also used two different Dutch bicycles: a 2008 Batavus Brower with a 3 speed hub and a 2008 Batavus Stratos Deluxe with

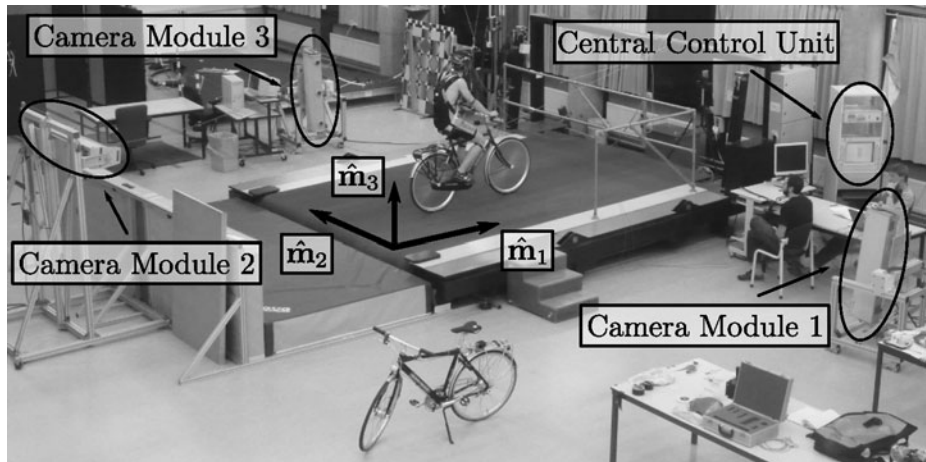


Fig. 1 The 3×5 m treadmill at the Vrije Universiteit Amsterdam

a 7 speed hub. The Browser is described by the manufacturer as “stable” and the Stratos Deluxe as “nervous.”

We made use of the Optotrak Certus Motion Capture System [8] to record the motion of the bicycle and rider during the stability tasks. The system is based on active infrared emitting markers that are placed on the moving bodies and connected to a central control unit. Each marker emits a sequential infrared signal and the infrared pulses are captured by camera modules each containing three cameras. The accuracy of the three dimensional measurements is ± 0.15 mm [8]. The system has no hardware-based noise reduction. Wiring harnesses were built for both the rider and the bicycles to facilitate easy bicycle and rider exchange Fig. 2.

The marker coordinates were measured with respect to an inertial frame, \mathbf{M} , where the plane normal to $\hat{\mathbf{m}}_3$ is coplanar with the treadmill surface and $\hat{\mathbf{m}}_3$ is directed upward. We collected the three dimensional locations of 31 markers, 11 of which were located on the bicycle and 20 mapped the rider Fig. 3.

The markers were placed on the bicycle so that we could easily extract the rigid body motion (i.e., body orientations and locations) of the bicycle frame and fork. Four markers were attached to the fork and seven markers were attached to the rear frame. A marker was attached on the right and left sides of the center of each wheel, the seat stays, the ends of the handlebars, and the head tube. A single marker was also attached to the back of the seat post.

We recorded the locations of 20 points on the rider Fig. 3: left and right sides of the helmet near the temple, back of the helmet, shoulders (greater tuberosity of the humerus), elbows (lateral epicondyle of the humerus), wrists (pisiform of the carpus), between the shoulder blades on the spine (T6 of the thoracic vertebrae), the tail bone (coccyx), midpoint on the spine between the coccyx and shoulder blades (L1 on the lumbar vertebrae), hips (greater trochanter of the femur), knees (lateral epicondyle of the femur), ankles (lateral malleolus of the fibula) and feet (proximal metatarsal joint). The body markers were not necessarily placed such that a complete rigid body model could easily be fit to the data. This was done to save setup and processing time because we only wanted a stick figure representation of the rider that allowed us to visually observe the dominant motions of the rider.

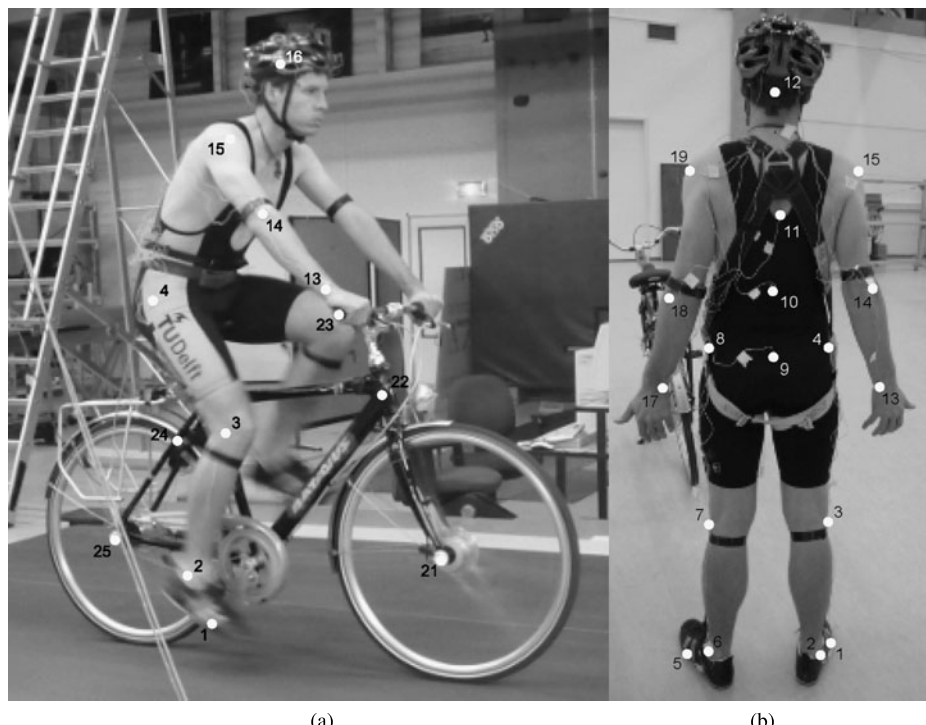


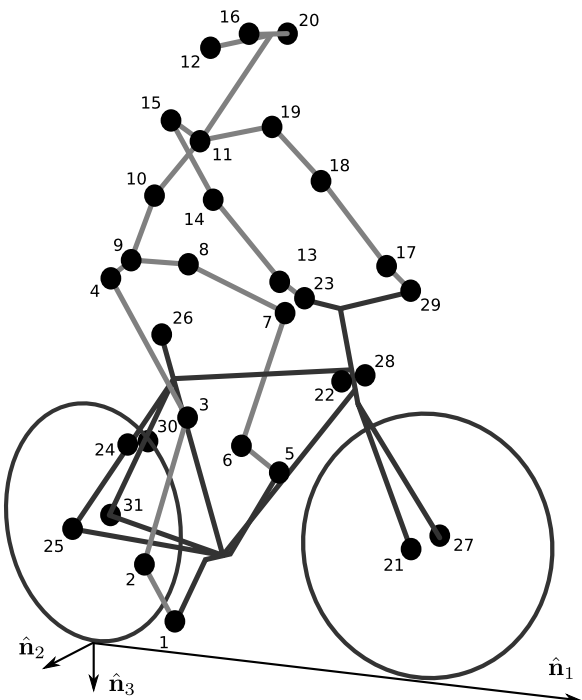
Fig. 2 (a) Rider 1 and the Batavus Stratos Deluxe with marker positions. (b) Body marker positions visible from the rear

The stability tasks were designed such that the rider would ride at a constant speed within the range of 2 to 30 km/h. The bicyclists were told to maintain an upright straight-ahead course on the treadmill and to look into the distance, with exception of the line tracking task. The bicyclists were instructed to bicycle comfortably at the designated speed and data recording was started at random. In all cases, the subject rode at the set speed until comfortable, then data was taken for 60 seconds at a 100 hertz sampling rate. Each task was performed on both bicycles with each rider. The following list describes the various tasks:

Normal pedaling The subject was instructed to simply stabilize the bicycle while pedaling and keep the heading in approximately the forward direction. The speed started at 5 km/h and increased in 5 km/h increments up to 30 km/h. The speeds were then decreased in the same fashion to 5 km/h. From then on the speed was decreased in 1 km/h increments until the subject was not able to stabilize the bicycle any longer. Therefore, there were two sets of data for each speed and each bicycle except speeds below 5 km/h. Several additional runs were also performed with the rider pedaling using a different gear, and thus a different cadence.

Without pedaling This was the same as the normal pedaling task except that a string was attached to the head tube of the bicycle such that the bicycle was fixed

Fig. 3 Schematic of the marker positions. The rider and bicycle are colored light gray and dark gray, respectively



longitudinally relative to the treadmill and no pedaling was required. The rider kept the feet in the same position throughout the task.

No-hands The riders stabilized the bicycle without using steering for control. They were instructed to keep their hands on their hips while bicycling. The rider started at 30 km/h and decreased in 5 km/h increments through 20 km/h and thereafter the speeds were decreased in 1 or 2 km/h increments until the rider was not able to comfortably stabilize the bicycle.

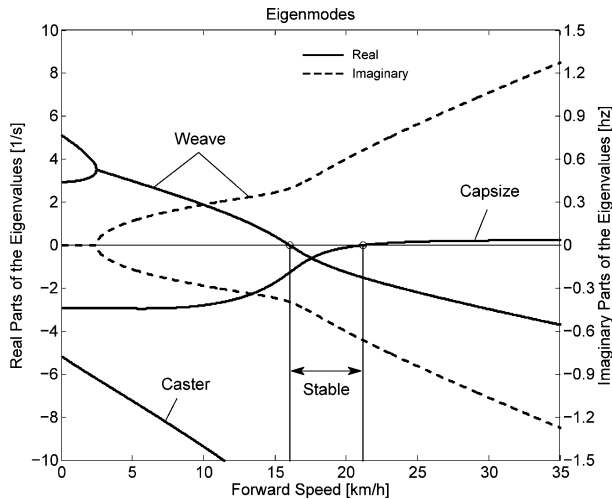
Line tracking This was the same as normal pedaling except that the rider was instructed to track a line on the treadmill surface with the front wheel. A smaller subset of speeds was performed.

These tasks were designed with the intent to answer several questions:

1. What upper body motions are used while bicycling?
2. How does the system motion change with respect to changes in forward speed?
3. How does pedaling influence the control actions?
4. Can the open loop rigid body dynamics be detected in the controlled state?
5. What does the rider do differently to control the bicycle when riding no-hands?
6. Do different bicyclists perform similar motions while performing the same task?
7. Is there a difference in motion when stabilizing and trying to track a line?

Since there is no room to address all of these questions in this paper, we focus on a single rider on the Brower bicycle and two of the tasks: normal pedaling and without pedaling. We were able to draw some conclusions on questions 1 through 4 with this smaller data set.

Fig. 4 Eigenvalues of the Browser bicycle with the third rider rigidly attached as a function of speed. Note that the initially unstable weave motion becomes stable above 16 km/h, the weave speed



3 Open loop rigid body dynamics

One question we have is whether or not the eigenfrequencies of the weave motion for the uncontrolled system can be detected in the results from the stabilization tasks. In order to predict the uncontrolled (open loop) eigenvalues of the rigid rider system, the basic geometry, mass, center of gravity locations, and moments of inertia of the bicycle were measured. Also, the riders were measured and weighed such that the body segment geometry, mass, center of gravity locations, and moments of inertia could be estimated. The physical parameter estimation methods are described in [9]. This data was used to calculate eigenvalues and eigenvectors of the uncontrolled open loop system Fig. 4.

4 Data processing

4.1 Missing markers

The Optotrak Certus Motion Capture System [8] is based on the cameras' ability to detect the infrared light from the sensors so there are occasional gaps in the coordinate data due to the markers going out of view. We attempted to minimize this by careful marker and camera placement but were not able to totally eliminate the error. Any missing markers on the bicycle were reconstructed using the assumption that the bicycle is a rigid body. We had more than three markers on both the frame and fork, so if one marker location was not detected we used the relative location of the remaining markers to reconstruct the missing marker. The gaps in the data of the markers on the human were repaired by fitting a cubic spline through the data. The spline estimated the marker coordinates during the gaps. We only used the splined data if the gaps were less than 10 time steps, or 0.1 sec; otherwise the trials were discarded.

4.2 Relative motion

We were interested in the analysis of three different marker combinations: the bicycle alone, the rider relative to the bicycle and the bicycle and rider together. The motion of the bicycle

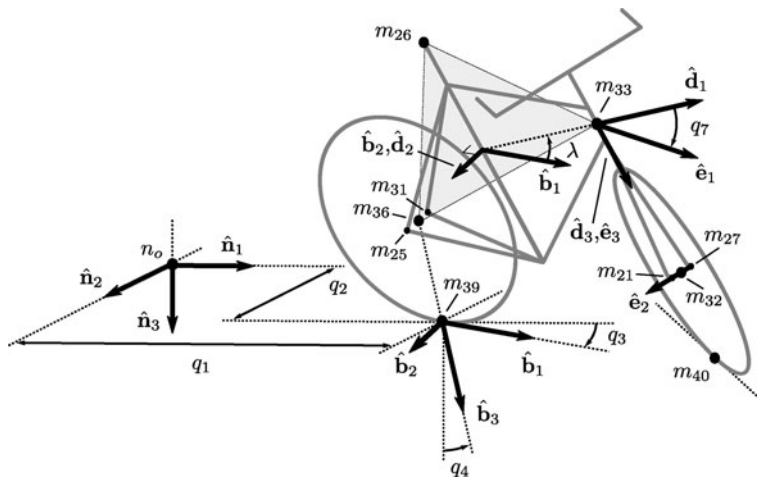


Fig. 5 Diagram of the bicycle's inertial frame **N**, rear frame **B**, front frame **E** and configuration variables

and the bicycle-rider were calculated with reference to the **N** inertial frame¹ and the motion of the rider was calculated with respect to the rear frame of the bicycle **B** Fig. 5. These three marker combinations allowed us to differentiate more easily between rider specific and bicycle specific motions. Furthermore, six of the variables that describe the configuration of the bicycle in time were calculated to give insight into the rigid body dynamics. The configuration variables q_1 and q_2 locate the contact point of the rear wheel of the bicycle. The **B** frame captures the yaw (q_3) and roll (q_4) motions of the bicycle frame, the **D** frame is an intermediate frame that differs from **B** only by the bike's headtube angle (λ), and the **E** frame captures the steering angle (q_7) of the bicycle fork relative to the bicycle frame. The pitch of the bicycle frame (q_6) is assumed to be zero. Details of these calculations are shown in Appendix.

4.3 Principal component analysis

We used Principal Component Analysis, PCA, [10] to extract and characterize the dominant motions of the system. Calculating the principal components effectively transforms the space of the data to a space that maximizes the variance of the data. The typical advantage of PCA is that the dimension of the system can be reduced and still retain enough information to adequately describe the system. We are primarily interested in the way that PCA is able to extract linear components and rank them in order of variance from the mean position. If we assume that the components with the largest kinematic variance are motions that are the dominant motions used for control and propulsion (which in general is not necessarily true for dynamical systems) the comparison of these components for different riding conditions can give insight into what motions may be important for developing a biomechanical control model of the bicyclist.

¹The **N** frame is used instead of the **M** frame to comply with the vehicle coordinate standards used in [1]. See Appendix for the derivation.

The repaired data from the motion capture measurements contained the x , y , and z coordinates of each marker 1 through l at each time step $j = 1, 2, \dots, n$. Each marker has three coordinates so there are a total of $m = 3l$ coordinates $i = 1, 2, \dots, m$. The coordinates at each time step can be collected in vector \mathbf{p}_j .

$$\mathbf{p}_j^T = [x_{1j} \quad \cdots \quad x_{lj} \quad y_{1j} \quad \cdots \quad y_{lj} \quad z_{1j} \quad \cdots \quad z_{lj}] = [p_{1j} \quad p_{2j} \quad \cdots \quad p_{mj}]$$

We can organize these coordinate vectors into a matrix, \mathbf{P} , where the rows, i , map a single coordinate of a marker through n time steps.

$$\mathbf{P} = \begin{bmatrix} | & | & & | & | \\ \mathbf{p}_1 & \mathbf{p}_2 & \cdots & \mathbf{p}_j & \cdots & \mathbf{p}_n \\ | & | & & | & | \end{bmatrix}$$

The principal components were calculated for the three marker combinations as described earlier where $n = 60 \times 100 = 6000$ time steps. The number of rows of \mathbf{P} were ($m = 3 \times 31 = 93$), ($m = 3 \times 11 = 33$) and ($m = 3 \times 20 = 60$) for the bicycle-rider, the bicycle alone and the rider alone, respectively.

One method of determining the principal components is to calculate the eigenvectors of the covariance matrix of the mean-subtracted data. We begin by calculating the mean \mathbf{u} (1) of the rows of \mathbf{P} and subtracting it from each column of \mathbf{P} to form the mean-subtracted data matrix $\bar{\mathbf{P}}$, (2).

$$\mathbf{u} = \frac{1}{n} \sum_{j=1}^n \mathbf{p}_j \quad (1)$$

A vector of ones

$$\mathbf{h}^T = [h_1 \quad h_2 \quad \cdots \quad h_j \quad \cdots \quad h_n] \quad \text{where } h_j = 1 \text{ for all } j$$

allows us to subtract \mathbf{u} from each column of \mathbf{P} ,

$$\bar{\mathbf{P}} = \mathbf{P} - \mathbf{u}\mathbf{h}^T \quad (2)$$

The covariance matrix \mathbf{C} of $\bar{\mathbf{P}}$ can then be calculated with (3).

$$\mathbf{C} = \frac{1}{n-1} \bar{\mathbf{P}} \bar{\mathbf{P}}^T \quad (3)$$

Calculating the eigenvectors \mathbf{v}_i and eigenvalues λ_i of the covariance matrix effectively transforms the space to one where the variances are maximized and the covariances are zero. The eigenvectors are the principal components of the data set and the corresponding eigenvalues represent the variance of each principal component. The eigenvectors are ordered by decreasing eigenvalue where \mathbf{v}_1 is the eigenvector corresponding to the largest eigenvalue. The eigenvalues and eigenvectors are calculated by finding the independent solutions to (4).

$$\mathbf{C}\mathbf{v}_i = \lambda_i \mathbf{v}_i \quad (4)$$

Each time step can now be represented as a linear combination of the principal components.

$$\mathbf{p}_j = \mathbf{u} + a_{1j}\mathbf{v}_1 + a_{2j}\mathbf{v}_2 + \cdots + a_{mj}\mathbf{v}_m \quad (5)$$

The coefficients a_{ij} can be solved at each time step j by reformulating (5) and solving the system of linear equations.

$$\mathbf{P} - \mathbf{uh}^T = \begin{bmatrix} | & | & & | \\ \mathbf{v}_1 & \mathbf{v}_2 & \cdots & \mathbf{v}_m \\ | & | & & | \end{bmatrix} \begin{bmatrix} a_{11} & \dots & a_{1n} \\ \vdots & \ddots & \vdots \\ a_{m1} & \dots & a_{mn} \end{bmatrix} = \mathbf{VA} \quad (6)$$

and

$$\mathbf{A} = \mathbf{V}^{-1}(\mathbf{P} - \mathbf{uh}^T). \quad (7)$$

With the principal components \mathbf{v}_i being constant, the behavior in time is described by the coefficients a_{ij} where the discretization in time is indexed by j . The order of the system can be reduced by eliminating principal components that have little variance. We arbitrarily decided to examine the first $k = 10$ principal components knowing that the first five would be based around the larger motions such as pedaling and that the remaining five may reveal some of the motions associated with control. The variance of each component, $\text{var}(\mathbf{a}_i) = \lambda_i$, is summed to determine the cumulative percentage of variance of the principal components, g_k .

$$g_k = 100 \frac{\sum_{i=1}^k \lambda_i}{\sum_{i=1}^m \lambda_i} \quad \text{where } 1 \leq k \leq m \quad (8)$$

Highly correlated data will show that even when $k \ll m$, g_k is close to 100%. Using 10 components g_{10} covers 100% (standard deviation, $\sigma = 10^{-14}\%$) of the variation in the data for the bicycle, rider and bicycle-rider. The matrix \mathbf{A} can then be reduced to a $k \times n$ matrix and eigenvectors greater than \mathbf{v}_k can be eliminated.

4.4 Data visualization

We developed a Graphical User Interface, GUI, in MATLAB that easily allows different trials to be compared with one another Fig. 6. The program loads in two different trials along with information on each trial. A graphical representation of the rider and bicycle are displayed in two adjacent screens and can be viewed from multiple perspectives. The animations of the runs can be played at different speeds, rewound and fast forwarded. The principal components are shown beside the corresponding animation display and combinations can be turned on and off for identification and comparison. Frequency and amplitude information for the temporal coefficients a_{ij} can also be displayed for comparison.

5 Results

5.1 Motion identification

The reduced set of data provides two important pieces of information for the identification of motion: the principal components \mathbf{v}_i and the corresponding coefficients a_{ij} . The principal components represent linear trajectories of the markers and the coefficients show how the markers follow the trajectories with time. We began processing the data by reviewing each principal component of each trial in the GUI and noting what type of motion we saw Table 1. These descriptions were subjective because we grouped marker movement based on



Fig. 6 Screen shot of the MATLAB graphical user interface (GUI) used to visualize principal components and compare between different components and trials

Table 1 Example raw trial description for the bicycle and rider during normal pedaling at 10 km/h

<i>i</i>	% Variance	Motion description	Frequency description
1	45.50	primarily longitudinal motion, some lateral	max amp = 0.6 m, most freq below 0.5 Hz, tiny spike at 1.6 Hz
2	29.39	primarily lateral motion, some longitudinal, small feet motion	max amp = 0.35 m, little spike at 0.8 Hz, most freq below 0.5 Hz
3	15.41	vertical pedaling, slight spine bend, hip/ head/shoulder sway out of phase with pedaling	max amp = 0.27 m, large dominant spike at 0.8 Hz
4	8.27	horizontal pedaling, head/shoulder sway	large dominant spike at 0.8 Hz with 0.19 m amp
5	0.82	yaw, knees stay still	max amp = 0.04 m at 0.33 Hz, most freq below 1 Hz
6	0.27	erratic left-hand movement	max amp = 0.018 m, most freq below 2 Hz
7	0.21	steer, left-hand movement, slight roll	most freq below 2 Hz, spike at 0.33 Hz and 1.58 Hz
8	0.07	knee and head bounce	dominant spike at 1.58 Hz
9	0.04	lateral knee movement, head jiggle	spikes at 1.58 Hz and 2.37 Hz, most freq below 2.5 Hz
10	0.02	head and knee jiggle	spikes at 1.58 Hz and 3.17 Hz, most freq below 3.5 Hz

Fig. 7 Coefficients a_{ij} versus time of the first five principal components for normal pedaling at 10 km/h

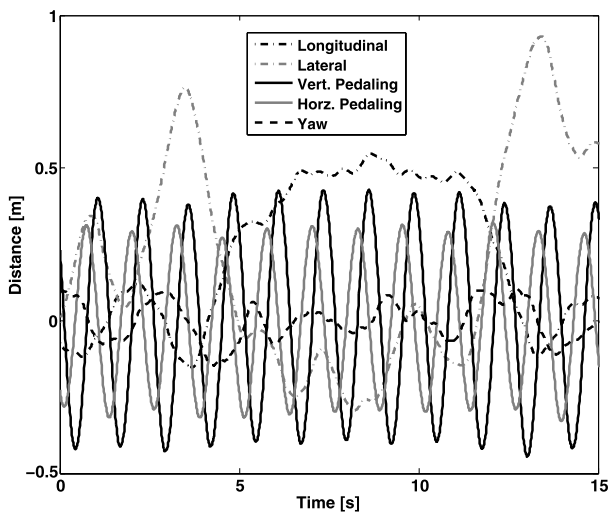
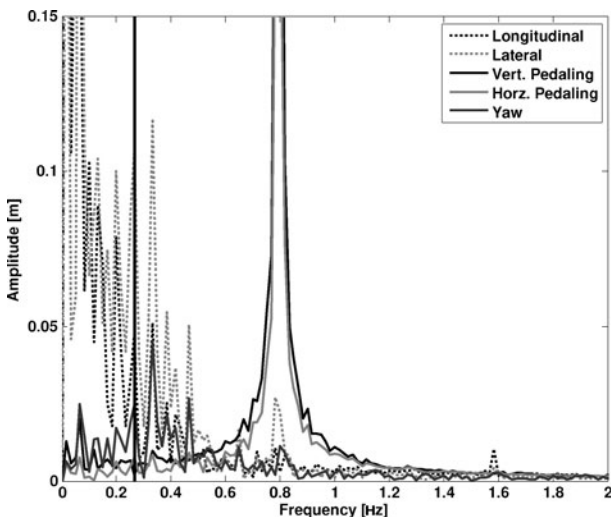


Fig. 8 The frequency content of the first five principal components for normal pedaling at 10 km/h. The vertical black line represents the open loop weave frequency (0.28 Hz) determined from Fig. 4 at this forward speed. The pedaling frequency is about 0.8 Hz at this speed; see Fig. 11



our preconceived understanding of rider and bicycle motion. Some of the components displayed motions that were not physically possible such as the upper leg stretching in length during the knee bounce. This is possible when examining a single component but when superimposed over the rest of the components the unrealistic motions are not present. Furthermore, for each component we examined amplitude and frequency content of the associated coefficients a_{ij} as shown in Figs. 7 and 8 and noted the shape of the frequency spectrum and the frequencies at any distinct spikes.

Several conclusions can be drawn from examining the coefficient data. First, some of the components are linked by the frequencies of the coefficients and describe an identifiable motion. The most obvious of these is that the vertical and horizontal pedaling components make up the circular pedaling motion. Both vary periodically and have a dominant frequency which is defined by the cadence. In the example trial, Table 1, the upper body motions are also linked to the pedaling. Components 8 and 9 both correspond to a frequency that is

twice the pedaling frequency, which may be due to the forces created during each pedal stroke. Component 6 seems to be the result of a bad marker signal. Components 5 and 7 are interesting because they display motions of the bicycle that are not dominated by the pedaling frequency and may be candidate control motions. The percentage variance of each component gives an idea of the relative amplitude of the components. The descriptions of each trial were used to compile a list of motions that contribute to the principal components. These motions, illustrated in Fig. 9, are:

- Drift** The bicycle and rider drift longitudinally and laterally on the surface of the treadmill. The motions are typically defined by two components that are not necessarily orthogonal or aligned with the inertial coordinate system. The motion is random and at low frequencies.

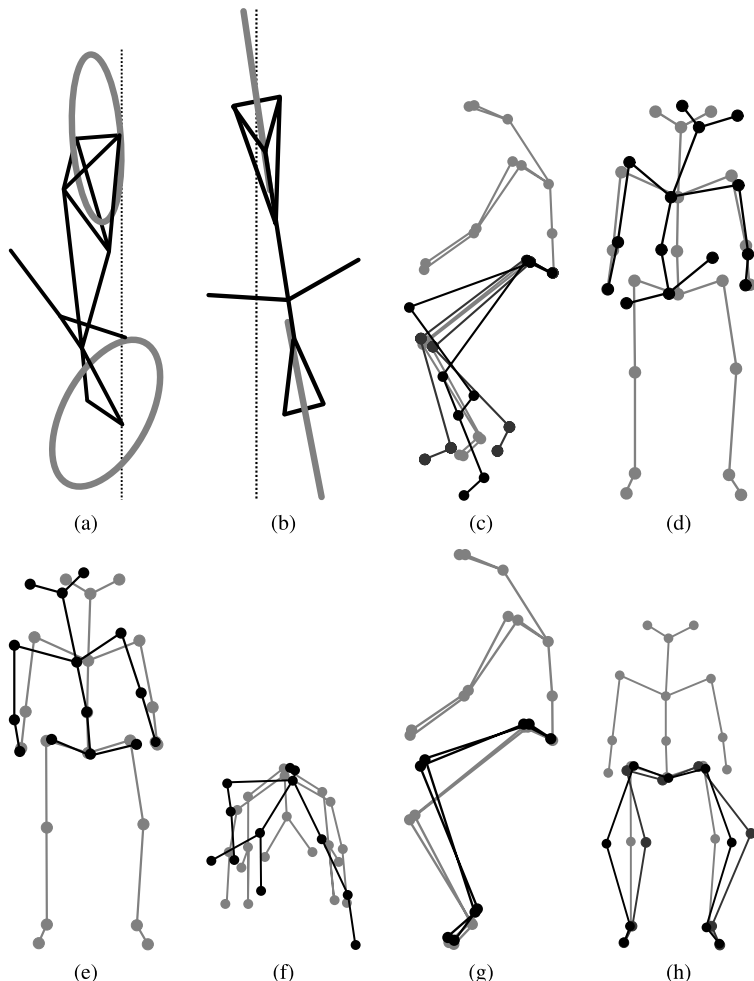


Fig. 9 Diagrams of the common motions. (a) Top view of bicycle steer and roll, (b) bicycle yaw, (c) horizontal and vertical components of pedaling, (d) spine bend, (e) rider lean, (f) top view of rider twist, (g) knee bounce and (h) two lateral knee motions. All but pedaling (c) are exaggerated for clarity

Steer	Rotation of the front assembly with respect to the rear frame. The steering may appear linked to one of the pedaling components at the pedaling frequency or may be in one or more components sometimes combined with roll and/or yaw at more random frequencies, Fig. 9(a).
Roll	The bicycle and the rider roll with respect to the ground plane. Roll is typically linked with steer and/or yaw and often at the pedaling frequency, Fig. 9(a).
Yaw	The heading angle of the bicycle and rider change together with respect to the ground plane. This is typically linked with steer, roll, and/or the drift, Fig. 9(b).
Pedaling	This motion is defined by two or more components, typically a vertical and horizontal motion of the feet, that show the feet rotating around the crank axle at a distinct frequency and the legs following suit, Fig. 9(c).
Bend	The spine bent laterally and was always connected with the vertical pedaling component, Fig. 9(d).
Lean	The upper body, shoulders and head lean laterally with respect to the rear frame and was always linked with the horizontal pedaling component, Fig. 9(e).
Twist	The shoulders rotate about the torso axis. This was linked to components that contained steering motions, both random and at the pedaling frequency, Fig. 9(f).
Bounce	The knee markers bounce up and down, the back straightens and the head nods at twice the pedaling frequency, Fig. 9(g).
Knees	The knees move laterally relative to the bicycle frame in both opposing directions and the same direction at random low frequencies, Fig. 9(h).
Head	Head twists and random head motions showed up often. These seemed to be due to the rider looking around randomly.

5.2 Motion characterization

To identify how bicycling changes with speed it would be ideal to investigate how the amplitude of each component varies with speed. However, the analysis does not return the same set of components for each run so such a comparison is typically not possible. Therefore, components were grouped into classes, where each class shows a specific physically relevant motion. The same total motion of the class can be described by one set of components in one trial and another, probably different, set of components in another trial. How the amplitudes of these classes vary among experiments can be used as a measure for how the rider and bicycle motion varies among trials.

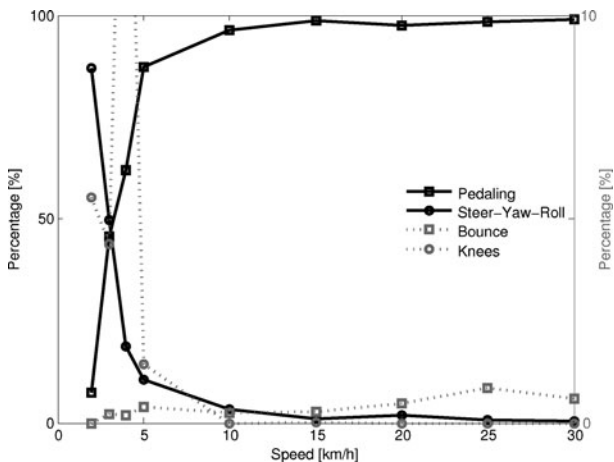
To objectively identify which coefficients show the same type of motion and could therefore form a class, the frequency content of each of the time coefficients in a single trial was correlated to that of each of the other components in that trial. Next, a minimum correlation value was set to determine which coefficients were correlated to each other. When the minimum was set at 0.9 only the coefficients making up the pedaling motion could be considered correlated. On the other hand, when a minimum level of 0.7 was used practically every coefficient was correlated to each other. The only exception was the coefficient that displayed the bounce. Its maximum correlation with another coefficient was no higher than 0.4 for any of the tested speeds. The 0.8 level gave a number of distinct classes of components, and thus this level was used to identify which coefficients were connected. Finally, the correlated coefficients were viewed simultaneously in the GUI enabling the determination of the motion class.

The correlated coefficients were used to form six different classes of motions, Table 2, each made up of combinations of the previously described motions in Fig. 9.

Table 2 The six primary motion classes

Class name	Class description
Drift	Drift
Pedaling	Pedaling 9(c), Bend 9(d), Lean 9(e), Twist 9(f)
Steer-Yaw-Roll	Steer and Roll 9(a), Yaw 9(b)
Bounce	Bounce 9(g)
Knees	Knees 9(h)
Other	Head and components that showed noise of some sort

Fig. 10 The relative percent variance of the four classes: Pedaling, Steer-Yaw-Roll, Bounce and Knees, at the different speeds when the Drift and Other classes were removed from the results for normal pedaling. The solid lines are scaled to 100% (left axis), the dotted lines are scaled to 10% (right axis)



In most cases, the correlated coefficients described a single class. However, sometimes, this was not the case and the coefficients were used to describe more than one class. An example is that at low speed the components containing the drift motions also contained large steer, yaw, and roll motions. Therefore, the motions were placed in both the Drift and the Steer-Yaw-Roll classes.

Since the rider was not instructed to hold a specific location on the treadmill the Drift class, which was usually the class with the largest amplitude, was not used in further analysis of the motion and neither was the ‘Other’ class. For each of the remaining classes, the percentages of variance of the remaining components were recalculated without the components placed in the Drift and the Other classes.

We also calculated various configuration variables from the bicycle marker locations (see Appendix) independent of the PCA perspective for more specific motion characterizations. This allowed us to investigate the bicycle’s configuration variable time histories and frequency content explicitly.

5.3 Characterization of motions during normal pedaling

Figure 10 shows how the relative percent variance of the four classes: Pedaling, Steer-Yaw-Roll, Bounce and Knees varies with speed for Rider 3 on the Batavus Brower bicycle. The percentage is the average of two runs at speeds 5 km/h and above. From the

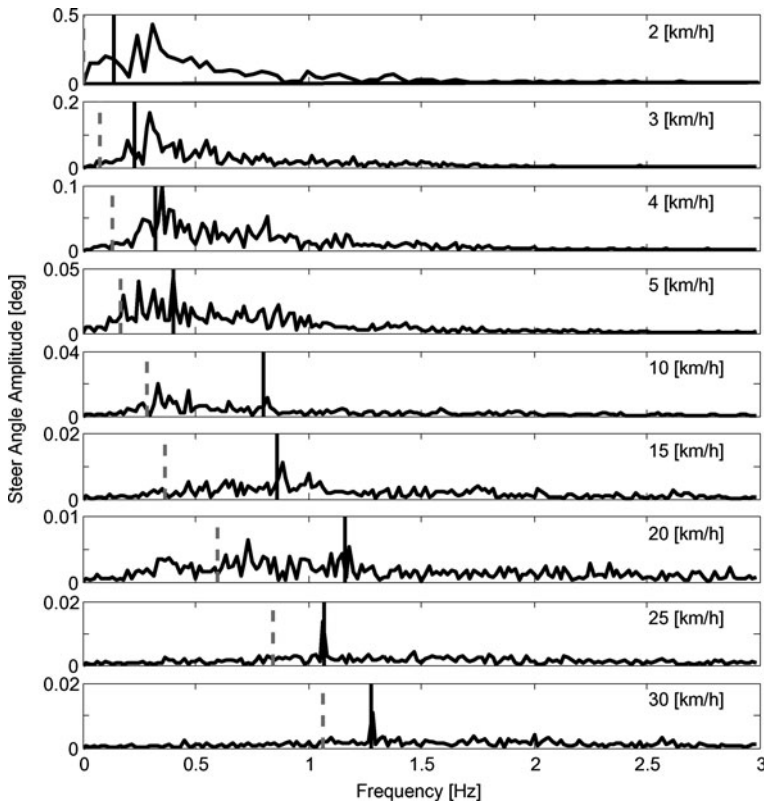
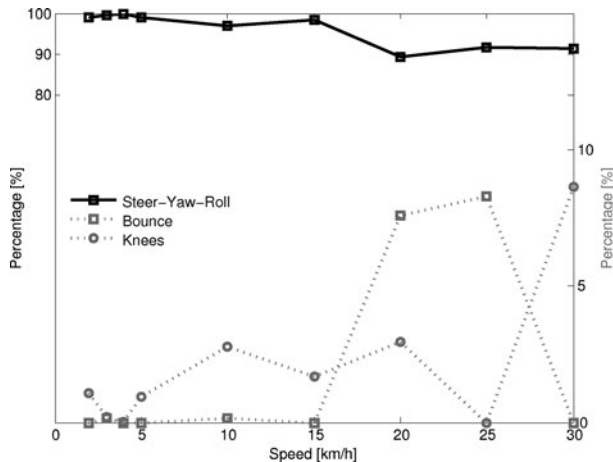


Fig. 11 Steer angle amplitude plot for the nine different speeds for normal pedaling experiment. *Solid vertical line* indicates the pedaling frequency. *Dashed vertical gray line* indicates the bicycle-rigid rider open loop weave eigenfrequency from Fig. 4

graph, it is clear that at 10 km/h and higher speeds practically all the motion that is taking place is the pedaling motion class. Below 10 km/h, the Steer-Yaw-Roll class becomes increasingly active and the relative percentage of the motion taking place in the pedaling class drops. Also, at speeds below 10 km/h, the lateral knee motion (Knees) class percentage increases with decreasing speed. The increase is not as significant as that of the Steer-Yaw-Roll class (increase to roughly 5% at 2 km/h), but it is certainly visible. The spike at 4 km/h can be attributed to the fact that the classes may contain higher variance motions because the classification method is based on principal components that are not necessarily consistent between runs. The Bounce roughly remains constant at all speeds.

The steer angle amplitude-frequency plot for each of the speeds calculated from the bicycle rigid body motions is given in Fig. 11. It clearly shows that the steering actions take place at or around the pedaling frequency for high and low speeds, respectively. It also shows that the amplitude of the steering angle increases by 5000% when the speed decreases from 30 km/h to 2 km/h. Figure 11 also shows the open loop, rigid rider, weave eigenfrequency for each speed obtained from Fig. 4. Apparently the open loop eigenfrequency is not a frequency at which the bicycle-rider operates.

Fig. 12 The percent variance of each of the three classes: Steer-Yaw-Roll, Bounce and Knees, at the different speeds when the Drift and Other classes were removed from the results for trials without pedaling. The solid lines are scaled to 100% (left axis), the dotted lines are scaled to 15% (right axis)



5.4 Characterization of motions without pedaling

During normal pedaling, all motions, including the control tasks, are dominated by the pedaling motions. Therefore we also looked at the motions of bicycle-rider system without the influence of pedaling. Figure 12 shows how the percent variance of Steer-Yaw-Roll, Bounce and Knees varies with speed for Rider 3 on the Batavus Brower bicycle without pedaling. Since the bicycle is towed and the riders feet remain in the same, constant, position relative to bicycle, there is no pedaling class present in analysis. Furthermore, no bend, lean or twist motions with high variance were detected during the experiments. It is clear that at all speeds most motion takes place in the Steer-Yaw-Roll class. Also interesting is that, unlike in the normal pedaling situation, the Knee motion percentage does not increase at low speeds. This may mean that the lateral knee motion is connected to pedaling in some way. Like for the pedaling case, the Bounce and Knee classes may contain different principal components and a statistical approach to evaluate the percent variance of the classes would provide clearer results. Also note that as the bicycle becomes self stable above 16 km/h the total variance is tiny and thus any sort of random knee motion can be a relatively large motion.

Figure 13 shows the bicycle rigid body steer angle frequency-amplitude plot for different speeds. Compared to normal pedaling, the amplitudes are about half the size at the low speeds and one tenth the size at high speeds, indicating that smaller steering angles were made. The frequency content now also shows a much wider, flatter spectrum compared to normal pedaling. At 10 and 15 km/h, the frequency with the largest amplitude is near the open loop weave eigenfrequency. However, at the other speeds, this is not the case, once again indicating that the rigid body open loop weave eigenfrequency is not the frequency at which the bicycle is controlled.

6 Conclusions

The view provided by principal component analysis into bicycle-rider interaction, biomechanics and control has led us to several conclusions. During normal bicycling there are

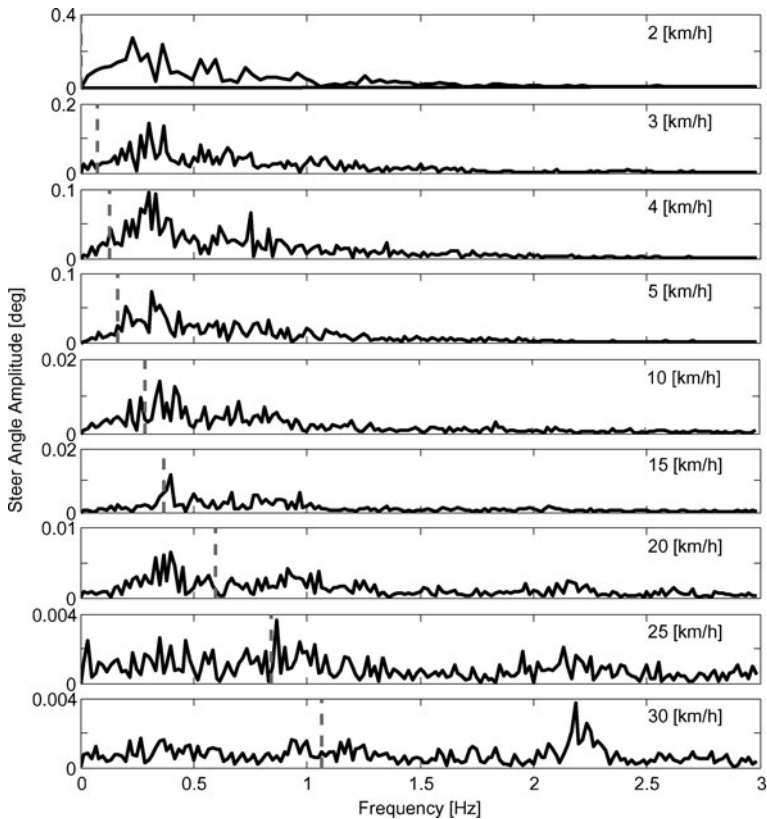


Fig. 13 Steer angle amplitude plot for the nine different speeds for the tasks without pedaling. *Dashed vertical grey line* indicates the bicycle-rigid rider open loop weave eigenfrequency obtained from Fig. 4

several dominant upper body motions: lean, bend, twist and bounce, all of which seem to be linked to the pedaling motion. This is important for understanding which inputs are related to fundamental balance control and which are reactions to pedaling. We hypothesize that lateral control is mainly accomplished by steering since only upper body motion was observed at the pedaling frequency. If upper body motions are used for control then this control is carried out at the pedaling frequency. Considering variations of motion with respect to speed, we observed that there is a great deal of steering at low speeds but this decreases in magnitude as speed increases. This is generally true for all motions and shows that the bicycle-rider system becomes more stable at higher speeds with few detectable control actions. At low speeds additional lateral knee motions are observed which are probably more effective at augmenting steering control for lateral balance than upper body motions.

The bicycle model predicts that the weave mode is stable above about 16 km/h. Intuition might possibly lead one to believe, if the weave mode is already stable, that the weave frequency might be relatively undisturbed by rider control actions and therefore present in the closed loop dynamics. However, we found no evidence of a distinct weave frequency in the steer angle time histories of any run. In fact, the only distinct frequency that sometimes appeared was the pedaling frequency.

Principal component analysis provided a unique view into the control actions of a rider on a bicycle, but limitations in data reduction and motion grouping leave room for more objective statistical views into the motion of the bicycle-rider system.

Acknowledgements We would like to thank Knoek van Soest and Richard Casius of the Faculty of Human Movement Sciences at the Vrije Universiteit, Amsterdam, for their cooperation and use of their equipment for the experiments and for Richard's expertise and help in operating the motion capture system and data processing. Also, we thank Victor Ahlm for a tireless day of bicycling and the Dutch bicycle manufacturer, Batavus, for supplying the bicycles.

Open Access This article is distributed under the terms of the Creative Commons Attribution Noncommercial License which permits any noncommercial use, distribution, and reproduction in any medium, provided the original author(s) and source are credited.

Appendix: Inertial frames and configuration variables

The transformation from marker coordinates to rigid body inertial frames and configuration variables shown in Fig. 5 is described here. A reference frame, \mathbf{N} , with origin n_o corresponding with the benchmark bicycle [1] is defined with respect to the Optotrak reference frame, \mathbf{M} , (9).

$$\mathbf{N} = \begin{bmatrix} \hat{\mathbf{n}}_1 \\ \hat{\mathbf{n}}_2 \\ \hat{\mathbf{n}}_3 \end{bmatrix} = \begin{bmatrix} 1 & 0 & 0 \\ 0 & -1 & 0 \\ 0 & 0 & -1 \end{bmatrix} \begin{bmatrix} \hat{\mathbf{m}}_1 \\ \hat{\mathbf{m}}_2 \\ \hat{\mathbf{m}}_3 \end{bmatrix} \quad (9)$$

Thirty-one marker locations were recorded and the vector to each is defined as \mathbf{r}^{m_k/n_o} where $k = 1, 2, \dots, l$ for the original markers and $k = l + 1, \dots$ for any additional virtual markers. To calculate the reference frame attached to the rear bicycle we formed a frame center plane from the seat post marker, m_{26} , and two new additional virtual markers at the center of the rear wheel, m_{36} , and the center of the head tube, m_{33} . For example, the center of the rear wheel was calculated by (10) where m_{25} and m_{31} are the left and right rear wheel markers.

$$\mathbf{r}^{m_{36}/n_o} = (\mathbf{r}^{m_{25}/n_o} + \mathbf{r}^{m_{31}/n_o})/2 \quad (10)$$

The normal vector to the plane through the rear wheel center, seat post, and the head tube center is

$$\hat{\mathbf{b}}_2 = \frac{\mathbf{r}^{m_{36}/m_{26}} \times \mathbf{r}^{m_{33}/m_{26}}}{|\mathbf{r}^{m_{36}/m_{26}} \times \mathbf{r}^{m_{33}/m_{26}}|} \quad (11)$$

The heading vector of the rear frame is then $\hat{\mathbf{b}}_1 = \hat{\mathbf{b}}_2 \times \hat{\mathbf{n}}_3$ and $\hat{\mathbf{b}}_3 = \hat{\mathbf{b}}_1 \times \hat{\mathbf{b}}_2$ follows. These unit vectors define a reference frame that leans and yaws with the rear frame. We assumed that the rear frame pitch is negligible. The marker locations of the rider can now be expressed relative to the bicycle's inertial frame with reference to a point on the bicycle frame m_{36} . Equation (12) shows that the vector from any marker on the rider relative to m_{36} can be expressed in the bicycle reference frame, \mathbf{B} , rather than the inertial frame, \mathbf{N} . This formulation was used in the PCA of the rider-only markers to look specifically at rider motion relative to the bicycle. The subscripts, \mathbf{N} and \mathbf{B} , in (12) signify which reference frame the position vectors are expressed in.

$$\mathbf{r}_{\mathbf{B}}^{m_k/m_{36}} = (\mathbf{r}_{\mathbf{N}}^{m_k/m_{36}} \cdot \hat{\mathbf{b}}_1)\hat{\mathbf{b}}_1 + (\mathbf{r}_{\mathbf{N}}^{m_k/m_{36}} \cdot \hat{\mathbf{b}}_2)\hat{\mathbf{b}}_2 + (\mathbf{r}_{\mathbf{N}}^{m_k/m_{36}} \cdot \hat{\mathbf{b}}_3)\hat{\mathbf{b}}_3 \quad (12)$$

A reference frame \mathbf{D} that is aligned with the steering axis of the rear frame can be formulated by rotation about the $\hat{\mathbf{b}}_2$ axis through the steer axis angle λ , which is measured for each bicycle [9].

$$\mathbf{D} = \begin{bmatrix} \hat{\mathbf{d}}_1 \\ \hat{\mathbf{d}}_2 \\ \hat{\mathbf{d}}_3 \end{bmatrix} = \begin{bmatrix} \cos \lambda & 0 & -\sin \lambda \\ 0 & 1 & 0 \\ \sin \lambda & 0 & \cos \lambda \end{bmatrix} \begin{bmatrix} \hat{\mathbf{b}}_1 \\ \hat{\mathbf{b}}_2 \\ \hat{\mathbf{b}}_3 \end{bmatrix} \quad (13)$$

The handlebar/fork inertial frame \mathbf{E} is then calculated by defining $\hat{\mathbf{e}}_2$ to be aligned with the front wheel axle (14).

$$\hat{\mathbf{e}}_2 = \frac{\mathbf{r}^{m_{21}/n_o} - \mathbf{r}^{m_{27}/n_o}}{|\mathbf{r}^{m_{21}/n_o} - \mathbf{r}^{m_{27}/n_o}|} \quad (14)$$

The handlebar/fork frame rotates around $\hat{\mathbf{d}}_3 = \hat{\mathbf{e}}_3$ and then $\hat{\mathbf{e}}_1 = \hat{\mathbf{e}}_3 \times \hat{\mathbf{e}}_2$. Equation (15) gives the instantaneous rear wheel radius which is used to formulate the vector to the rear wheel contact point (16).

$$r_R = -\frac{\mathbf{r}^{m_{36}/n_o} \cdot \hat{\mathbf{n}}_3}{\hat{\mathbf{b}}_3 \cdot \hat{\mathbf{n}}_3} \quad (15)$$

$$\mathbf{r}^{m_{39}/n_o} = \mathbf{r}^{m_{36}/n_o} + r_R \hat{\mathbf{b}}_3 \quad (16)$$

This now allows us to calculate six of the eight configuration variables of the bicycle as a function of time (q_5 and q_8 are the rear and front wheel rotations, respectively).

$$\text{Distance to the ground contact point: } q_1 = \mathbf{r}^{m_{39}/n_o} \cdot \hat{\mathbf{n}}_1, \quad (17)$$

$$\text{Distance to the ground contact point: } q_2 = \mathbf{r}^{m_{39}/n_o} \cdot \hat{\mathbf{n}}_2, \quad (18)$$

$$\text{Yaw angle: } q_3 = \arccos(\hat{\mathbf{b}}_1 \cdot \hat{\mathbf{n}}_1), \quad (19)$$

$$\text{Roll angle: } q_4 = \arccos(\hat{\mathbf{b}}_3 \cdot \hat{\mathbf{n}}_3), \quad (20)$$

$$\text{Pitch angle: } q_6 = 0, \quad (21)$$

$$\text{Steer angle: } q_7 = \arccos(\hat{\mathbf{d}}_1 \cdot \hat{\mathbf{e}}_1), \quad (22)$$

References

1. Meijaard, J.P., Papadopoulos, J.M., Ruina, A., Schwab, A.L.: Linearized dynamics equations for the balance and steer of a bicycle: a benchmark and review. Proc. R. Soc., A Math. Phys. Eng. Sci. **463**(2084), 1955–1982 (2007)
2. Kooijman, J.D.G., Schwab, A.L., Meijaard, J.P.: Experimental validation of a model of an uncontrolled bicycle. Multibody Syst. Dyn. **19**, 115–132 (2008)
3. Peterson, D.L., Hubbard, M.: Yaw rate and velocity tracking control of a hands-free bicycle. In: International Mechanical Engineering Congress and Exposition, Boston, Oct. 2008. ASME, New York (2008)

4. Schwab, A.L., Kooijman, J.D.G., Meijaard, J.P.: Some recent developments in bicycle dynamics and control. In: Belyaev, A.K., Indeitsev, D.A. (eds.) Fourth European Conference on Structural Control (4ECSC), pp. 695–702. Institute of Problems in Mechanical Engineering, Russian Academy of Sciences, Moscow (2008)
5. Sharp, R.S.: On the stability and control of the bicycle. *Appl. Mech. Rev.* **61**(6), 1–24 (2008)
6. Kooijman, J.D.G., Schwab, A.L., Moore, J.K.: Some observations on human control of a bicycle. In: Proceedings of the ASME 2009 International Design and Engineering Technical Conferences & Computers and Information in Engineering Conference, 2009
7. Troje, N.F.: Decomposing biological motion: a framework for analysis and synthesis of human gait patterns. *J. Vis.* **2**(5), 371–387 (2002)
8. Northern Digital Incorporated. Optotrak Certus Motion Capture System (2009)
9. Moore, J.K., Kooijman, J.D.G., Hubbard, M., Schwab, A.L.: A method for estimating physical properties of a combined bicycle and rider. In: Proceedings of the ASME 2009 International Design Engineering Technical Conferences & Computers and Information in Engineering Conference, IDETC/CIE 2009, San Diego, CA, USA, August–September 2009. ASME, New York (2009)
10. Jolliffe, I.T.: Principal Component Analysis. Springer Series in Statistics, 2nd edn. Springer, New York (2002)

An elaborate data set on human gait and the effect of mechanical perturbations

Jason K. Moore, Sandra K. Hnat and Antonie J. van den Bogert

Department of Mechanical Engineering, Cleveland State University, Cleveland, OH, USA

ABSTRACT

Here we share a rich gait data set collected from fifteen subjects walking at three speeds on an instrumented treadmill. Each trial consists of 120 s of normal walking and 480 s of walking while being longitudinally perturbed during each stance phase with pseudo-random fluctuations in the speed of the treadmill belt. A total of approximately 1.5 h of normal walking (>5000 gait cycles) and 6 h of perturbed walking (>20,000 gait cycles) is included in the data set. We provide full body marker trajectories and ground reaction loads in addition to a presentation of processed data that includes gait events, 2D joint angles, angular rates, and joint torques along with the open source software used for the computations. The protocol is described in detail and supported with additional elaborate meta data for each trial. This data can likely be useful for validating or generating mathematical models that are capable of simulating normal periodic gait and non-periodic, perturbed gaits.

Subjects Bioengineering, Kinesiology, Computational Science

Keywords Gait, Data, Control, Perturbation

INTRODUCTION

The collection of dynamical data during human walking has a long history beginning with the first motion pictures and now with modern marker based motion capture techniques and high fidelity ground reaction load measurements. Even though years of data on thousands of subjects now exist, this data is not widely disseminated, well organized, nor available with few or no restrictions. David Winter's published normative gait data ([Winter, 1990](#)) is widely used in biomechanical studies, yet it comes from few subjects and only a small number of gait cycles per subject. This small source has successfully enabled many other studies, such as powered prosthetic control design ([Sup, Bohara & Goldfarb, 2008](#)) but success in other research fields using large sets of data for discovery lead us to believe that more elaborate data sets may benefit the field of human motion studies. To enable such work, biomechanical data needs to be shared extensively, organized, and curated to enable future analysts.

There are some notable gait data sets and databases besides Winter's authoritative set that are publicly available. The International Society of Biomechanics has maintained a web page (<http://isbweb.org/data>) since approximately 1995 that includes data sets for download and mostly unencumbered use. For example, the kinematic and force plate measurements from several subjects from [Vaughan, Davis & O'Connor \(1992\)](#) is available on the site. At another website, the CGA Normative Gait Database, [Kirtley \(2014\)](#) curates

Submitted 19 December 2014

Accepted 7 April 2015

Published 28 April 2015

Corresponding author

Jason K. Moore,
moorepants@gmail.com

Academic editor
Arti Ahluwalia

Additional Information and
Declarations can be found on
page 19

DOI [10.7717/peerj.918](https://doi.org/10.7717/peerj.918)

© Copyright
2015 Moore et al.

Distributed under
Creative Commons CC-BY 4.0

OPEN ACCESS

and shares normative clinical gait data collected from multiple labs and these datasets have influenced other studies, for example [Van den Bogert \(2003\)](#) made use of the average gait cycles from the child subjects.

[Chester, Tingley & Biden \(2007\)](#) report on a large gait database comparison where one database contained kinematic data of 409 gait cycles of children from 1 to 7 years old but the data does not seem to be publicly available. This is unfortunately typical. [Tirosh, Baker & McGinley \(2010\)](#) recognized the need for a comprehensive data base for clinical gait data and created the Gaitabase. This database may contain a substantial amount of data but it is encumbered by a complicated and restrictive license and sharing scheme. [Yun et al. \(2014\)](#) provides lower body kinematic data of single gait cycles from over one hundred subjects extracted from the large KIST Human Gait Pattern Data database which may also include a substantial amount of raw data but it is private. However, there are examples of data with less restrictions. The University of Wisconsin at LaCrosse has an easily accessible normative gait data set ([Willson & Kernozeck, 2014](#)) from 25 subjects with lower extremity marker data from multiple gait cycles and force plate measurements from a single gait cycle. The CMU Graphics Lab Motion Capture Database ([Hodgins, 2015](#)) is also a good example and contains full body marker kinematics for a fair number of trials with small number of gait cycles during both walking and running.

More recent examples of biomechanists sharing their data alongside publications are: [Van den Bogert et al. \(2013\)](#) which includes full body joint kinematics and kinetics from eleven subjects walking on an instrumented treadmill and [Wang & Srinivasan \(2014\)](#) who include a larger set of data from ten subjects walking for five minutes each at three different speeds but only a small set of lower extremity markers are present. The second is notable because they publish the data in Dryad, a modern citable data repository. It is also worth noting purely visual data collections of gait, like the one presented in [Makihara et al. \(2012\)](#), which contain videos of subjects walking on a treadmill in full clothing. This database is also unfortunately tightly secured with an extensive release agreement for reuse.

The amount of publicly available gait data is small compared to the number of gait studies that have been performed over the years. The data that is available generally suffers from limitations such as few subjects, few gait cycles, few markers, highly clinical, no raw data, limited force plate measurements, lack of meta data, non-standard formats, and restrictive licensing. To help with this situation we are making the data we collected for our research purposes publicly available and free of the previously mentioned deficiencies. Not only do we provide a larger set of normative gait data that has been previously available, we also include an even larger set of data in which the subject is being perturbed, something that does not currently exist. We believe both of these sets of data can serve a variety of use cases and hope that we can save time and effort for future researchers by sharing it.

But our reasons are not entirely altruistic, as governments and granting agencies are also encouraging researchers to share data with recent policy changes. For example, the [European Commission \(2012\)](#) has outlined publicly funded data's role in innovation and the [White House \(2013\)](#) laid out a plan for public access to publications and data in 2013. The National Science Foundation, which partially funds this work, was ahead of the White

House and required all grants to include a data management plan in 2011. This work is a partial fulfillment of the grant requirements laid out in our grant's data management plan and we hope that this work can be a good model for dissemination of biomechanical data.

Our use case for the data is centered around the need for bio-inspired control systems in emerging powered prosthetics and orthotics. Ideally, a powered prosthetic would behave in such a way that the user would feel like their limb was never disabled. There are a variety of approaches to developing bio-inspired control systems, some of which aim to mimic the reactions and motion of an able-bodied person. A modern gait lab is able to collect a variety of kinematic, kinetic, and physiological data from humans during gait. This data can potentially be used to drive the design of the human-mimicking controller. With a rich enough data set, one may be able to identify control mechanisms used during a human's natural gait and recovery from perturbations. We hypothesize that by forcing the human to recover from external perturbations, the resulting reactive actions can be used along with system identification techniques to expose the feedback related relationships among the human's sensors and actuators. With this in mind, we have collected data that is richer than previous gait data sets and may be rich enough for control identification. The data can also be used for verification purposes for controllers that have been designed in other manners, such as those constructed from first principles (e.g., [Geyer & Herr, 2010](#)).

With all of this in mind, we collected over seven and a half hours of gait data from fifteen able bodied subjects which amounts to over 25,000 gait cycles ([Moore, Hnat & Van den Bogert, 2014](#)). The subjects walked at three different speeds on an instrumented treadmill while we collected full body marker locations and ground reaction loads from a pair of force plates. The final protocol for the majority of the trials included two minutes of normal walking and eight minutes of walking under the influence of pseudo-random belt speed fluctuations. The data has been organized complete with rich meta data and made available in the most unrestrictive form for other research uses following modern best practices in data sharing ([White et al., 2013](#)).

Furthermore, we include a small Apache licensed open source software library for basic gait analysis and demonstrate its use in the paper. The combination of the open data and open software allow the results presented within to be computationally reproducible and instructions are included in the associated repository (<https://github.com/csu-hmc/perturbed-data-paper>) for reproducing the results.

METHODS

In this section, we describe our experimental design beginning with descriptions of the participants and equipment. This is then followed by the protocol details and specifics on the perturbation design.

Participants

Fifteen able bodied subjects including four females and eleven males with an average age of 24 ± 4 years, height of 1.75 ± 0.09 m, mass of 74 ± 13 kg participated in the study.

The study was approved by the Institutional Review Board of Cleveland State University (# 29904-VAN-HS) and written informed consent was obtained from all participants.

Table 1 Information about the 15 study participants in order of collection date. The subjects are divided into those that were used for the protocol pilot trials, i.e., the first three, and those used for the final protocol. The final three columns provide the trial numbers associated with each nominal treadmill speed. The measured mass is computed from the mean total vertical ground reaction force just after the calibration pose event, if possible. If the mass is reported without an accompanying standard deviation, it is the subject's self-reported mass. Additional trials found in the data set with a subject identification number 0 are trials with no subject, i.e., unloaded trials that can be used for inertial compensation purposes, and are not shown in the table. Generated by `src/subject_table.py`.

Id	Gender	Age (yr)	Height (m)	Mass (kg)	0.8 m/s	1.2 m/s	1.6 m/s
1	male	25	1.87	101	NA	6, 7, 8	NA
11	male	22	1.85	80	9	10	11
4	male	30	1.76	74	12, 15	13	14
7	female	29	1.72	64.5 ± 0.8	16	17	18
8	male	20	1.57	74.9 ± 0.9	19	20	21
9	male	20	1.69	67 ± 2	25	26	27
5	male	23	1.73	71.2 ± 0.9	32	31	33
6	male	26	1.77	86.8 ± 0.6	40	41	42
3	female	32	1.62	54 ± 2	46	47	48
12	male	22	1.85	74.2 ± 0.5	49	50	51
13	female	21	1.70	58 ± 2	55	56	57
10	male	19	1.77	92 ± 2	61	62	63
15	male	22	1.83	80.5 ± 0.8	67	68	69
17	male	23	1.86	88.3 ± 0.8	73	74	75
16	female	28	1.69	56.2 ± 0.6	76	77	78

The data has been anonymized with respect to the participants' identities and a unique identification number was assigned to each subject. A selection of the meta data collected for each subject is shown in **Table 1**.

Equipment

The data were collected in the Laboratory for Human Motion and Control at Cleveland State University, using the following equipment:

- A R-Mill treadmill which has dual 6 degree of freedom force plates, independent belts for each foot, along with lateral translation and pitch rotation capabilities (Forcelink, Culemborg, Netherlands).
- A 10 Osprey camera motion capture system paired with the Cortex 3.1.1.1290 software (Motion Analysis, Santa Rosa, CA, USA).
- USB-6255 data acquisition unit (National Instruments, Austin, Texas, USA).
- Four ADXL330 Triple Axis Accelerometer Breakout boards attached to the treadmill (Sparkfun, Niwot, Colorado, USA).
- D-Flow software (versions 3.16.1 to 3.16.2) and visual display system, (Motek Medical, Amsterdam, Netherlands).

The Cortex software delivers high accuracy 3D marker trajectories from the cameras along with data from the force plates and analog sensors (e.g., EMG/Accelerometer)



Figure 1 The treadmill with coordinate system, cameras (circled in orange), projection screen, and safety rope. The direction of travel is in the $-z$ direction.

through a National Instruments USB-6255 data acquisition unit. D-Flow then receives streaming data from Cortex and any other digital sensors. It is also responsible for controlling the treadmill's motion (lateral, pitch, belts). D-Flow can process the data in real time and/or export data to file.

Our motion capture system's coordinate system is such that the X coordinate points to the right, the Y coordinate points upwards, and the Z coordinate follows from the right-hand-rule, i.e., points backwards with respect to the walking direction. The camera's coordinate system is aligned to an origin point on the treadmill's surface during camera calibration. The same point is used as the origin of the ground reaction force measuring system. **Figure 1** shows the layout of the equipment.

Early on, we discovered that the factory setup of the R-Link treadmill had a vibration mode as low as 5Hz that was detectable in the force measurements; this was likely due to the flexible undercarriage and pitch motion mechanism. Trials 6–8 are affected by this vibration mode. During trials 9–15 the treadmill was stabilized with wooden blocks. During the remaining trials (>15) the treadmill was stabilized with metal supports; both with ones we fabricated in-house and ones supplied by the vendor. These supports aimed to improve the stiffness and frequency response of the force plate system. See the Data Limitations Section for more details.

The acceleration of the treadmill base was measured during each trial by the ADXL330 accelerometers placed at the four corners of the machine. These accelerometers were intended to provide information for inertial compensation purposes when the treadmill moved laterally or in pitch, but are extraneous for trials greater than number 8 due to the treadmill being stabilized in those degrees of freedom by the aforementioned supports.

Protocol

The experimental protocol consisted of both static measurements and walking on the treadmill for 10 min under unperturbed and perturbed conditions. Before a set of trials on the same day, the motion capture system was calibrated using the manufacturer's recommended procedure. Before each subject's gait data were collected, the subject changed into athletic shoes, shorts, a sports bra, a baseball cap,¹ and a rock climbing harness. All 47 markers were applied directly to the skin at the landmarks noted in [Table 2](#) except for the heel, toe, and head markers, which were placed on the respective article of clothing.² Then the subject self-reported their age, gender, and mass. Finally, their height was measured by the experimentalist and four reference photographs (front, back, right, left) were taken of subject's marker locations.

¹ A cap was used to avoid having to shave participants' hair at the expense of accuracy.

² The sacrum and rear pelvic markers were placed on the shorts for a small number of the subjects.

After obtaining informed consent and a briefing by the experimentalist on the trial protocol, the subject followed the verbal instructions of the experimentalist and the on-screen instructions from the video display. The final protocol for a single trial was as follows:

1. The subject stepped onto the treadmill and markers were identified with Cortex.
2. The safety rope was attached loosely to the rock climbing harness such that no forces were acting on the subject during walking, but so that the harness would prevent a full fall.
3. The subject started by stepping on sides of treadmill so that feet did not touch the force plates and the force plate signals are zeroed. This corresponds to the "Force Plate Zeroing" event.
4. Once notified by the video display, the subject stood in the calibration pose: standing straight up, looking forward, arms out by their sides (approximately 45 degree abduction) and the event, "Calibration Pose," was manually recorded by the operator.
5. A countdown to the first normal walking phase was displayed. At the end of the countdown the event "First Normal Walking" was recorded and the treadmill ramped up to the specified speed and the subject was instructed to walk normally, to focus on the "endless" road on the display, and not to look at their feet.
6. After 1 min of normal walking, the longitudinal perturbation phase begun and was recorded as "Longitudinal Perturbation."
7. After 8 min of walking under the influence of the perturbations, the second normal walking phase begun and was recorded as "Second Normal Walking."
8. After 1 min of normal walking, a countdown was shown on the display and the treadmill decelerated to a stop.
9. The subject was instructed to step off of the force plates for 10 s and the "Unloaded End" event was recorded.
10. The subject could then take a rest break before each additional trial.

Pilot protocols

Trials 3–15 were pilot tests for finalizing the protocol design and thus have some slight variations with respect to the subsequent trials. We include these trials due to the

Table 2 Descriptions of the 47 subject markers used in this study. The “Set” column indicates whether the marker exists in the lower and/or full body marker set. The label column matches the column headers in the `mocap-xxx.txt` files and/or the marker map in the `meta-xxx.yml` file.

Set	#	Label	Name	Description
F	1	LHEAD	Left head	Just above the ear, in the middle.
F	2	THEAD	Top head	On top of the head, in line with the LHEAD and RHEAD.
F	3	RHEAD	Right head	Just above the ear, in the middle.
F	4	FHEAD	Forehead	Between line LHEAD/RHEAD and THEAD a bit right from center.
L/F	5	C7	C7	On the 7th cervical vertebrae.
L/F	6	T10	T10	On the 10th thoracic vertebrae.
L/F	7	SACR	Sacrum bone	On the sacral bone.
L/F	8	NAVE	Navel	On the navel.
L/F	9	XYPH	Xiphoid process	Xiphoid process of the sternum.
F	10	STRN	Sternum	On the jugular notch of the sternum.
F	11	BBAC	Scapula	On the inferior angle of the right scapular.
F	12	LSHO	Left shoulder	Left acromion.
F	13	LDELT	Left deltoid muscle	Apex of the deltoid muscle.
F	14	LLEE	Left lateral elbow	Left lateral epicondyle of the elbow.
F	15	LMEE	Left medial elbow	Left medial epicondyle of the elbow.
F	16	LFRM	Left forearm	On 2/3 on the line between the LLEE and LMW.
F	17	LMW	Left medial wrist	On styloid process radius, thumb side.
F	18	LLW	Left lateral wrist	On styloid process ulna, pinky side.
F	19	LFIN	Left fingers	Center of the hand. Caput metatarsal 3.
F	20	RSHO	Right shoulder	Right acromion.
F	21	RDELT	Right deltoid muscle	Apex of deltoid muscle.
F	22	RLEE	Right lateral elbow	Right lateral epicondyle of the elbow.
F	23	RMEE	Right medial elbow	Right medial epicondyle of the elbow.
F	24	RFRM	Right forearm	On 1/3 on the line between the RLEE and RMW.
F	25	RMW	Right medial wrist	On styloid process radius, thumb side.
F	26	RLW	Right lateral wrist	On styloid process ulna, pinky side.
F	27	RFIN	Right fingers	Center of the hand. Caput metatarsal 3.
L/F	28	LASIS	Pelvic bone left front	Left anterior superior iliac spine.
L/F	29	RASIS	Pelvic bone right front	Right anterior superior iliac spine.
L/F	30	LPSIS	Pelvic bone left back	Left posterior superio iliac spine.
L/F	31	RPSIS	Pelvic bone right back	Right posterior superior iliac spine.
L/F	32	LGTRO	Left greater trochanter of the femur	On the cetner of the left greater trochanter.
L/F	33	FLTHI	Left thigh	On 1/3 on the line between the LGTRO and LLEK.
L/F	34	LLEK	Left lateral epicondyle of the knee	On the lateral side of the joint axis.
L/F	35	LATI	Left anterior of the tibia	On 2/3 on the line between the LLEK and LLM.
L/F	36	LLM	Left lateral malleoulus of the ankle	The center of the heel at the same height as the toe.
L/F	37	LHEE	Left heel	Center of the heel at the same height as the toe.
L/F	38	LTOE	Left toe	Tip of big toe.
L/F	39	LMT5	Left 5th metatarsal	Caput of the 5th metatarsal bone, on joint line midfoot/toes.
L/F	40	RGTRO	Right greater trochanter of the femur	On the cetner of the right greater trochanter.
L/F	41	FRTHI	Right thigh	On 2/3 on the line between the RFTRO and RLEK.
L/F	42	RLEK	Right lateral epicondyle of the knee	On the lateral side of the joint axis.

(continued on next page)

Table 2 (continued)

Set	#	Label	Name	Description
L/F	43	RATI	Right anterior of the tibia	On 1/3 on the line between the RLEK and RLM.
L/F	44	RLM	Right lateral malleolus of the ankle	The center of the heel at the same height as the toe.
L/F	45	RHEE	Right heel	Center of the heel at the same height as the toe.
L/F	46	RTOE	Right toe	Tip of big toe.
L/F	47	RMT5	Right 5th metatarsal	Caput of the 5th metatarsal bone, on joint line midfoot/toes.

uniqueness of trials 6–8 and the fact that the kinematic data is valid. We believe there may be useful analyses that only require the kinematic data. Additional information needed to interpret the data in the pilot trials can be found in the associated meta data files and the Data Limitations Section of this paper.

Trials 3–8 use an early experimental protocol which divided the walking period into three sections: no perturbation, longitudinal perturbation, and a combination of longitudinal and lateral perturbation. The calibration pose and zeroing events are present in the data but lumped into one event. These trials only use the lower body marker set described in Table 2. Additionally, there are five markers that have labels beginning with ROT that were attached to the treadmill base to capture the lateral motion. Trials 9–15 use the final protocol but have corrupt ground reaction loads due to the wooden treadmill base stabilizers.

Perturbation signals

As previously described, the protocol included a phase of normal walking, followed by longitudinal belt speed perturbations, and ended with a second segment of normal walking. Three pseudo-random belt speed control signals, with mean velocities of 0.8 m s^{-1} , 1.2 m s^{-1} and 1.6 m s^{-1} , were pre-generated with MATLAB and Simulink (Mathworks, Natick, Massachusetts, USA) and are available for download from Zenodo ([Hnat, Moore & Van den Bogert, 2015](#)). The same control signal was used for all trials at that given speed.

To create the signals, we started by generating random acceleration signals, sampled at 100 Hz, using the Simulink discrete-time Gaussian white noise block followed by a saturation block set at the maximum belt acceleration of 15 m s^{-2} . The signal was then integrated to obtain belt speed and high-pass filtered with a second-order Butterworth filter to eliminate drift. One of the three mean speeds were then added to the signal and limited between 0 m s^{-1} to 3.6 m s^{-1} . The cutoff frequencies of the high-pass filter, as well as the variance in the acceleration signal, were manually adjusted until acceptable standard deviations for each mean speed were obtained: 0.06 m s^{-1} , 0.12 m s^{-1} and 0.21 m s^{-1} for the three speeds, respectively. These ensured that the test subjects were sufficiently perturbed at each speed, while remaining within the limits of our equipment and testing protocol. To ensure that the treadmill belts could accelerate to the desired values, the high performance mode in the D-Flow software was enabled. The MATLAB script and Simulink model produce a comma-delimited text file of with the desired belt speed signals indexed by the time stamp.

Figure 2 gives an idea of the effect of the treadmill and controller dynamics by plotting the measured speed of the treadmill belts from loaded trials (76, 77, 78) against the

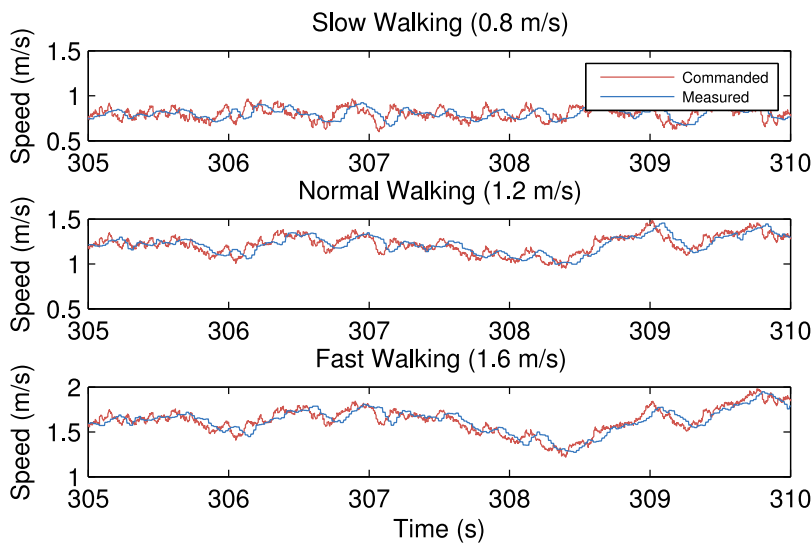


Figure 2 Commanded treadmill belt speed (red) and the recorded speed (blue) for average belt speeds of 0.8 m s^{-1} , 1.2 m s^{-1} and 1.6 m s^{-1} , respectively. Generated by `src/input_output_plot.m`.

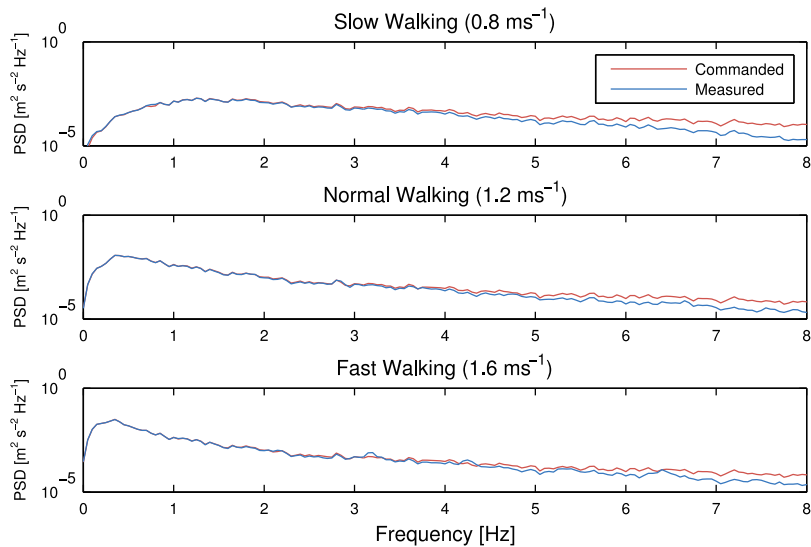


Figure 3 Power spectral density of the commanded treadmill belt speed (red) and the recorded speed (blue) for average belt speeds of 0.8 m s^{-1} , 1.2 m s^{-1} and 1.6 m s^{-1} , respectively. Generated by `src/frequency_analysis.m`.

commanded treadmill control input signal. The system introduces a delay and seems to act as a low pass filter. The standard deviations of the measured speeds do not significantly differ from those of the commanded speeds: 0.05 m s^{-1} , 0.12 m s^{-1} and 0.2 m s^{-1} for the three speeds, respectively.

Figure 3 gives a frequency domain view of the effects of the treadmill dynamics. These spectral density plots were created by averaging a spectrogram of a twenty second Hamming window. For all speeds, the frequency content of the commanded and measured

Table 3 A list of unloaded trials collected for each speed. Each loaded trial includes a compensation file listed in its meta data which matches it to these unloaded trials. Generated by `src/subject_table.py`.

Speed	Trial Numbers
0.8 m/s	22, 30, 34, 43, 52, 58, 64, 70, 79
1.2 m/s	3, 4, 5, 23, 29, 35, 44, 53, 59, 65, 71, 80
1.6 m/s	24, 28, 36, 45, 54, 60, 66, 72, 81

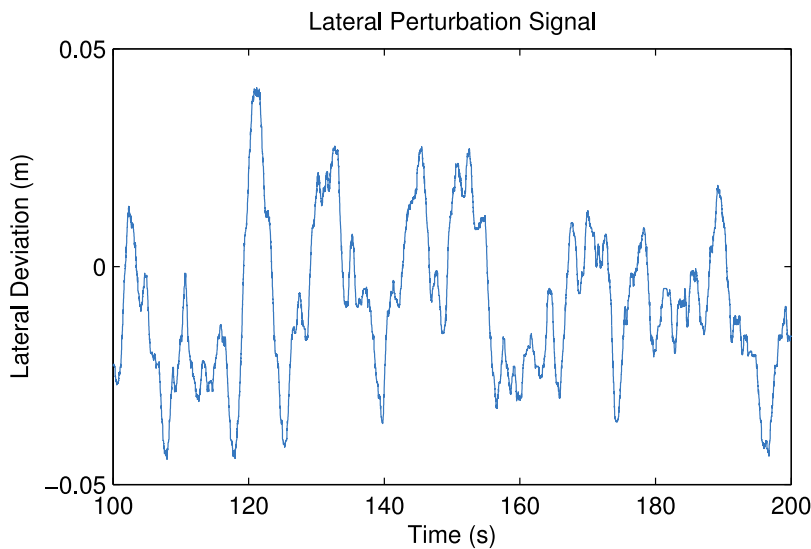


Figure 4 The measured lateral deviation of the treadmill base from trial 6. Generated by `src/lateral_perturbation_plot.m`.

time series show similarity below 4 Hz and attenuation in the measured spectral density above 4 Hz.

When belt speed is not constant, the inertia of the rollers and motor will likely induce error in the force plate x axis moment, and hence, the anterior-posterior coordinate (z axis) of the center of pressure that is measured by the instrumentation in the treadmill. This error may or may not be pertinent to different analyses. If needed, this error can be partially compensated by a linear model as shown in [Hnat & Van den Bogert \(2014\)](#). The model coefficients can be identified from the unloaded trials given in **Table 3**. The error due to inertia is random and does not affect the averaged joint moments presented in [Fig. 5](#). Compensation should, however, be done if joint moments from individual gait cycles are of interest rather than the ensemble average.

In addition to the longitudinal perturbations, lateral perturbations were also prescribed for a duration of four minutes in the pilot trials 3–8. [Figure 4](#) shows an example of the measured lateral deviation of the treadmill base. These signals were generated in a similar manner using MATLAB and Simulink in which a Gaussian white noise block was twice integrated to obtain the lateral deviation. The signal was then high-pass filtered with a second-order Butterworth filter to eliminate drift and then saturated so that the signal

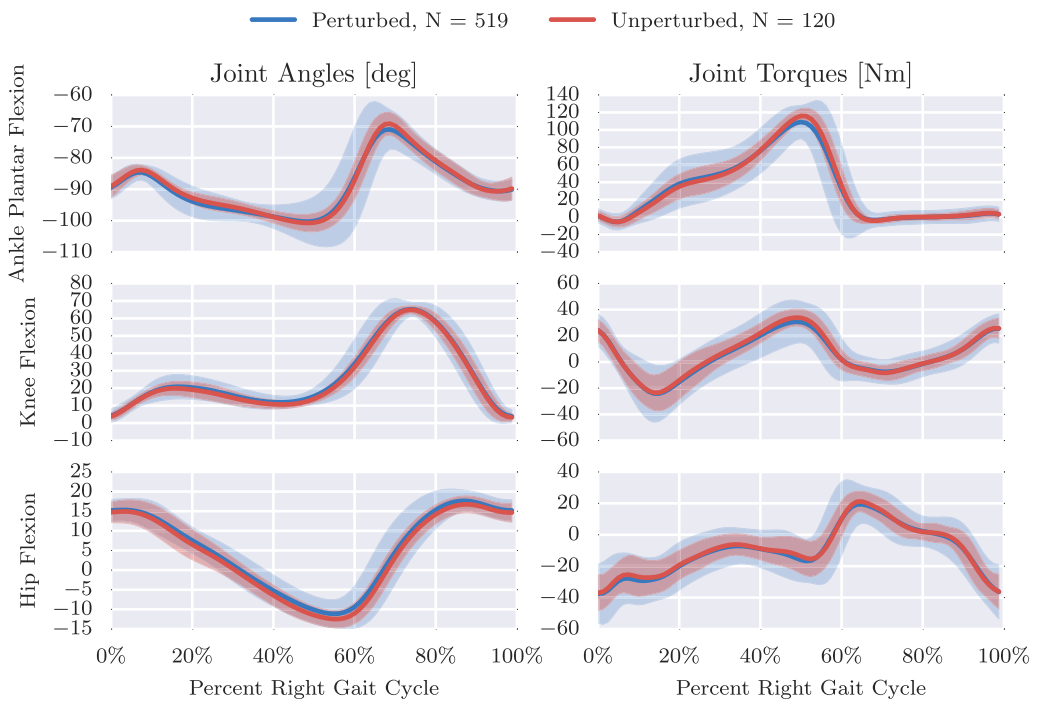


Figure 5 Right leg mean and 3σ (shaded) joint angles and torques from both unperturbed (red) and perturbed (blue) gait cycles from trial 20. We define the nominal configuration, i.e., all joint angles equal to zero, such that the vectors from the shoulder to the hip, the hip to the knee, the knee to the ankle, and the heel to the toe are all aligned. Produced by `src/unperturbed_perturbed_comparison.py`.

remained within the 5 cm lateral range of the physical hardware. The same perturbation signal was used for each of the three trials.

RESULTS

Here we present some basic results. We first provide a detailed description of the raw data followed by an overview of several computed variables that give an idea of the characteristics of both the unperturbed and perturbed gait.

Raw data

The raw data consists of a set of ASCII tab delimited text files output from both the “mocap” and “record” modules in D-Flow in addition to a manually generated YAML³ file that contains all of the necessary meta data for the given trial. These three files are stored in a hierarchy of directories with one trial per directory. The directories are named in the following fashion T001/ where T stands for “trial” and the following three digits provide a unique trial identification number.

mocap-xxx.txt

The output from the D-Flow mocap module is stored in a tab separated value (TSV) file named `mocap-xxx.txt` where `xxx` represents the trial id number. The file contains a number of time series. The numerical values of the time series are provided in decimal fixed point notation with 6 decimals of precision, e.g., 123456.123456, regardless of the

³ YAML is a human readable data serialization format. See [Listing 1](#) for an example.

units. The first line of the file holds the header. The header includes time stamp column, frame number column, marker position columns, force plate force/moment columns, force plate center of pressure columns, and other analog columns. The columns are further described below:

TimeStamp The monotonically increasing computer clock time when D-Flow receives a frame from Cortex. These are recorded approximately at 100 Hz sampling rate and given in seconds. Due to data buffering, it is preferred to derive sample times from the FrameNumber column rather than TimeStamp.

FrameNumber Monotonically increasing positive integers that correspond to each frame received from Cortex.

Marker Coordinates Any column that ends in .PosX, .PosY, or .PosZ are marker coordinates expressed in Cortex's Cartesian reference frame. The prefixes match the marker labels given in [Table 2](#). These values are in meters.

Ground Reaction Loads There are three ground reaction forces and three ground reaction moments recorded by each of the two force plates in Newtons and Newton-Meters, respectively. The prefix for these columns is either FP1 or FP2 and represents either force plate 1 (left) or 2 (right). The suffixes are either .For[XYZ], .Mom[XYZ] for the forces and moments, respectively. The force plate voltages are sampled at a much higher frequency than the cameras, but delivered at the Cortex camera sample rate, approximately 100 Hz, through the D-Flow mocap module. A force/moment calibration matrix stored in Cortex converts the voltages to forces and moments before sending it to D-Flow. The software also computes the center of pressure from the forces, moments, and force plate dimensions. These have the same prefixes for the plate number, have the suffix .Cop[XYZ], and are given in meters.

Analog Channels Several analog signals are recorded under column headers Channel[1-99].Anlg. These correspond to analog signals sampled by Cortex and correspond to the 96 analog channels in the National Instruments USB-6255. The first twelve are the voltages from the force plate load cells. We also record the acceleration of 4 points on the treadmill base in analog channels 61–72 that were in place in case inertial compensation for the lateral treadmill movement was required.

We make use of the full body 47 marker set described in [Van den Bogert et al. \(2013\)](#) and presented in detail in [Table 2](#). As with all camera based motion capture systems, the markers sometimes go missing in the recording. When a marker goes missing, if the data was recorded in a D-Flow version less than 3.16.2rc4, D-Flow continues to record the last non-missing value in all three axes until the marker is visible again. In D-Flow versions greater than or equal to 3.16.2rc4, the missing markers are indicated in the TSV file as either 0.000000 or -0.000000. The D-Flow version must be provided in the meta data YAML file to be able to distinguish this detail.

record-xxx.txt

The record module also outputs a tab delimited ASCII text file with numerical values at six decimal digits. It includes a Time column which records the D-Flow system time in

seconds. This time corresponds to the time recorded in the `TimeStamp` column in mocap module TSV file which is necessary for time synchronization. There are two additional columns `RightBeltSpeed` and `LeftBeltSpeed` which provide the independent belt speeds measured in meters per second by a factory installed encoder in the treadmill.

Additionally, the record module is capable of recording the time at which various preprogrammed events occur, as detected or set by D-Flow. It does this by inserting commented (#) lines in between the rows when the event occurred. The record files have several events that delineate the different phases of the protocol:

- A: Force Plate Zeroing** Marks the time at the beginning of the trial at which there is no load on the force plates and when the force plate voltages were zeroed.
- B: Calibration Pose** Marks the time at which the person is in the calibration pose.
- C: First Normal Walking** Marks the time when the treadmill begins Phase 1: constant belt speed.
- D: Longitudinal Perturbation** Marks the time when the treadmill begins Phase 2: longitudinal perturbations in the belt speed.
- E: Second Normal Walking** Marks the time when phase 3 starts: constant belt speed.
- F: Unloaded End** Marks the time at which there is no load on the force plates and the belts are stationary.

meta-xxx.yml

Each trial directory contains a meta data file in the YAML format named in the following style `meta-xxx.yml` where `xxx` is the three digit trial identification number. There are three main headings in the file: `study`, `subject`, and `trial`. An example meta data file is shown in [Listing 1](#).

The `study` section contains identifying information for the overall study, an identification number, name, and description. This is the same for all meta data files in the study. Details are given below:

- id** An integer specifying a unique identification number of the study.
- name** A string giving the name of the study.
- description** A string with a basic description of the study.

The `subject` section provides key value pairs of information about the subject in that trial. Each subject has a unique identification number along with basic anthropomorphic data. The following details the possible meta data for the subject:

- age** An integer age in years of the subject at the time of the trial.
- ankle-width-left** A float specifying the width of the subjects left ankle.
- ankle-width-right** A float specifying the width of the subjects right ankle.
- ankle-width-units** A string giving the units of measurement of the ankle widths.
- id** An unique identification integer for the subject.
- gender** A string specifying the gender of the subject.
- height** A float specifying the measured height of the subject (with shoes and hat on) at the time of the trial.

height-units A string giving the units of the height measurement.
knee-width-left A float specifying the width of the subjects left knee.
knee-width-right A float specifying the width of the subjects right knee.
knee-width-units A string giving the units of measurement of the knee widths.
mass A float specifying the self-reported mass of the subject.
mass-units A string specifying the units of the mass measurement.

The trial section contains the information about the particular trial. Each trial has a unique identification number along with a variety of other information, detailed below:

analog-channel-map A mapping of the strings D-Flow assigns to signals emitted from the analog channels of the NI USB-6255 to names the user desires.
cortex-version The version of Cortex used to record the trial.
datetime A date formatted string giving the date of the trial in the YYYY-MM-DD format.
dflow-version The version of D-Flow used to record the trial.
events A key value map which prescribes names to the alphabetic events recorded in the record file.
files A key value mapping of files associated with this trial where the key is the D-Flow file type and the value is the path to the file relative to the meta file. The compensation file corresponds to an unloaded trial collected on the same day that could be used for inertial compensation purposes, if needed.
hardware-settings There are tons of settings for the hardware in both D-Flow, Cortex, and the other software in the system. This contains any non-default settings.
high-performance A boolean value indicating whether the D-Flow high performance setting was on (True) or off (False).
id An unique three digit integer identifier for the trial. All of the file names and directories associated with this trial include this number.
marker-map A key value map which maps marker names in the mocap file to the user's desired names for the markers.
marker-set Indicates the HBM ([Van den Bogert et al., 2013](#)) marker set used during the trial, either full, lower, or NA.
nominal-speed A float representing the nominal desired treadmill speed during the trial.
nominal-speed-units A string providing the units of the nominal speed.
notes A string with any notes about the trial.
pitch A boolean that indicates if the treadmill pitch degree of freedom was actuated during the trial.
stationary-platform A boolean that indicates whether the treadmill sway or pitch motion was actuated during the trial. If this flag is false, the measured ground reaction loads must be compensated for the inertial affects and be expressed in the motion capture reference frame.
subject-id An integer corresponding to the subject in the trial.
sway A boolean that indicates if the treadmill lateral degree of freedom was actuated during the trial.

```
study:
  id: 1
  name: Gait Control Identification
  description: Perturb the subject during walking and running.
subject:
  id: 8
  age: 20
  mass: 70.0
  mass-units: kilograms
  height: 1.572
  height-units: meters
  knee-width-left: 107.43
  knee-width-right: 107.41
  knee-width-units: millimeters
  ankle-width-left: 70.52
  ankle-width-right: 67.66
  ankle-width-units: millimeters
  gender: male
trial:
  id: 58
  subject-id: 8
  datetime: 2014-03-28
  notes: >
    The subject did a somersault during this trial instead of following
    instructions to walk. Will have to use for another study.
  nominal-speed: 0.8
  nominal-speed-units: meters per second
  stationary-platform: True
  pitch: False
  sway: False
  hardware-settings:
    high-performance: True
    dfflow-version: 3.16.1
    cortex-version: 3.1.1.1290
  marker-set: full
  marker-map:
    M1: LHEAD
    M2: THEAD
    M3: RHEAD
    M4: FHEAD
    M5: C7
  analog-channel-map:
    Channel1.Anlg: F1Y1
    Channel2.Anlg: F1Y2
    Channel3.Anlg: F1Y3
    Channel4.Anlg: F1X1
events:
  A: Force Plate Zeroing
  B: Calibration Pose
  C: First Normal Walking
  D: Longitudinal Perturbation
  E: Second Normal Walking
  F: Unloaded End
files:
  compensation: ./T057/mocap-057.txt
  mocap: mocap-058.txt
  record: record-058.txt
  meta: meta-058.yml
```

Listing 1: A fictitious example of a YAML formatted meta data file. Examples of all of the possible keys in the data set are shown.

Processed data

We developed a toolkit for data processing, GaitAnalysisToolKit v0.1.2 ([Moore et al., 2014](#)) for common gait computations and provide an example processed trial to present the nature of the data. The tool was developed in Python, is dependent on the SciPy Stack [NumPy ([Walt, Colbert & Varoquaux, 2011](#)), SciPy ([Jones et al., 2001](#)), matplotlib ([Hunter, 2007](#)), Pandas ([McKinney, 2010](#)), etc] and Octave ([Octave community, 2014](#)), and provides two main classes: one to do basic gait data cleaning from D-Flow's output files, DFlowData, and a second to compute common gait variables of interest, GaitData.

The DFlowData class collects and stores all the raw data presented in the previous section and applies several “cleaning” operations to transform the data into a usable form. The cleaning process follows these steps:

1. Load the meta data file into a Python dictionary.
2. Load the D-Flow mocap module TSV file into Pandas DataFrame.
3. Relabel the column headers to more meaningful names if this is specified in the meta data.
4. Optionally identify the missing values in the mocap marker data and replace them with `numpy.nan`.
5. Optionally interpolate the missing marker values and replaces them with interpolated estimates using a variety of interpolation methods.
6. Load the D-Flow record module TSV file into a Pandas DataFrame.
7. Extract the events and create a dictionary mapping the event names in the meta data to the events detected in the record module file.
8. Inertially compensate the ground reaction loads based on whether the meta data indicates there was treadmill motion.
9. Merge the data from the mocap module and record module into one data frame at the maximum common constant sample rate.

Once the data is cleaned there are two methods that allow the user to extract the cleaned data: either extract sections of the data bounded by the events recorded in the `record-xxx.txt` file or save the cleaned data to disk. These operations are available as a command line application and as an application programming interface (API) in Python. An example of the DFlowData API in use is provided in [Listing 2](#).

The GaitData class is then used to compute gait events (toe off and heel strike times), basic 2D inverse kinematics and dynamics, and to store the data into a Pandas Panel with each gait cycle on the item axis at a specified sampling rate. This object can also be serialized to disk in HDF5 format. An example of using the Python API is shown in [Listing 3](#).

A similar work flow was used to produce [Fig. 5](#) which compares the mean and standard deviation of sagittal plane joint angles and torques from the perturbed gait cycles to the unperturbed gait cycles computed from trial 20. This gives an idea of the more highly variable dynamics required to walk while being longitudinally perturbed.

```
>>> from gaitanalysis.motek import DFlowData
>>> data = DFlowData('mocap-020.txt', 'record-020.txt',
...                   'meta-020.yml')
>>> mass = data.meta['subject']['mass']
>>> data.clean_data()
>>> event_df = data.extract_processed_data(
...     event='Longitudinal Perturbation')
```

Listing 2: Python interpreter session showing how one could load a trial into memory, extract the subject's mass from the meta data, run the data cleaning process, and finally extract a Pandas DataFrame containing all of the time histories for a specific event in the trial.

```
>>> from gaitanalysis.gait import GaitData
>>> gdata = GaitData(event_df)
>>> gdata.inverse_dynamics_2d(left_markers, right_markers,
...                             left_loads, right_loads, mass, 6.0)
>>> gdata.grf_landmarks('Right Fy', 'Left Fy', threshold=20.0)
>>> gdata.split_at('right')
>>> gdata.plot_gait_cycles('Left Hip Joint Torque', mean=True)
>>> gdata.save('gait-data.h5')
```

Listing 3: Python interpreter session showing how one could use the `GaitData` class to load in the result of `DFlowData` and compute the inverse dynamics (joint angles and torques), identify the gait events (e.g., heel strikes), split the data with respect to the gait events into a Pandas Panel, plot the mean and standard deviation of one time history with respect to the gait cycles, and save the data to disk.

For more insight into the difference in the unperturbed and perturbed data, Fig. 6 compares the distribution of a few gait cycle statistics. One can see that the perturbed strides have a much larger variation in frequency and length and even larger variation in stride width. It is also interesting to note that the coupled nature of the system's degrees of freedom can be exploited to increase the stride width with only longitudinal perturbations, although not relatively as much as is in the other statistics.

Data limitations

The data is provided in good faith with great attention to detail but as with all data there are anomalies that may affect the use and interpretation of results emanating from the data. The following lists give various notes and warnings about the data that should be taken into account before use.

All trials

- Be sure to read the notes in each meta data file for details about possible anomalies in that particular trial. Things such as marker dropout, ghost markers, and marker movement are the more prominent notes. Details about variations in the equipment on the day of the trial are also mentioned.

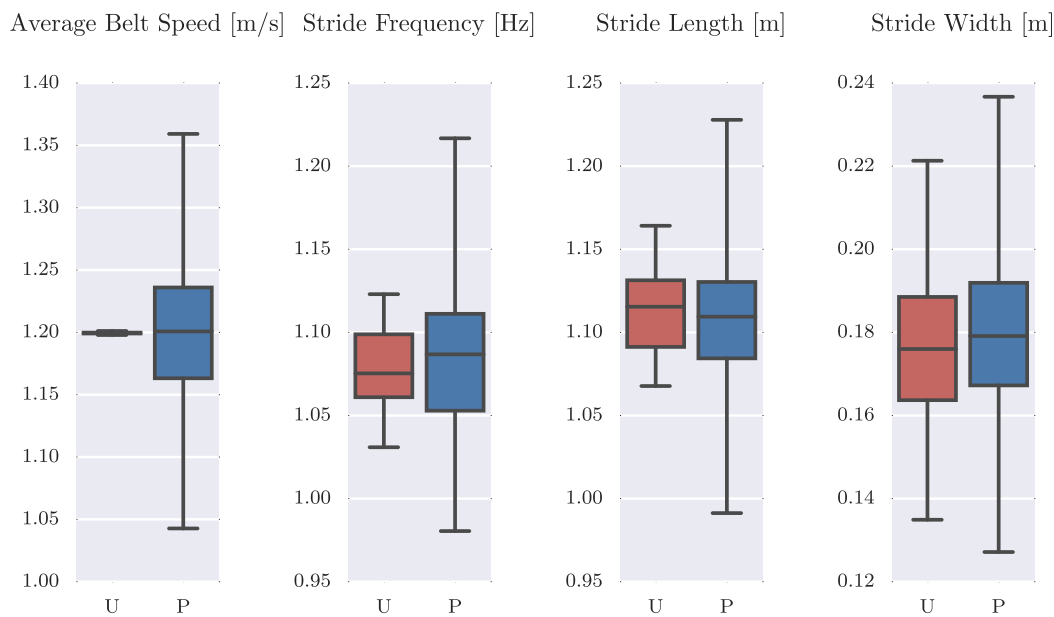


Figure 6 Box plots of the average belt speed, stride frequency, stride length, and stride width which compare 120 unperturbed (U: red) and 519 perturbed (P: blue) gait cycles. The median is given with the box bounding the first and third quartiles and the whiskers bound the range of the data. Produced by `src/unperturbed_perturbed_comparison.py`.

- The subject identification number 0 represents the “null subject” and was used whenever data was collected from the system with no subject on the treadmill, for example during the trials that were intended to be used for inertial compensation purposes. These trials play through the exact protocol as those with a human subject and the matching trials are indicated in the meta data. Matching unloaded trials were recorded on the same day as the loaded trials and is noted in the `trial:files:compensation` section of the meta data file. See [Table 3](#) for a list of all the compensation trials.
- Trials 1 and 2 were not recorded as part of this study. Those trial identification numbers were reserved for early data exploration from data collected in other studies and are not included in this dataset.
- Trials 37, 38, and 39 do not exist. The numbers were accidentally skipped.
- The ankle joint torques computed from subject 9’s data in trials 25–27 are abnormal and should be used with caution or not at all. We were not able to locate the source of the error, but it is likely related to the force calibration.

Pilot trials

- Subject 1 walked only at a single speed with three trial repetitions.
- Trials 6–8 included a calibration pose at the start of the trial but the event was not explicitly recorded. In those trials, the “TreadmillPerturbation” event marks the beginning of longitudinal perturbations and the “Both” event marks the beginning of combined longitudinal and lateral perturbations. The force plate zeroing at the end was also not explicitly recorded.

- Trials 6–8's force measurements are affected by the treadmill vibration mode mentioned in the equipment section and the force plate data should not be used.
- Trials 9–11 used a slightly different event definition where the calibration poses were not explicitly tagged by an event, yet the protocol was identical to the following trials. The calibration pose will have to be determined manually.
- During trials 9–15, we used wooden blocks to fix the treadmill to the concrete floor to eliminate the treadmill's low vibration mode. But these blocks seem to have corrupted the force plate measurements by imposing frictional stresses on the system. The force plate measurements should not be used from these trials.
- We did not record unloaded compensation trials for trials 9–15. Regardless, they would likely be useless due to the corruption from the wooden blocks and are not needed because the treadmill base is fixed.

CONCLUSION

We have presented a rich and elaborate data set of motion and ground reaction loads from human subjects during both normal walking and when recovering from perturbations. The raw data is provided for reuse with complete meta data. In addition to the data, we provide software that can process the data for both cleaning purposes and to produce typical sagittal plane gait variables of interest. Among other uses, we believe the dataset is ideally suited for control identification purposes. Many researchers are working on mathematical models for control in gait and this dataset provides both a way to validate these models and a source for generating them.

ACKNOWLEDGEMENTS

We thank Roman Boychuk and Obinna Nwanna for assistance with the experiments. We also thank Sabrina Abram, Brad Humphreys, and Anne Koelewijn for reviewing the preprint and being our guinea pigs on the software/data instructions. Dan Simon also gave valuable feedback on the preprint. Furthermore, we thank the academic editor, Arti Ahluwalia, and three reviewers, Morgan Sangeux, Paul Lee, and Manoj Srinivasan, for their valuable feedback which helped improve the quality of the paper and data.

ADDITIONAL INFORMATION AND DECLARATIONS

Funding

The work was partially funded by the State of Ohio Third Frontier Commission through the Wright Center for Sensor Systems Engineering (WCSSE) and by the National Science Foundation under Grant No. 1344954. The funders had no role in study design, data collection and analysis, decision to publish, or preparation of the manuscript.

Grant Disclosures

The following grant information was disclosed by the authors:

Wright Center for Sensor Systems Engineering (WCSSE).

National Science Foundation: 1344954.

Competing Interests

The authors declare there are no competing interests.

Author Contributions

- Jason K. Moore and Sandra K. Hnat conceived and designed the experiments, performed the experiments, analyzed the data, contributed reagents/materials/analysis tools, wrote the paper, prepared figures and/or tables, reviewed drafts of the paper.
- Antonie J. van den Bogert conceived and designed the experiments, contributed reagents/materials/analysis tools, wrote the paper, reviewed drafts of the paper.

Human Ethics

The following information was supplied relating to ethical approvals (i.e., approving body and any reference numbers):

The study was approved by the Institutional Review Board of Cleveland State University (# 29904-VAN-HS) and informed consent was obtained from all participants.

Data Deposition

The following information was supplied regarding the deposition of related data:

Zenodo:

- <http://dx.doi.org/10.5281/zenodo.13030>
- <http://dx.doi.org/10.5281/zenodo.13253>
- <http://dx.doi.org/10.5281/zenodo.13159>
- <http://dx.doi.org/10.5281/zenodo.16064>

REFERENCES

- Chester VL, Tingley M, Biden EN. 2007. Comparison of two normative paediatric gait databases. *Dynamic Medicine* 6(8) DOI 10.1186/1476-5918-6-8.
- European Commission. 2012. Scientific data: Open access to research results will boost Europe's innovation capacity. Press release. Available at http://europa.eu/rapid/press-release_IP-12-790_en.htm?locale=en.
- Geyer H, Herr H. 2010. A muscle-reflex model that encodes principles of legged mechanics produces human walking dynamics and muscle activities. *Neural Systems and Rehabilitation Engineering, IEEE Transactions on* 18(3):263–273 DOI 10.1109/TNSRE.2010.2047592.
- Hnat S, Van den Bogert AJ. 2014. Inertial compensation for belt acceleration in an instrumented treadmill. *Journal of Biomechanics* 47(15):3758–3761 DOI 10.1016/j.jbiomech.2014.10.014.
- Hnat SK, Moore JK, Van den Bogert AJ. 2015. Commanded treadmill motions for perturbation experiments. Available at <http://zenodo.org/record/16064>.
- Hodgins J. 2015. CMU graphics lab motion capture database. Available at <http://mocap.cs.cmu.edu>.
- Hunter JD. 2007. Matplotlib: a 2D graphics environment. *Computing in Science & Engineering* 9(3):90–95 DOI 10.1109/MCSE.2007.55.
- Jones E, Oliphant T, Peterson P. 2001. SciPy: open source scientific tools for Python. Available at <http://www.scipy.org/>.
- Kirtley C. 2014. CGA normative gait database. Available at <http://www.clinicalgaitanalysis.com/data/>.

- Makihara Y, Mannami H, Tsuji A, Hossain M, Sugiura K, Mori A, Yagi Y.** 2012. The OU-ISIR gait database comprising the treadmill dataset. *IPSJ Transactions on Computer Vision and Applications* 4:53–62 DOI 10.2197/ipsjtcva.4.53.
- McKinney W.** 2010. Data structures for statistical computing in Python. In: *Proceedings of the 9th Python in Science Conference*. Austin: Enthought, Inc., 51–56. Available at https://conference.scipy.org/scipy2010/slides/wes_mckinney_data_structure_statistical_computing.pdf.
- Moore JK, Hnat S, Van den Bogert A.** 2014. An elaborate data set on human gait and the effect of mechanical perturbations. Available at <https://zenodo.org/record/13030>.
- Moore JK, Nwanna O, Hnat S, Van den Bogert A.** 2014. *GaitAnalysisToolKit*. Version 0.1.2. Available at <http://dx.doi.org/10.5281/zenodo.13159>.
- Octave community.** 2014. GNU Octave 3.8.1. Available at <https://www.gnu.org/software/octave/>.
- Sup F, Bohara A, Goldfarb M.** 2008. Design and control of a powered transfemoral prosthesis. *The International Journal of Robotics Research* 27(2):263–273 DOI 10.1177/0278364907084588.
- Tirosh O, Baker R, McGinley J.** 2010. GaitaBase: web-based repository system for gait analysis. *Computers in Biology and Medicine* 40(2):201–207 DOI 10.1016/j.combiomed.2009.11.016.
- Van den Bogert AJ.** 2003. Exotendons for assistance of human locomotion. *BioMedical Engineering OnLine* 2(17) DOI 10.1186/1475-925X-2-17.
- Van den Bogert AJ, Geijtenbeek T, Even-Zohar O, Steenbrink F, Hardin EC.** 2013. A real-time system for biomechanical analysis of human movement and muscle function. *Medical & Biological Engineering & Computing* 51(10):1069–1077 DOI 10.1007/s11517-013-1076-z.
- Vaughan C, Davis B, O'Connor J.** 1992. *Dynamics of Human Gait*. 1st edition. Champaign: Human Kinetics Publishers.
- Walt Svd, Colbert SC, Varoquaux G.** 2011. The NumPy array: a structure for efficient numerical computation. *Computing in Science & Engineering* 13(2):22–30 DOI 10.1109/MCSE.2011.37.
- Wang Y, Srinivasan M.** 2014. Stepping in the direction of the fall: the next foot placement can be predicted from current upper body state in steady-state walking. *Biology Letters* 10(9):20140405 DOI 10.1098/rsbl.2014.0405.
- White EP, Baldridge E, Brym ZT, Locey KJ, McGlinn DJ, Supp SR.** 2013. Nine simple ways to make it easier to (re)use your data. *PeerJ PrePrints* 1:e7v2 DOI 10.7717/peerj.72.
- White House.** 2013. Increasing access to the results of federally funded scientific research. Available at https://www.whitehouse.gov/sites/default/files/microsites/ostp/ostp_public_access_memo_2013.pdf.
- Willson JD, Kernozeck T.** 2014. Gait data collected at University of Wisconsin-LaCrosse. Available at <http://www.innsport.com/related-products/data-sets/uw-l-gait-data-set.aspx>.
- Winter DA.** 1990. *Biomechanics and motor control of human movement*. 2nd edition. Hoboken: John Wiley & Sons.
- Yun Y, Kim H-C, Shin SY, Lee J, Deshpande AD, Kim C.** 2014. Statistical method for prediction of gait kinematics with Gaussian process regression. *Journal of Biomechanics* 47(1):186–192 DOI 10.1016/j.jbiomech.2013.09.032.

Adaptive smartphone-based sensor fusion for estimating competitive rowing kinematic metrics

Bryn Cloud¹, Britt Tarien¹, Ada Liu¹, Thomas Shedd¹, Xinfan Lin¹, Mont Hubbard¹, R. Paul Crawford², Jason K. Moore^{1*}

1 Mechanical and Aerospace Engineering, University of California, Davis, California, USA

2 Hegemony Technologies LLC, Davis, California, USA

* jkm@ucdavis.edu

Abstract

Competitive rowing highly values boat position and velocity data for real-time feedback during training, racing and post-training analysis. The ubiquity of smartphones with embedded position (GPS) and motion (accelerometer) sensors motivates their possible use in these tasks. In this paper, we investigate the use of two real-time digital filters to achieve highly accurate yet reasonably priced measurements of boat speed and distance traveled. Both filters combine acceleration and location data to estimate boat distance and speed; the first using a complementary frequency response-based filter technique, the second with a Kalman filter formalism that includes adaptive, real-time estimates of effective accelerometer bias. The estimates of distance and speed from both filters were validated and compared with accurate reference data from a differential GPS system with better than 1 cm precision and a 5 Hz update rate, in experiments using two subjects (an experienced club-level rower and an elite rower) in two different boats on a 300 m course. Compared with single channel (smartphone GPS only) measures of distance and speed, the complementary filter improved the accuracy and precision of boat speed, boat distance traveled, and distance per stroke by 44%, 42%, and 73%, respectively, while the Kalman filter improved the accuracy and precision of boat speed, boat distance traveled, and distance per stroke by 48%, 22%, and 82%, respectively. Both filters demonstrate promise as general purpose methods to substantially improve estimates of important rowing performance metrics.

Introduction

Non-intrusive collection of data from athletes during practice and competition provides opportunities for evidenced-based performance evaluation and coaching. Traditional kinematic measurement techniques in sports have frequently required elaborate equipment to capture the motion of human body segments and associated sports equipment; see examples in [1]. With the growing functionality and ubiquity of smartphones, athletes and coaches have access to an increasingly capable and sophisticated measurement system that includes the phone's inertial measurement unit (three dimensional angular rate gyroscope, accelerometer, and magnetometer) and determinants of location (GPS, GLONASS, etc.). Modern smartphone technology provides position measurements that can be sampled up to about 1 Hz with stationary absolute accuracy between 0.5 m to 16 m and stationary root mean square error (RMSE)

between 14 m to 71 m, making them more precise than accurate [2]. The phones also output acceleration and angular velocity data at rates up to about 200 Hz [3].

Competitive rowing aims at maximizing the average boat speed over a specified race distance. For competitions over a typical race distance, the time domain race-to-race variability for elite rowers is approximately 1% and this has been proposed as “an irreducible error for any measure of rowing performance” [4]. However, the discrete unit of action and control in rowing is the stroke and this accordingly represents the domain in which many training and racing parameters are communicated and analyzed. For example, rowing speed is represented in the stroke domain as the product of stroke rate and distance per stroke.

In Olympic rowing races, the historical speed difference between finish positions (first and second; second and third; etc.) has averaged at 0.42% [5]. Contextualized in the approximately 200 strokes that it takes to complete a 2000 m race, rowers who generate an additional 5 cm per stroke will ordinarily gain a one place improvement in race finish. Thus, it follows that the accuracy and precision of distance per stroke measurements must be better than 5 cm in order to generate meaningful insight and feedback. Satellite-based positioning systems (GPS, etc.) do not ordinarily afford this level of accuracy and precision thus limiting their effectiveness in the analysis of any individual stroke. We posit that more accurate and precise measures of boat movements for individual strokes will enable a more direct examination of the causal relationships between rower-oar-boat system mechanics and race performance. Therefore this study seeks to improve the accuracy and precision of rowing performance metric measurements.

The paper begins with a brief review of the immediately related literature and is followed by an explanation of the problem and statistics used to quantify accuracy and precision of the desired kinematic performance metrics. Two methods are then presented for fusing the smartphone position and motion data to generate more accurate estimates of these metrics. Finally, the estimates are presented against ground truth data collected from a differential GPS (DGPS) system for validation. We close with discussion of the implications and use cases.

Related work

Real-time water-relative boat speed in rowing has traditionally been measured by either a pitot tube or a small impeller attached to the hull. Modern speedometers make use of GPS receivers to calculate Earth-relative speed and distance in the distance, time, and stroke domains. For example, the popular SpeedCoach GPS (Nielsen Kellerman, Boothwyn, PA, USA) outputs metrics such as boat speed, stroke rate, distance, and elapsed time based on GPS and/or impeller measurements. The accuracy and utility of these systems are limited by the position measurement accuracy and/or the uncertain and frequently fluctuating current velocity. GPS alone has been used to measure position during long distance (15,000 m) rowing events [6] and low cost GPS systems have also been shown to be capable of providing real-time speed estimates during rowing [7].

Other references exist with high accuracy (0.1 m s^{-1} to 0.3 m s^{-1}) GPS measurements for rowing [8] and the use of high accuracy differential GPS [9], but these systems are often impractical for ordinary rowing applications because they require establishing and operating an additional stationary base station. There has been success in creating differential GPS systems from a network of smartphones that improve location estimates to 1 cm accuracy at 1 Hz [10] and a differential GPS-tailored Kalman filter has been used for the specific task of rowing position prediction [11].

Researchers have improved the accuracy of position and speed estimates in rowing

63
64
65
66
67
68
69
70
71
72
73
74
75
76
77
78
79
80
81
82
83
84
85
86
87
88
89
90
91
92
93
94
95
96
97
98
99
100
101
102
103
104
105
106
107
108
109
110

by incorporating acceleration measures. Accelerometer-derived speed shows strong correlation to impeller-derived speed measurements in still water [12]. GPS and accelerometer sensor fusion have been used to estimate position and velocity during GPS network downtime [13, 14]. Reference [15] compares GPS accelerometer-derived velocity to high speed video footage, and [16] measures differential GPS and acceleration showing the utility of advanced sensors.

A network of IMUs on the rower can capture rowing with results similar to motion capture cameras [17] and real-time accelerometer-based feedback has been found to improve rowing consistency when used on indoor ergometers [18]. Tessendorf et. al [19] use an elaborate IMU sensor array (Xsens, Enschede, Netherlands) to demonstrate the utility of metrics for characterizing on-water rowing performance but this system requires extensive setup time and expertise and is cost prohibitive for the typical rower. Various filters have been used to improve smartphone position estimates for walking in [20], but the large sensor error causes difficulties when applied to this more general problem.

Among the various methods that have been proposed to improve measurement results during rowing, the most similar to the present paper is that of Hermsen [21]. Hermsen's primary goal was to estimate the position, speed, and stroke rate of the boat based on a consumer-grade accelerometer and GPS sensor for real-time wireless transmission and display to viewers of the rowing event. The proposed linear Kalman filter-based approach fused data from the two sensors and estimated rowing speed. The found finish times are 14% more accurate than those estimated with GPS data alone. Although real-time estimates were desired, this solution to handling sensor orientation bias required an offline after-the-fact computation leaving real-time implementation infeasible.

None of these prior methods offer an accurate and precise estimate of boat distance traveled and boat speed that is inexpensive, simple, works with a single consumer grade GPS sensor, and can operate in real-time. In this paper, we present two methods that can do so. These methods provide a strong foundation for further improvements to the desired estimates.

Problem formulation

We desire highly accurate estimates of the distance the boat travels along its path during each individual stroke using readily available and easy to use consumer products, such as, a smartphone. High accuracy allows for inter-rower, -race, and -day repeatable comparisons in both distance traveled and boat speed. In competitive rowing, boats move on the order of 10 m per stroke. We have found smartphones to have raw accuracy on the order of 1 m and a precision of 0.8 m by comparison with our differential GPS measurements; see Table 1. Our ultimate goal is to improve this distance accuracy by roughly two orders of magnitude, allowing distance per stroke estimates that approach 1 cm accuracy. Additionally, we want the capability of calculating these estimates in real time and to not rely on knowledge of the specific boat and rower to facilitate easy to use and simple real-time training feedback to coaches and rowers. Our proposed methods to accomplish these goals consist of four major components:

Data collection A smartphone is rigidly attached to a boat and used to collect GPS data at an average sampling rate of 0.3 Hz and accelerometer data at approximately 100 Hz. (A differential GPS unit is also attached to the boat to measure boat position at approximately 5 Hz for validation purposes, but this is not part of the evaluated method.)

Table 1. Sensor measurement accuracy and precision.

The rows corresponding to the smartphone GPS provide the accuracy (central error, CE [2]) and precision (standard deviation, SD) of the GPS-derived position relative to simultaneously collected DGPS position of the moving pair of sensors (see the following section for our definitions of these statistics). The smartphone accelerometer rows provide a measure of precision of the sensor's body fixed acceleration when the smartphone is motionless. Similarly, the differential GPS rows provide a measure of precision of the motionless rower position relative to the motionless base station. The duration of the data logs used to derive these metrics and the frequency at which they were sampled are listed for each sensor.

Sensor	Measurement	Value
Smartphone GPS (Moving, 32 sec, 0.3 Hz)	CE of NS position	1.01 m
	CE of EW position	0.89 m
	SD in the NS position	0.81 m
	SD in the EW position	0.70 m
Smartphone Accelerometer (Motionless, 96 sec, 100 Hz)	SD along the X axis	2.67 mg
	SD along the Y axis	2.45 mg
	SD along the Z axis	1.59 mg
Differential GPS (Motionless, 57 sec, 10 Hz)	SD in the N-S position	3.2 mm
	SD in the E-W position	1.7 mm

Sensor fusion Fusion of the raw GPS and accelerometer measurements to estimate distance traveled at the accelerometer sampling rate (100 Hz).

Rowing metric computation Stroke transition detection is used to calculate the distance traveled per stroke, stroke rate, and boat speed.

Error estimates Estimates from the sensor fusion are compared to “true” values obtained from the differential GPS measurements.

Fig 1 provides a schematic of the aforementioned general flow of data and processing algorithms. The primary algorithms, i.e. transforming raw smartphone data to distance and speed estimates, are designed for real-time computing, but the actual results for the purposes of the paper were computed offline and are available in the companion software (see https://gitlab.com/mechmotum/row_filter). In this section we elaborate on the four components listed above, beginning with the characterization of the measurement data. We then propose the desired accuracy of the metrics, and finally provide the details of the two sensor fusion methods.

Accuracy and precision

It is worth carefully defining the accuracy and precision of repeated measurements of a motionless sensor and those of a moving sensor [2].

Accuracy specifies how close a given measurement is to the true value. In the case of planar Cartesian horizontal position measurements $(x_1 \dots x_n, y_1 \dots y_n)$ derived from latitude and longitude of a motionless sensor, we use the Central Error, CE, defined in [2] as a measure of accuracy. This is the Euclidean distance between the average of a set of measurements, (\bar{x}, \bar{y}) , and the sensor's true position, (x_s, y_s) .

$$\text{CE}_{xy}^2 = \left[\frac{1}{n} \sum_{i=1}^n (x_i - x_s)^2 \right]^{\frac{1}{2}} + \left[\frac{1}{n} \sum_{i=1}^n (y_i - y_s)^2 \right]^{\frac{1}{2}} = (\bar{x} - x_s)^2 + (\bar{y} - y_s)^2 \quad (1)$$

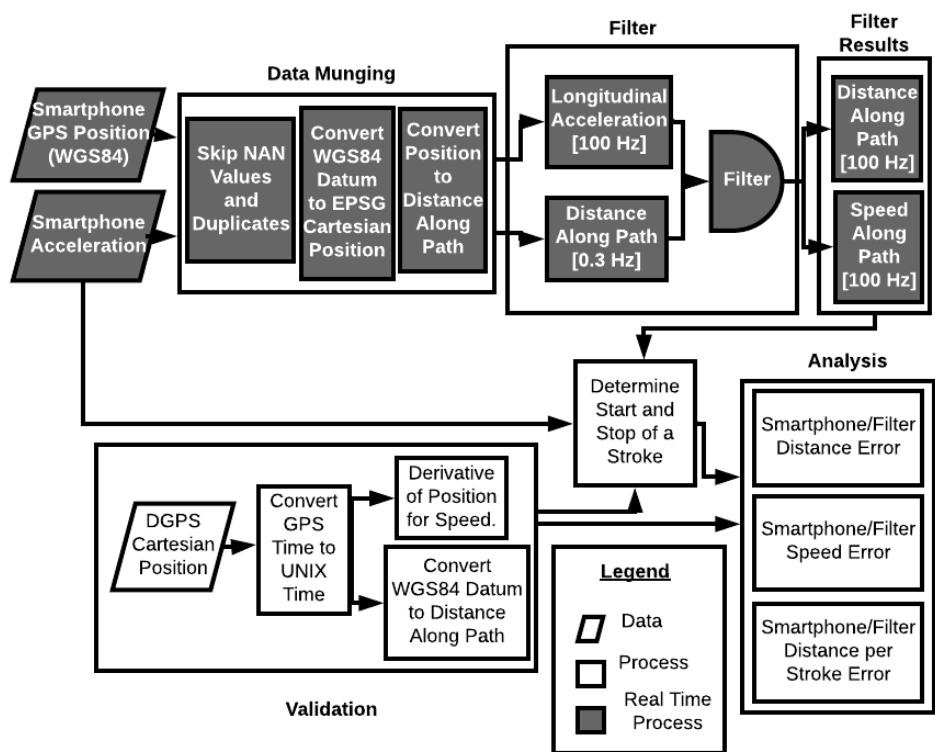


Fig 1. Data processing pipeline flow chart.

Grey rectangles indicate the real-time algorithm process. White rectangles indicate the validation process. Parallelograms represent raw data from the sensors.

Precision characterizes how repeatable measurements are. For measurements from a motionless sensor the standard deviation, σ , about the mean position in the planar Cartesian coordinates is a measure of precision.

$$\sigma_x^2 = \frac{1}{n} \sum_{i=1}^n (x_i - \bar{x})^2, \quad \sigma_y^2 = \frac{1}{n} \sum_{i=1}^n (y_i - \bar{y})^2 \quad (2)$$

The Federal Geographic Data Committee recommends using the Root Mean Square Error (RMSE) to characterize error in geographic position measurements [2]. It is important to note that RMSE is a function of both accuracy and precision. For example, increases in either the Central Error or the standard deviation will increase RMSE:

$$\text{RMSE}_{xy}^2 = \frac{1}{n} \sum_{i=1}^n [(x_i - x_s)^2 + (y_i - y_s)^2] = \text{CE}_{xy}^2 + \frac{n-1}{n} (\sigma_x^2 + \sigma_y^2) \quad (3)$$

We have elected to report RMSE values in this paper to follow this convention. We calculate the error between the smartphone measurements (or smartphone derived estimates) and the measurements from the differential GPS, which we define as ground truth.

Furthermore, we are primarily concerned with estimates of the distance, $d(t)$, and speed, $v(t)$, along the boat's nearly straight path during rowing. So we additionally define the accuracy and precision of these time varying estimates. We calculate the distance for the smartphone, d_{SP} , and DGPS, d_{DGPS} , at any given discrete time measurement, t_i , with the following equation, using smartphone or DGPS data respectively:

$$d(t_i) = d(t_{i-1}) + \sqrt{[x(t_i) - x(t_{i-1})]^2 + [y(t_i) - y(t_{i-1})]^2}. \quad (4)$$

The boat speed is then estimated from the DGPS data using backward differences.

$$v_{\text{DGPS}}(t_i) = \frac{d_{\text{DGPS}}(t_i) - d_{\text{DGPS}}(t_{i-1})}{t_i - t_{i-1}} \quad (5)$$

Additionally, the boat speed is also reported directly from the smartphones internal estimates.

Given the boat distance and speed along the path we calculate the RMSE of any estimate of the two prior quantities by comparing them with the counterparts derived from the differential GPS data to quantify accuracy and precision (Eqs (6) and (7)). In this case n is taken as the number of samples associated with the signal of higher sampling rate, and linear interpolation is used to find intermediate samples of the signal with lower sampling rate.

$$\text{RMSE}_d^2 = \frac{1}{n} \sum_{i=1}^n d_e(t_i)^2 = \frac{1}{n} \sum_{i=1}^n [d(t_i) - d_{\text{DGPS}}(t_i)]^2 \quad (6)$$

$$\text{RMSE}_v^2 = \frac{1}{n} \sum_{i=1}^n v_e(t_i)^2 = \frac{1}{n} \sum_{i=1}^n [v(t_i) - v_{\text{DGPS}}(t_i)]^2 \quad (7)$$

With given errors d_e and v_e at every time sample, the mean of the errors (Eqs (8) and (9)), and the standard deviation of the errors, (Eqs (10) and (11)) can be computed

with

$$\bar{d}_e = \frac{1}{n} \sum_{i=1}^n d_e(t_i) = \frac{1}{n} \sum_{i=1}^n [d(t_i) - d_{\text{DGPS}}(t_i)] \quad (8)$$

$$\bar{v}_e = \frac{1}{n} \sum_{i=1}^n v_e(t_i) = \frac{1}{n} \sum_{i=1}^n [v(t_i) - v_{\text{DGPS}}(t_i)] \quad (9)$$

$$\sigma_{d_e}^2 = \frac{1}{n} \sum_{i=1}^n [d_e(t_i) - \bar{d}_e]^2 \quad (10)$$

$$\sigma_{v_e}^2 = \frac{1}{n} \sum_{i=1}^n [v_e(t_i) - \bar{v}_e]^2 \quad (11)$$

The central errors are then simply

$$\text{CE}_{d_e} = \sqrt{\bar{d}_e^2} = |\bar{d}_e|, \quad \text{CE}_{v_e} = \sqrt{\bar{v}_e^2} = |\bar{v}_e|. \quad (12)$$

The RMSE is related to the error mean and standard deviation by

$$\text{RMSE}_d^2 = \text{CE}_{d_e}^2 + \sigma_{d_e}^2, \quad \text{RMSE}_v^2 = \text{CE}_{v_e}^2 + \sigma_{v_e}^2. \quad (13)$$

Lastly, we calculate the RMSE of the actual distance per stroke relative to the estimated distance per stroke for all strokes, or subsets of strokes.

$$\text{RMSE}_{d_s} = \sqrt{\frac{\sum_{i=1}^m [d_{si} - d_{\text{DGPS}si}]^2}{m}} \quad (14)$$

where d_{si} is the i th distance per stroke from an estimate and m is the number of strokes. 143

Data collection

Smartphone GPS

The smartphone provides global position estimates accessed via the iPhone software development kit. Latitude and longitude are received at a variable sampling rate between 0.1 and 1Hz, usually at an average of about 0.3 Hz when the sensor is in motion. Once the data is transformed into an Earth-local Cartesian coordinate system with respect to the WGS84 coordinate system [22], the precision of motionless measurements can be determined; see Table 1. For repeated measurements over a short duration (<15 min) we assume that any inherent systematic bias of the GPS relative to true position is constant and does not degrade our distance calculations. None of the metrics of interest we describe later requires knowledge of the absolute position of the boat on the earth; instead we require only relative sample-to-sample (x, y) position differences. Even though systematic bias can be quite large, e.g. 16 m, the precision of repeated measurements over a short duration can be at least an order of magnitude higher [2], which is advantageous in our case.

Using a Piksi differential GPS system (SwiftNav, San Francisco, USA) as a measure of ground truth relative position (with better than 1 cm precision) we characterized the motionless and moving mean-subtracted distribution of smartphone position measurement errors; see Table 1. The cumulative distance traveled along the boat's path is calculated from the relative distance between each (x, y) coordinate; see Eq (4). We rely on numerical differentiation (backward differences, see Eq (5)) using the sensor-recorded time stamps to compute speed from the DGPS position measurements.

Smartphone acceleration

The smartphone accelerometer provides three dimensional body-fixed acceleration measurements with an average precision (SD) of about 0.02 m s^{-2} , updated at approximately 100 Hz. When affixed to the boat, we are interested in the component of acceleration tangent to the boat's travel path on the water surface, which is approximately the smartphone's y component in our case.

The small yaw (typically $<1^\circ$) angular motion during typical rowing [5] allows us to ignore the lateral acceleration component. We also ignore effects of any boat rolling motion, because it is typically negligible as well [5]. Pitch angular motion is similarly small ($<1^\circ$) [5] but because of the relatively large gravitational acceleration, even small changes in pitch mounting orientation, or static boat pitch mean that the longitudinal smartphone acceleration measurement will be biased; see Fig 2.

In general, we use only the smartphone-fixed longitudinal component of acceleration, α_y to estimate distance, but must take into account the pitch effects and accumulation of error from twice integrating the biased accelerometer measurement. Although this could be corrected by a calibration procedure [21], it is generally not practical in the expected smartphone consumer use case. Fig 2 illustrates how the smartphone body-fixed sensed acceleration relates to the actual acceleration parallel to the water's surface. The acceleration vector $\mathbf{a} = \boldsymbol{\alpha} - g\hat{\mathbf{z}}'$ can be written as two scalar equations by projecting onto the $\hat{\mathbf{y}}'$, $\hat{\mathbf{z}}'$ axes.

$$a_y = \alpha_y \cos \theta - \alpha_z \sin \theta \quad (15)$$

$$a_z = \alpha_y \sin \theta - \alpha_z \cos \theta - g \quad (16)$$

These two equations can be combined to show that the longitudinal acceleration is:

$$a_y = \frac{\alpha_y}{\cos \theta} - (a_z + g) \tan \theta \quad (17)$$

If the smartphone pitch, θ , and the vertical acceleration, a_z , of the boat are small, then the longitudinal acceleration a is given by the following linear approximation:

$$a = a_y \approx \alpha_y - g\theta. \quad (18)$$

For example, if θ were 6 degrees due to off-level mounting and average boat pitch, the gravity term could cause up to a meter per second squared error in the estimate.

Desired kinematic metrics

Stroke rate

Rowing involves periodic propulsive strokes by the rower(s) delivered through the oars to generate boat movement. These create a periodic kinematic pattern of boat accelerations and pitching that reliably maps to the characteristic phases of the stroke. Similar to others [14], we defined the endpoints of the stroke (the end of one and start of the next) as the timepoint that corresponds to the minimum peak values of longitudinal boat acceleration. This instant in time reliably corresponds to the transition from the recovery phase to the beginning of the propulsive phase of the stroke, commonly referenced in rowing as the “catch” [5]. These time instants can be detected in real-time using the method from [23], for example. Fig 3 illustrates the reliability of individual stroke endpoints detected using this method as well as the consistency of the rowing technique and the data quality during the experiments. On the rare occasion when visual inspection of the data demonstrated a clear stroke detection misidentification, the data from that stroke was excluded from any relevant analyses. These stroke timepoints are then used to calculate the stroke-domain metrics of interest: distance per stroke and stroke rate.

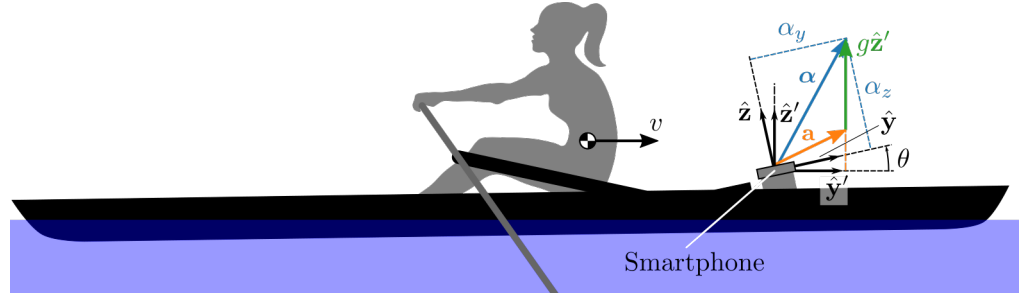
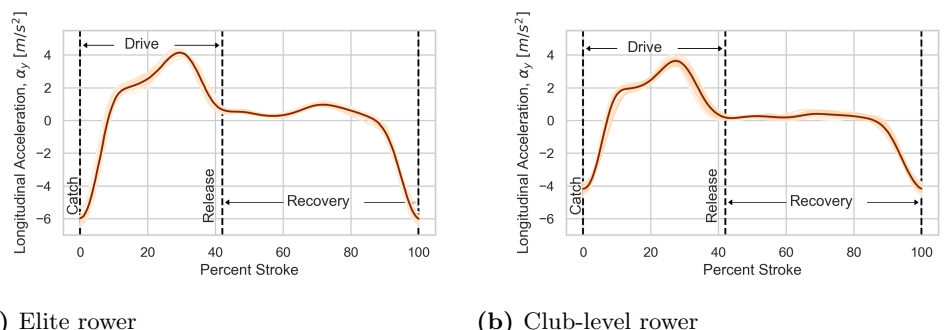


Fig 2. Diagram of a rowing boat under speed with an imperfectly aligned bow-mounted smartphone.

The smartphone coordinate system $\hat{\mathbf{y}}, \hat{\mathbf{z}}$ is oriented relative to the horizontal coordinate system $\hat{\mathbf{y}}', \hat{\mathbf{z}}'$ by a varying pitch angle θ . The accelerometer-reported acceleration α differs from the actual $\hat{\mathbf{y}}'$ component because it includes a gravitational component. The actual acceleration \mathbf{a} of the phone is then $\mathbf{a} = \alpha - g\hat{\mathbf{z}}'$. We desire the magnitude of the acceleration \mathbf{a} projected onto the horizontal plane but we do not know θ at any given time. As described in the “smartphone acceleration” section, the sensed $\hat{\mathbf{y}}$ acceleration differs from the true $\hat{\mathbf{y}}'$ acceleration by a moderate intrinsic bias and a larger term $g\theta$ which accounts for the projection of the gravity vector on the pitched $\hat{\mathbf{y}}$ axis.

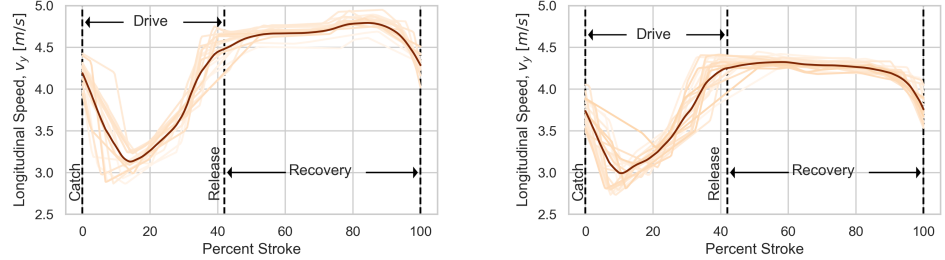


(a) Elite rower

(b) Club-level rower

Fig 3. Boat-fixed longitudinal acceleration as a function of percent stroke from two trials (elite and club-level 24SE.).

Each stroke is plotted as an orange line and the mean of all strokes as a dark line. The repeatability of the measured longitudinal acceleration, especially for the elite rower, validate the consistency of rowing technique, the robustness of the stroke endpoint identification, and the quality of the accelerometer data itself.



(a) Elite rower

(b) Club-level rower

Fig 4. DGPS computed boat speed as a function of percent stroke for two trials (elite and club-level 24SE).

Each stroke is plotted as a orange line and the mean of all strokes as a dark line. Because the DGPS data is sampled at only 10 Hz and the relative precision is lower than the accelerometer, the measured speed profile is less smooth and repeatable than the acceleration profiles in Fig 3.

Boat speed

Average boat speed along the shortest path to the finish is the primary metric rowers must maximize to win a race. We can compute reference boat speed by using the differential GPS measurements and Eq (5), and for the smartphone we rely on its internal speed estimate directly as it seems to be estimated via an algorithm that is more accurate than simple numerical differentiation of the distance. Fig 4 shows the DGPS computed speed measures for two trials at the same stroke rate.

Determining instantaneous earth-relative boat speed relies on accurate distance estimates. The smartphone provides a moderately accurate but reasonably precise position update at a sample rate on the same order of magnitude as the stroke rate, i.e. 0.3 Hz, which is only useful for average speed estimates over a number of strokes. Given a 0.8m precision in the distance measurements (Table 1), the accuracy of the speed estimates from the phone are on the order of 0.3 m s^{-1} . If the desired location precision of 5 cm was achieved at sampling rates approaching 100 Hz, the speed accuracy and frequency updates could potentially increase to 0.02 m s^{-1} and thus deliver data on intra-stroke speed variations.

Distance per stroke

Boat speed is the product of two separate but correlated variables in the stroke domain: stroke rate and distance per stroke. We calculate distance per stroke for each stroke by subtracting the interpolated distance, Eq (4), at each pair of subsequent stroke start/stop times. The same synchronized start/end time values are used for the smartphone-derived and reference differential GPS data allowing a direct comparison of the various estimations of boat distance. This comparison will allow an estimate of the accuracy and precision of each estimate method presented below.

As another indication of the effectiveness of the stroke endpoint identification procedure and the subsequent calculations of stroke time, distance per stroke and average speed, Table 2 reports the derived data and statistics on the strokes of the two trials portrayed in Figs 3 and 4.

Table 2. Summary DGPS data for strokes from elite and club-level 24SE trials depicted in Figs 3 and 4.

Stroke	elite			club-level		
	Duration [s]	Distance [m]	Speed [ms ⁻¹]	Duration [s]	Distance [m]	Speed [ms ⁻¹]
1	2.52	10.10	4.03	2.50	9.80	3.90
2	2.48	10.10	4.05	2.43	9.43	3.80
3	2.37	9.89	4.15	2.44	9.71	3.98
4	2.36	9.98	4.18	2.37	9.49	4.02
5	2.35	10.03	4.26	2.52	10.02	3.93
6	2.31	9.79	4.27	2.62	10.28	3.95
7	2.29	9.89	4.32	2.37	9.42	3.95
8	2.33	10.06	4.30	2.41	9.59	3.99
9	2.25	9.59	4.22	2.49	9.82	3.91
10	2.28	9.84	4.39	2.49	9.84	3.86
11	2.28	9.89	4.36	2.47	9.63	3.90
12	2.43	10.52	4.36	2.37	9.32	3.95
13	2.41	10.36	4.26	2.57	10.07	3.90
14	2.40	10.27	4.34	2.44	9.66	3.93
15	2.39	10.21	4.32	2.61	10.34	3.97
16	2.42	10.20	4.24	2.43	9.47	3.93
17	2.37	9.98	4.20	2.47	9.76	3.92
18	2.38	10.09	4.24	2.46	9.68	3.96
19	2.34	9.95	4.20	2.46	9.56	3.86
20	2.33	9.66	4.16	2.56	9.98	3.92
21				2.42	9.34	3.91
22				2.43	9.54	3.97
23				2.46	9.62	3.93
24				2.44	9.30	3.78
AVG	2.36	10.02	4.24	2.46	9.69	3.92
STD	0.07	0.23	0.10	0.07	0.29	0.05

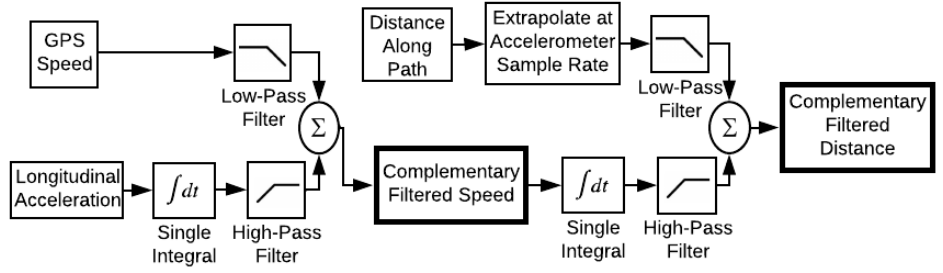


Fig 5. Block diagram depicting the complementary filter algorithm.

The smartphone speed and acceleration are fused to create an improved speed estimate and then that estimate is fused with the smartphone GPS-derived distance to create an improved distance estimate.

Sensor fusion method 1: complementary filter

The first method of combining smartphone accelerometer and GPS data stems from the classical idea of characterizing input-output behavior based on frequency response. We utilize two complementary filters in series, Fig 5, with each filter made up of two real-time discrete 2nd order Butterworth filters, namely one low-pass presented in [24] and one high-pass of similar design. Integrating the biased and noisy acceleration measurement introduces drift in the resulting speed and distance estimates, as expected. The high-pass filter is used to extract the high frequency portion of these estimates and to exclude the low frequency drift component. The low-pass filter extracts the low frequency portion of the smartphone speed and GPS-derived distance estimates. Each pair of two filtered signals is then summed at each accelerometer sample time to update the estimates. The results are more accurate speed and distance estimates.

Extrapolating GPS data

Since the GPS measurements occur less frequently than the accelerometer measurements, the smartphone speed and GPS-derived distance are linearly extrapolated, Eq (19), between GPS updates at each accelerometer update. This process uses the prior two GPS samples to provide an smoothed complementary filter input. This simple additional "filtering" procedure improves the distance estimate by 37% and the speed estimate by 20%. In the equation below the i index represents the accelerometer update time and the k index represents the last GPS update prior to t_i . This amounts to using the average speed derived from the GPS to make the extrapolation.

$$d(t_i) = d(t_{i-1}) + \frac{d(t_k) - d(t_{k-1})}{t_k - t_{k-1}}(t_i - t_{i-1}) \quad (19)$$

Bias and the Butterworth filter

A Butterworth filter creates a maximally flat passband and is relatively easy to implement digitally. At the cutoff frequency it rolls off gradually but is sufficient for many biomechanical filtering needs [1]. The transfer functions for the low- and high-pass 2nd order Butterworth filters are shown in Eqs (20) and (21) together with

Table 3. Average optimal Butterworth filter cutoff frequencies.

Distance Filter		Speed Filter	
low [Hz]	high [Hz]	low [Hz]	high [Hz]
0.189	3.789	0.0166	0.0457

the equations for the magnitudes of frequency response.

$$H_{\text{low}}(s) = \frac{\omega_c}{s^2 + \sqrt{2}\omega_c s + \omega_c}, \quad |H_{\text{low}}(j\omega)| = \frac{1}{\sqrt{1 + \left(\frac{\omega}{\omega_c}\right)^4}} \quad (20)$$

$$H_{\text{high}}(s) = \frac{s^2}{s^2 + \sqrt{2}\omega_c s + \omega_c}, \quad |H_{\text{high}}(j\omega)| = \frac{1}{\sqrt{1 + \left(\frac{\omega_c}{\omega}\right)^4}} \quad (21)$$

In the first filter in this series, we low-pass filter the smartphone GPS speed estimate and high-pass filter the longitudinal accelerometer measurement. The accelerometer output is the sum of the acceleration along the travel path minus a term that varies with boat pitch around a constant bias, i.e. $\alpha_y - g\theta$. In the frequency domain, these two input signals can be written as

$$X_{\text{low}}(j\omega) = V(j\omega) \quad (22)$$

$$X_{\text{high}}(j\omega) = A(j\omega) + a_0 \quad (23)$$

where a_0 represents the bias. Once filtered, the magnitude of each signal becomes

$$|Y_{\text{low}}(j\omega)| = \frac{|V(j\omega)|}{\sqrt{1 + \left(\frac{\omega}{\omega_c}\right)^4}} \quad (24)$$

$$|Y_{\text{high}}(j\omega)| = \frac{|A(j\omega)|}{\sqrt{1 + \left(\frac{\omega_c}{\omega}\right)^4}} + \frac{a_0}{\sqrt{1 + \left(\frac{\omega_c}{\omega}\right)^4}}. \quad (25)$$

In order to filter the effects of the accelerometer bias from the speed estimate, the high-pass cutoff frequency must be tuned to maximize the desired signal and to minimize the bias term in Eq (25). If the bias term has significant frequency content in the same bandwidth as the desirable signal, it is difficult to separate them. Fig 6 shows that the frequency content of the bias term, a_0 , is very low and that the high pass filter is effective at removing the bias. Thus, this filter is very suitable for this application where the accelerometer bias is approximately constant.

Cutoff frequency selection

A unique cutoff frequency is computed for each filter (low-pass and high-pass, each for distance and speed) for each trial. We calculate these parameters using an offline nonlinear least squares procedure to minimize the squared error between the filtered distance and the differential GPS distance. These optimal cutoff frequencies are averaged across all trials and the result is used in the real-time implementation, see Table 3. Since the high-pass cutoff frequencies for distance were large and did not have much effect on the performance of the filter above 10 Hz, the average was computed only over cutoff frequencies below 10 Hz.

Using the optimal cutoff frequency for each trial as opposed to the average over all trials would decrease the distance RMSE by an average of 20% and the speed RMSE by an average of 8%. However, calculating optimal cutoff frequencies would require post-processing and would render this filter unsuitable for real-time estimation.

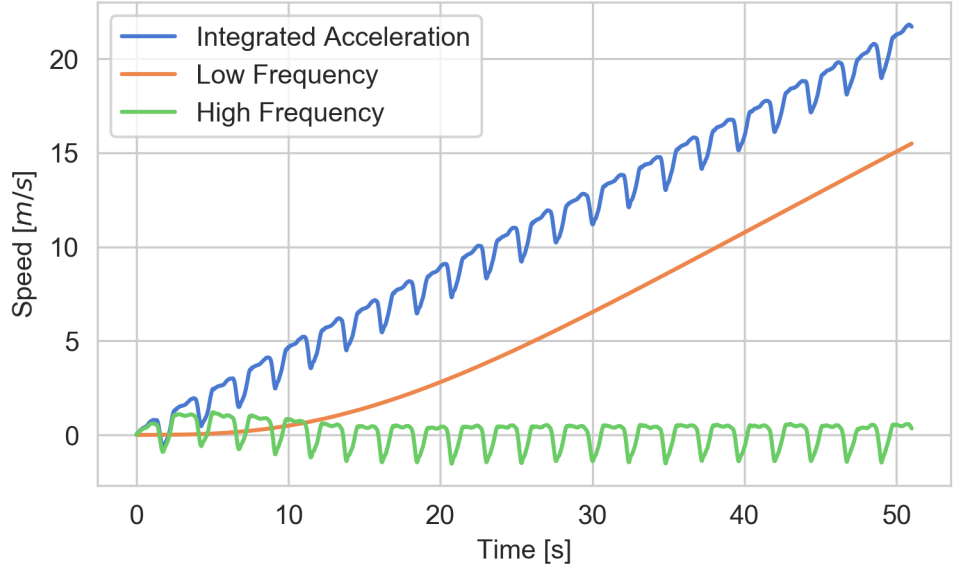


Fig 6. Example of low and high frequency components of speed derived from the integrated accelerometer measurement.

The blue curve shows the effect of the accelerometer bias on the speed estimate. The approximately constant slope of this curve indicates that the accelerometer bias is also approximately constant. The orange and green curves show the measurement separated into low and high frequency components.

Sensor fusion method 2: Kalman filter

The Kalman filter algorithm fuses data collected from different sensors with a predictive dynamic physical model to estimate the target time-varying variables of interest, known as states. The estimation results are expected to be more accurate than those obtained from any individual sensor [25]. Although the Kalman filter formalism makes several fundamental mathematical assumptions, perhaps the most important of which are random Gaussian process and measurement noise to guarantee the ultimate optimality, these assumptions are often relaxed in practice and the technique still works [26].

In our case, the body-fixed longitudinal acceleration of the boat is measured and used as an input to a kinematic model to predict the displacement and speed of the boat along its path. The predictions are then compared with the smartphone GPS-derived distance traveled and speed measurement, and the errors are used as feedback to adjust the estimation in real time. The Kalman filter gain can be tuned to balance the sensor and model uncertainty to achieve optimal accuracy. Details regarding the application of Kalman filtering to this estimation problem will be discussed in this section.

Boat kinematic model

The Kalman filter relies on a discrete dynamic model describing the kinematic relationships along the path. The actual horizontal acceleration a is integrated twice in discrete time to obtain distance d and speed v ,

$$d_{k+1} = d_k + v_k \Delta t. \quad (26)$$

$$v_{k+1} = v_k + a_k \Delta t \quad (27)$$

where the subscripts are shorthand for $d_k = d(t_k)$, etc.

As noted previously and illustrated in Fig 2, the smartphone's accelerometer axis $\hat{\mathbf{y}}$ is not, in general, perfectly aligned with the boat's horizontal travel path. Additionally, the accelerometer has an inherent bias due to its construction and nature. Neither are stationary but can be modeled as such for improved filter performance. If we want to use the smartphone acceleration α_y in place of a in Eq (27), we must compensate for these biases adjusting the accelerometer's measurement. To do so, we introduce an unknown constant bias state, ϕ_k , as

$$\phi_{k+1} = \phi_k \quad (28)$$

and replace a with $\alpha_{y,k} - \phi_k$, where ϕ_k is a model for the sum of the inherent accelerometer bias and the mean of $g\theta(t)$ that characterizes the bias due to boat pitch from (Eq 18). The augmented speed state equation becomes

$$v_{k+1} = v_k + (\alpha_{y,k} - \phi_k)\Delta t. \quad (29)$$

This bias can be thought of as the “effective” bias, in that it is the sum of the “real” sensor bias and the mean value of $g\theta$. It has now become a new state to be estimated by the filter which will effectively account for drift of integration error accumulation. The time varying component of $g\theta(t)$ is the sum of two parts: a roughly periodic remnant and a small truly random measurement noise. These two parts are lumped together as “process noise” \mathbf{w}_k below.

Lastly, we make use of two measurements, d and v , which are the smartphone GPS derived distance and speed along the travel path to correct our kinematic model predictions. Eqs (26) and (29) can be written in state space form to facilitate the design of the filter.

$$\mathbf{x}_{k+1} = \mathbf{Ax}_k + \mathbf{Bu}_k + \mathbf{w}_k \quad (30)$$

$$\mathbf{y}_k = \mathbf{Cx}_k + \mathbf{Du}_k + \boldsymbol{\nu}_k \quad (31)$$

where

$$\mathbf{x}_k = [d_k, v_k, \phi_k]^T, \quad \mathbf{u}_k = [\alpha_{y,k}], \quad \mathbf{y}_k = [d_k, v_k]^T, \quad (32)$$

and

$$\mathbf{A} = \begin{bmatrix} 1 & \Delta t & 0 \\ 0 & 1 & -\Delta t \\ 0 & 0 & 1 \end{bmatrix}, \quad \mathbf{B} = \begin{bmatrix} 0 \\ \Delta t \\ 0 \end{bmatrix}, \quad \mathbf{C} = \begin{bmatrix} 1 & 0 & 0 \\ 0 & 1 & 0 \end{bmatrix}, \quad \mathbf{D} = \begin{bmatrix} 0 \\ 0 \end{bmatrix}. \quad (33)$$

The terms \mathbf{w}_k and $\boldsymbol{\nu}_k$ are the process and measurement noise representing model and sensor uncertainty, respectively.

Kalman filter formulation

Based on the state space model of boat kinematics, we design a Kalman filter to estimate the states \mathbf{x}_k over time. The Kalman filter generates the estimates in two steps: the model prediction update and the measurement update. In the prediction update, an *a priori* estimate is made based on the input, the estimated state at the previous time instant, and the model,

$$\hat{\mathbf{x}}_k^- = \mathbf{Ax}_{k-1}^+ + \mathbf{Bu}_{k-1}, \quad (34)$$

where the superscript $-$ denotes the *a priori* estimate and $+$ denotes the final (*a posteriori*) estimate. In our case, the acceleration measurement is fed as the input to

the kinematic model to calculate the instantaneous speed and distance. Meanwhile, the Kalman filter provides an estimate of the covariance \mathbf{P} of the state estimate according to

$$\mathbf{P}_k^- = \mathbf{A}_{k-1} \mathbf{P}_{k-1}^+ \mathbf{A}_{k-1}^T + \mathbf{Q}, \quad (35)$$

which characterizes the estimate accuracy. In Eq (35), \mathbf{Q} is the assumed covariance of the process noise \mathbf{w}_k .
288
289

In the measurement update step, an *a posteriori* estimate is made based on the difference between the model prediction and the output measurement error feedback,
290

$$\hat{\mathbf{x}}_k^+ = \hat{\mathbf{x}}_k^- + \mathbf{L}_k (\mathbf{y}_k - \hat{\mathbf{y}}_k^-) \quad (36)$$

where

$$\hat{\mathbf{y}}_k^- = \mathbf{C}_k \hat{\mathbf{x}}_k^- + \mathbf{D}_k \mathbf{u}_k, \quad (37)$$

and where \mathbf{L}_k is the Kalman gain matrix calculated as
290

$$\mathbf{L}_k = \mathbf{P}_k^- \mathbf{C}_k^T (\mathbf{C}_k \mathbf{P}_k^- \mathbf{C}_k^T + \mathbf{R})^{-1}. \quad (38)$$

In Eq (38), \mathbf{R} is the covariance of the assumed random output measurement noise ν_k . During this step, the estimate covariance is also updated
291
292

$$\mathbf{P}_k^+ = (1 - \mathbf{L}_k \mathbf{C}_k^T) \mathbf{P}_k^-. \quad (39)$$

If both the process noise \mathbf{w}_k and measurement noise ν_k are indeed Gaussian, the *a posteriori* estimate obtained in Eq (36) is optimal in the sense that it has minimum covariance \mathbf{P} . In our case, the smartphone GPS derived distance and speed measurements are used to compare with and correct the *a priori* estimate of boat distance and speed.
293
294
295
296
297

The model prediction is performed at approximately 100 Hz in accordance with the sampling rate of the accelerometer, while the measurement update is carried out at the less frequent update rate of the GPS, about 0.3 Hz.
298
299
300

The performance of the Kalman filter relies heavily on the choice of values for the \mathbf{Q} and \mathbf{R} matrices. The optimal values for both are difficult, if not sometimes impossible, to know, and the noises are often not actually Gaussian. But in practice, the \mathbf{Q} and \mathbf{R} can often be tuned to create a good estimate. We are able to directly calculate the smartphone measurement variances by using the DGPS measurements as the true values (see Eqs (10) and (11)) and use them to populate the diagonals of \mathbf{R} .
301
302
303
304
305
306

$$\mathbf{R} = \begin{bmatrix} 25.279 & 0 \\ 0 & 100 \end{bmatrix} \quad (40)$$

$$\mathbf{P}_0 = \begin{bmatrix} 1 & 0 & 0 \\ 0 & 1 & 0 \\ 0 & 0 & 0.51 \end{bmatrix}, \quad \mathbf{x}_0 = \begin{bmatrix} d_0 \\ v_0 \\ 0.42 \end{bmatrix} \quad (41)$$

Our process model is a simple and exact kinematic model so the only terms that may have appreciable process noise are the acceleration input and the bias. We assume that the process noise is negligible because of the quality of the acceleration measurement and the dominance of the bias term (over variance) in the development of error in the estimate. We thus, set $\mathbf{Q} = \mathbf{0}$ to reflect this, and the filter trusts the model fully when no measurements are available, relying completely on the bias estimate to provide accurate estimates between measurement updates. The model is initialized with the first distance and speed measurement and an initial guess of the bias (see Eq 41)
307
308
309
310
311
312
313
314

using the mean value raw acceleration, $\alpha_{y,k}$, for a single trial. It is noted that the initial state variance \mathbf{P}_0 are non-zero as we do not have confident knowledge about the initial values of states (including acceleration bias). Hence the measurements are used in the initial stage to adjust the state and bias estimation (even though $\mathbf{Q} = \mathbf{0}$), which is critical for achieving accurate estimation. We found the values for \mathbf{Q} and \mathbf{R} generally robust with respect to variations in rower and boat (see
https://gitlab.com/mechmotum/row_filter for details). Note that we could obtain incremental gains in model accuracy if we further turned \mathbf{Q} and \mathbf{R} for individual rowers and boat configurations, however this choice would be inconsistent with our intent to build an easy-to-use, general purpose solution.

A Note on real-time algorithm implementation

We did not implement these filtering algorithms on an actual smartphone in real-time, but our algorithms, written in Python, can be directly translated to a smartphone's associated programming language. The complementary filter, Kalman filter, and peak detection algorithms have 110, 440, and 160 floating point operations per time step, respectively. The maximum floating point operations per time step is then the sum of the Kalman filter and peak detection, 600. We desire real-time updates at 100 Hz so the total neccesary FLOPS is 60 thousand. Contemporary smartphones have FLOPS capabilities between 5 billion to 35 billion. Thus the real-time implementation of these algorithms is relatively trivial and have little consequence on overall computation time.

Experimental methodology

Experiments were performed two days apart to validate the effectiveness of the proposed sensor fusion methods using a different rower-boat combination on each day: an experienced club-level (18 years rowing experience, age=63, height=1.68 m, weight=70 kg) sculling a 2 person boat (2002 Hudson mid-weight, 2X) alone, and an elite rower (2016 Olympic participant, age=31 height=2.00 m, weight=100 kg) sculling a single person boat (2004 Hudson heavy-weight, 1X). The 2X boat was used with a single rower to allow for ease om mounting of the measurement equipment to the empty bow seat before a mounting option for the single scull was developed. In each experiment, the rower performed a series of trials (each over a distance of approximately 300 m) in an inlet to a lake (Lake Washington, West Sacramento, CA, USA) that is part of deep water ship channel in both the northwest and southeast directions (Fig 7). A SpeedCoach GPS (Model 2, Nielson-Kellerman, Boothwyn, PA) was used onboard to display to the rower their current stroke rate. An example trial path is shown in Fig 7.

An iPhone 7 smartphone with iOS 11.3 (Apple, Cupertino, USA) running a custom data-logger app SwingRow 1.1 (Hegemony Technologies, Davis, CA) was rigidly attached to the deck of the 1X boat using positive-locking fasteners (Dual Lock, 3M, St. Paul, MN) at the position and orientation shown in Fig 8. A second smartphone running the same data-logger app was put into a "rowers wallet" (Hegemony Technologies, Davis, CA), positioned flat against the back of the rower at the top of the pelvis, and worn throughout the experiments. A ruggedized, waterproof camera (HERO4 Session, GoPro, San Mateo, USA) was mounted to the stern hull facing the rower to collect video. A differential GPS roving antenna (Piksi, Swiftnav, San Francisco, USA) was also attached to the hull as shown in Fig 8 (or in the spare seat in the case of the 2X boat).

Each rower performed a series of trials over a range of assigned stroke rates (target= 16, 20, 22, 24, 26, 28, max) in opposing directions (NW and SE) on the same 300 m



Fig 7. Satellite image showing a typical trial path.

The single red dot on the shore is the location of the DGPS base station. The mean latitude and longitude are 38.566435° and -121.556365° , respectively.



Fig 8. Sensor locations during elite trials.

2004 Hudson heavy-weight with the elite rower, annotated for experimental hardware. Note the DGPS antenna is clearly visible to the sky (above 15 degrees from horizontal in all directions it with a clear view to the sky). The individual pictured has given written informed consent (as outlined in PLOS consent form) to publish these case details.

course. The water current in the inlet was investigated and found to be negligible. The
362
collected data is available in the supplementary materials.
363

The UC Davis IRB determined that this study is not research involving human
364
subjects as defined by DHHS and thus IRB review was not required (IRB ID:
365
1430682-1). Informed consent was not formally obtained from the participants because
366
it was not required under the IRB determination. The collected and shared data is
367
anonymized and the portion of the data provided by Hegemony Technologies was
368
anonymized before the authors' analysis.
369

Results

Both the smartphone and the DGPS provide time measurements originating from the
370
same GPS satellites. We use these times to synchronize the measurements between
371
devices and we calculate estimates of the three variables distance, speed, and distance
372
per stroke at those times using the two aforementioned filters and directly from the
373
smartphone position data. This section discusses the comparisons among these three
374
estimates (smartphone: SP, complementary filter: CF, and Kalman filter: KF) of each
375
of the variables. A description of the detailed analysis procedure can be found in the
376
accompanying software (https://gitlab.com/mechmotum/row_filter). We present
377
data summaries for each subject (rower-boat combination) in the following figures. We
378
do so simply to show that the two filters are able to improve the metric estimates for
379
subjects that have significant differences (mass, performance, etc.) and purposely make
380
no claims about filter performance between subjects due to having too few subjects.
381

Filter convergence

The Kalman filter's performance relies on the effective bias ϕ converging to a constant
382
value, because our model assumes the bias is constant. The state estimates will
383
necessarily be erroneous if the bias is not constant in time. Fig 9 shows ϕ as a function
384
of time for a single example trial. In this case it takes almost 20 seconds (or
385
approximately 6 strokes) for convergence, which is about one fourth of the length of the
386
trial. For this reason we limited the calculation of steady state performance data
387
(RMSE) to the last ten strokes of each trial.
388

The filter converges to a different value of ϕ for each rower-boat combination and
389
stroke rate. Fig 10 shows the steady state values of ϕ for every trial. The effective bias
390
increases with stroke rate as does the average boat pitch angle.
391

Rowing races at amateur and professional levels typically range from 1000-5000
392
meters in length and are completed in timeframes that range from 3 minutes to 20+
393
minutes. Every boat before a race will execute an extensive warmup involving many
394
hundreds and probably thousands of strokes over 30+ minutes. This warmup period
395
provides ample opportunity to complete all of the filter convergence for this
396
implementation so that it will be optimally tuned and operational for the totality of a
397
race.
398

Distance estimates

Fig 11 shows, using an example from a single elite trial (16NW) after filter convergence,
401
all estimates of total distance travelled. Fig 12 shows the errors of these estimates
402
relative to the DGPS-derived distance. The Kalman filter estimate is similar to the
403
smartphone at the GPS updates and provides a reasonably drift free estimate between
404
adjacent smartphone updates; that is, it is similar in accuracy to the smartphone but
405
much more precise. The complementary filter is less influenced by the smartphone
406

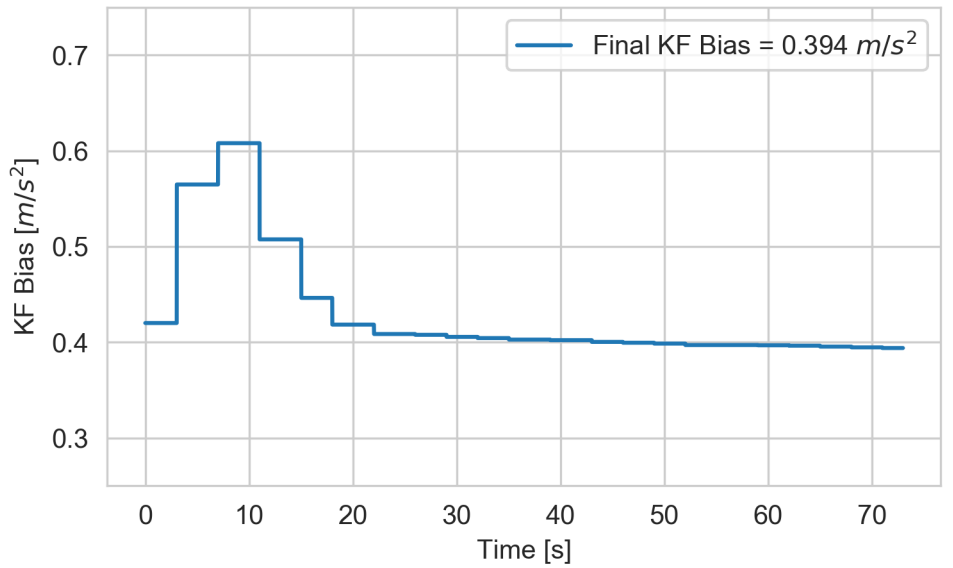


Fig 9. Convergence of the Kalman filter bias state over a single trial (elite 16NW).

The filter bias state typically takes about 20 seconds to converge to a relatively constant value.

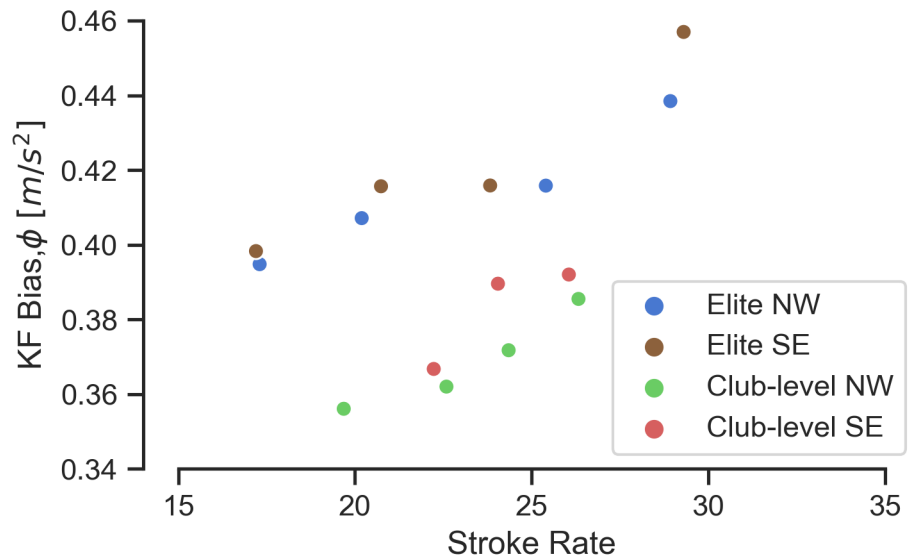


Fig 10. Terminal values of the Kalman filter bias state ϕ_k for each trial.

Each dot represents a single trial at the mean stroke rate. The bias is dependent on the rower/boat combination and boat speed.

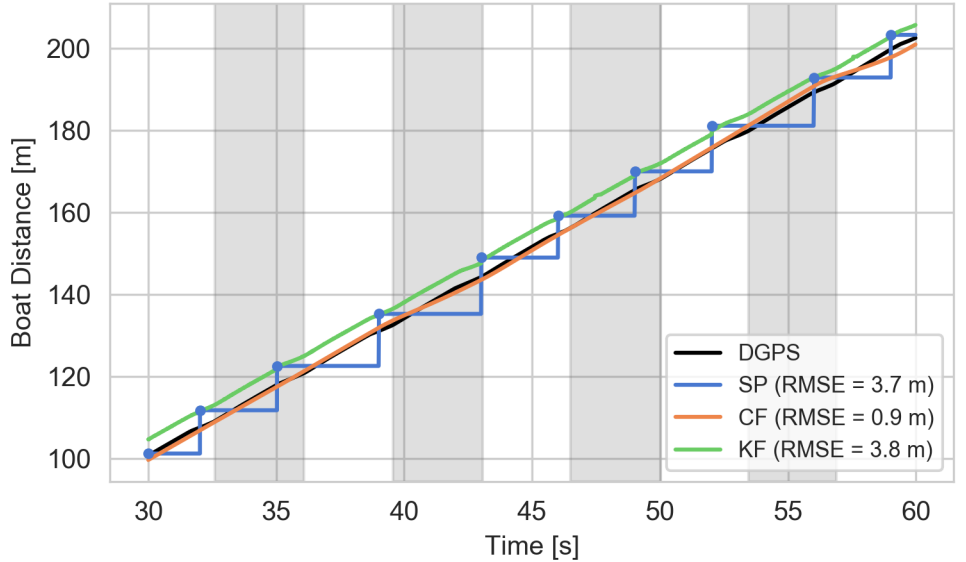


Fig 11. Example total boat distance traveled estimates.

The figure indicates distance traveled as a function of time for the last 30 s of the elite 16NW trial as estimated by the smartphone, complementary filter, and Kalman filter. The blue dots indicate the actual smartphone measurement update and the blue line is the piecewise constant interpolation in between updates. The alternating gray and white sections indicate each stroke. The reported RMSE values are relative to the DGPS distance shown in black. Each RMSE is calculated at the accelerometer sampling rate, i.e. 100 Hz.

distance measurements and provides a better estimate of the true distance traveled, both with respect to accuracy and precision. This is because the complementary filter corrects the integration bias solely from the speed measurement and mostly ignores the position measurement.

Fig 13 portrays the distribution of RMSE for the distance estimates relative to the DGPS for all trials for the elite and club-level rowers. The complementary filter shows improvement for both rowers and the Kalman filter shows improvement for the club-level rower. The Kalman filter actually is more than a meter worse for the elite rower when comparing the medians. The large distance RMSE for the filters is attributable to the relatively poor accuracy in the GPS measurement. In contrast, the errors in distance per stroke estimates are primarily influenced by measurement precision, which are improved by the filters relative to the smartphone. Nevertheless, the complementary and Kalman filters improve the median estimate by 42% and 22% when all trials are considered.

Boat speed estimates

Fig 14 shows example speed estimates for a typical trial after convergence from both the complementary and Kalman filters compared to those derived from the raw smartphone GPS and the differential GPS measurements. The RMSE of the estimates relative to differential GPS are tabulated for the post-convergence portion and shown on the graph for that trial. Both filters track the differential GPS derived speed throughout the stroke much more closely than the smartphone GPS derived speed, which is more like

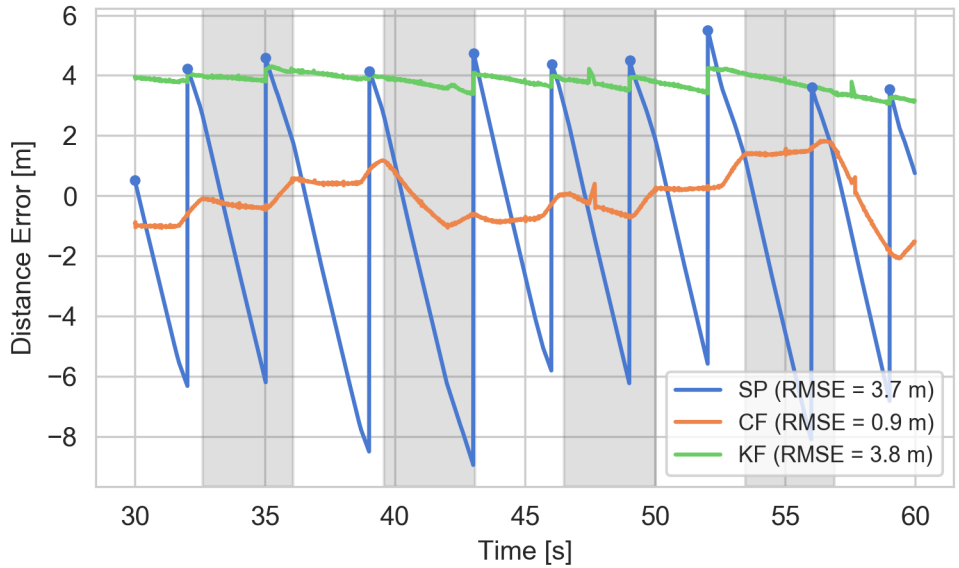


Fig 12. Example boat distance estimate errors.

Error in the smartphone, complementary filter, and Kalman filter distance estimates relative to the DGPS for the last 30 s of the elite 16NW trial. The “saw-tooth” smartphone error curve is derived from the piece-wise constant curve shown in Fig 11 to highlight the issue it poses when one desires to calculate distance per stroke. The alternating gray and white sections indicate each stroke. The RMSE values are the same as in Fig 11.

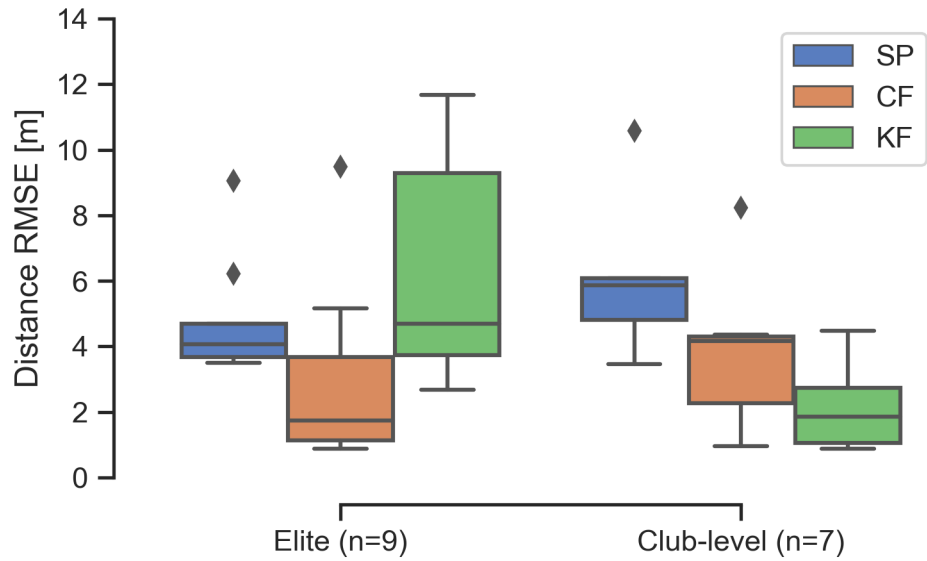


Fig 13. Summary of the distance estimate errors for all trials.

Comparisons of the distributions of RMSE_d of the distance estimates from the three methods for the last 10 strokes of each trial.

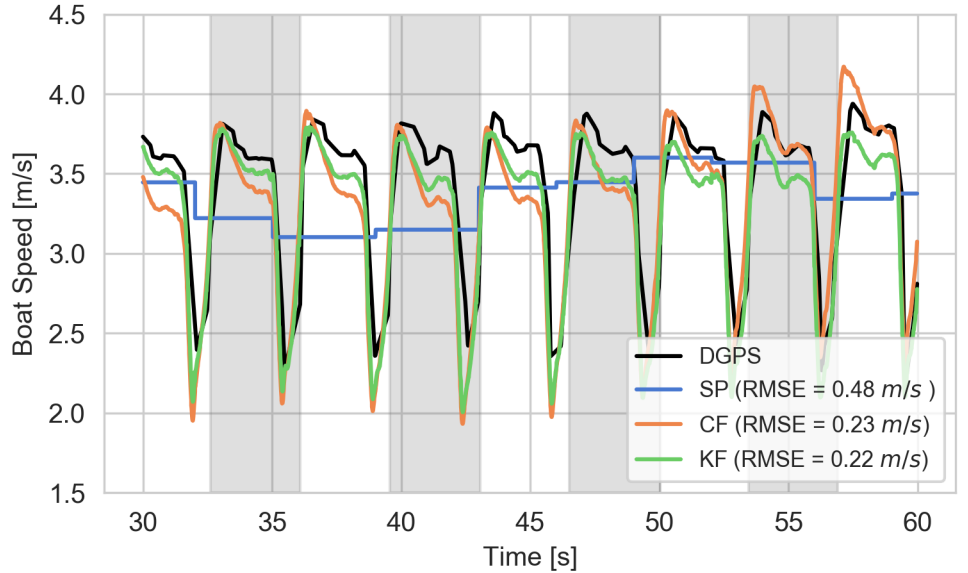


Fig 14. Example boat speed estimates.

The figure indicates the speed as a function of time for the last 30 s of the elite 16NW trial as estimated by the smartphone, complementary filter, and Kalman filter. The alternating gray and white sections indicate each stroke. The reported RMSE values are relative to the DGPS computed speed shown in black. Each RMSE_v is calculated at the 100 Hz accelerometer sampling rate.

an average speed. Both of the filters improve the estimate by over a factor of 2 in this trial.

Fig 15 shows the summary of the calculated speed RMSEs for each rower. It is clear that both of the filters improve the speed estimates for all trials, also by about a factor 2 or more when comparing the medians. Overall, the complementary and Kalman filters improve the median estimate by 44% and 48% when all trials are considered.

Distance per stroke estimates

Fig 16 compares the distance per stroke estimates computed from the smartphone, complementary filter, and Kalman filter with respect to the differential GPS derived estimates. The percentage improvement for the complementary filter is 62% and 81% for the elite and club-level rowers whereas for the Kalman filter it is 75% and 87%, respectively. The average of the error median values of the filters is 49 cm, which is still an order of magnitude larger than the goal of less than 5 cm. It is important to note that distance per stroke estimates are not affected by any constant bias present in the distance error (Fig 12). As long as the distance estimate has good precision and equivalent slope to the actual distance traveled across each stroke, the distance per stroke errors can be low.

Discussion

Rowing research, training, and racing methodologies are necessarily linked to the accuracy and precision of the available measurement systems. The emergence of location technologies like GPS make it possible to derive and report speed and related

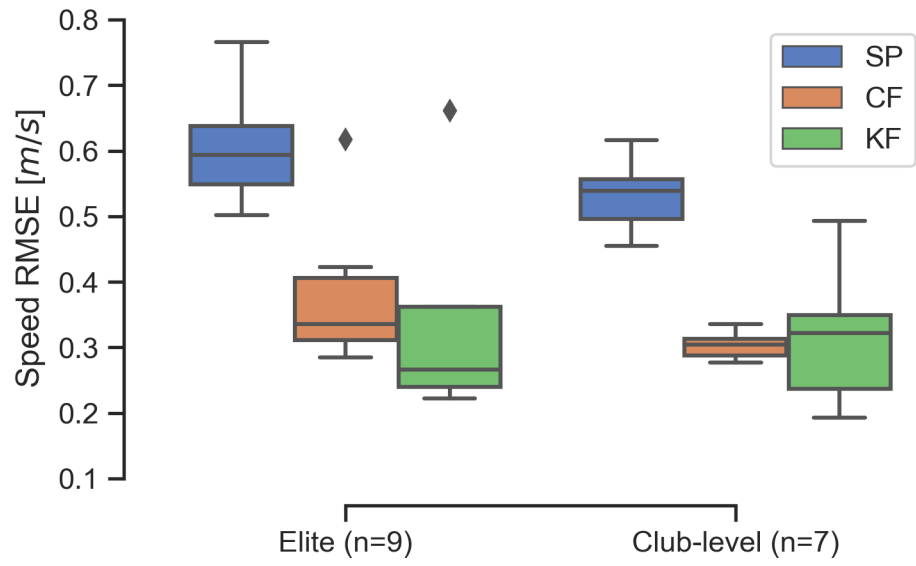


Fig 15. Summary of the speed estimate error for all trials.

Comparisons of the distributions of RMSE_v of the speed estimates from the three methods for the last 10 strokes of each trial.

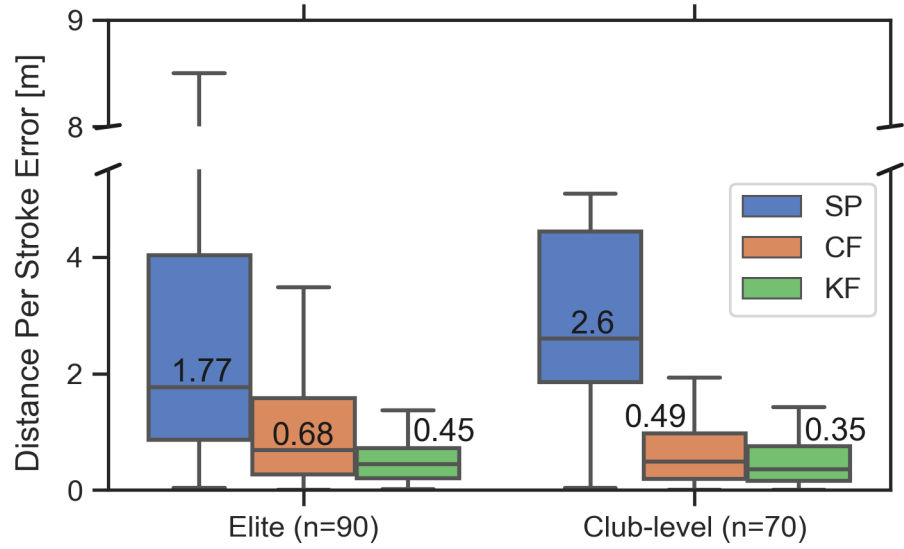


Fig 16. Summary of the distance per stroke error for the last 10 strokes of each trial.

Comparison of the distance per stroke error relative to the DGPS-derived value for all trials for the elite and club-level rowers, respectively. The numbers indicate the median values.

metrics in the stroke domain, e.g., stroke rate and distance per stroke. However, efforts to monitor and effect meaningful elite-level race result at an individual stroke level were shown in the introduction to require location accuracy and precision better than 5 cm, which systems like GPS cannot deliver. Thus, the aforementioned stroke level metrics derived from available systems should be recognized as approximations. These instrumentation limitations prevent direct and quantitative investigations of the complex causal relationships between rower-oar-boat system mechanics and boat performance at and within the level of an individual stroke. For these purposes, this study has explored methods for achieving more accurate and precise measures of boat movement. We created a system using consumer electronics and services and focused on designing a general purpose and easy-to-use solution that could be broadly deployed in the rowing community.

We have presented two alternative estimation methods for boat distance traveled, boat speed, and distance per stroke. Both methods similarly perform better (are more accurate) in most cases than direct output from the smartphone, but neither reach the desired sub 5 cm distance per stroke accuracy. The complementary filter has the disadvantage that the filter cutoff frequencies were not updated to optimal values in real-time, and the optimal offline values we found do not robustly handle all stroke rates for the two rowers and boats investigated. This makes the Kalman filter method more attractive because the bias term is adaptively updated for every rower and boat; i.e. the filter tunes itself. Nevertheless the complementary filter performs as good as or better than the Kalman filter for our set of trials. Both filters take time to converge to a steady error from a zero speed start, so the first few strokes in a race will produce less accurate results. A future study could consider minimizing the startup time by tuning the filters further, but there is likely a tradeoff in accuracy and precision of the estimates.

Both of our presented methods provide better estimates of boat speed and distance per stroke over any prior work that uses a single low-cost commercially available GPS system. The closest prior work on rowing is the thesis from Hermsen [21]. Hermsen's concept was similar but did not offer the online adaptation that our Kalman filter design provides and there were no reported improvements in any metric but predicted time. Our methods do not provide estimates as accurate as the measurements available using differential GPS systems, but considering the cost and convenience of use our methods are more attractive for general consumer use cases.

We have sought to develop a general purpose boat motion model that is independent of stroke rate, and the models presented in this paper were constructed from experiments involving single rowers with rowing rates that ranged from 16 to 34 strokes per minute. The markedly inferior performance of distance per stroke measures in the smartphone (SP) estimate relative to the CF and KF methods is largely attributed to the smartphone's limitation of having only a relatively low position sampling frequency. In the case of high stroke rate rowing where stroke frequency (at the high end faster than 0.5 Hz) exceeds the smartphone location sampling frequency (0.3-0.5 Hz), there are numerous instances between location samples where a stroke ends, a second stroke is completed, and a third stroke begins. In these cases, the distance per stroke error of the second stroke is the entire distance traveled. Accordingly, the CF and KF models stand to add the most value for high rate rowing, *e.g.*, racing rates.

It may be possible to further reduce estimation errors by implementing changes to the model that reflect unique or special aspects of rowing. For example, rowing necessarily occurs on a level plane (water) and boat movement dominantly occurs along the longitudinal axis of the boat. Both of these conditions imply kinematic constraints that were not completely modeled in this study. If the choice to build a general-purpose model was relaxed and special purpose models were developed that were tuned to specified ranges of rowing rates, rowing ability, and boat class, then special purpose

model accuracies would definitely improve. Additionally, relatively expensive commercial sports position and speed sensors can sample position at higher rates than a smartphone and thus can be useful to address the significant errors due to the low frequency sampling of the smartphone. However, these high frequency sampling solutions do not eliminate the inaccuracies and imprecision of the position measurements and thus at present do not represent a viable method for realizing the distance per stroke estimation accuracy of 5 cm or less. Rowers and teams could also invest in a DGPS and immediately gain the necessary accuracy and precision, but the costs are higher and the hardware is more cumbersome. Once we accomplish improvements that can achieve this level of accuracy and thus can enable more microscopic analyses of rowing mechanics, we anticipate the emergence of a new generation of tools for testing and coaching the boat-racing performance.

Conclusion

We have presented two methods to estimate the distance, speed, and distance per stroke along a rowing boat's path in real time that provide improved accuracy and precision results from the relatively low accuracy sensors in a single smartphone attached to the boat. These improved estimates can be used to create a more detailed analysis of the rower's performance. Specifically, we show that the distance per stroke can be estimated to an accuracy and precision of about 50 cm, which is an improvement over smartphone estimates but still insufficient for detailed stroke-by-stroke level differentiation of boats in a racing event with relatively close elapsed times. The more continuous data on boat speed that our methods create open up opportunities to analyze rowing mechanics and performance *within* a stroke. Overall, this paper demonstrates the capability that carefully crafted, activity-specific sensor fusion algorithms can have with low accuracy sensors. Accessible inertial measurement units, like those in smartphones, are continually decreasing in cost and size and stand to play a larger role in collecting field data in sports. The utility of these systems will depend on the development and improvement of application-specific sensor fusion algorithms.

Nomenclature

Complementary Filter

ω	frequency	532
ω_c	cutoff frequency	533
A	smartphone accelerometer input signal	534
a_0	accelerometer bias	535
D	smartphone GPS input signal	536
H	transfer function	537
j	unit imaginary number	538
k	index for prior GPS update	539
s	denotes the frequency domain ($s = jw$)	540
V	smartphone speed inpu signal	541

X	input signal	542
Y	output signal	543
Error Calculations		544
\bar{d}_e, \bar{v}_e	mean errors of distance and speed estimates	545
\bar{x}, \bar{y}	mean of Cartesian coordinates	546
σ_{d_e, v_e}	standard deviation of distance and speed estimate errors	547
$\sigma_{x,y}$	standard deviation of the Cartesian coordinates	548
CE_{d_e, v_e}	central errors of the distance and speed estimates	549
CE_{xy}	central errors of the Cartesian location	550
RMSE_{d, v, d_s}	root mean square errors of distance, speed, and distance per stroke	551
RMSE_{xy}	root mean square errors of the Cartesian location	552
d	distance traveled along the boat's path	553
d_e, v_e	errors in distance and speed estimates, respectively, relative to differential GPS measurements	554 555
d_s	distance per stroke	556
i	sample index	557
m	Number of strokes	558
n	number of time samples	559
t	time	560
v	magnitude of the velocity along the boat's path	561
x	east-west position on the local EPSG 3310 WGS84 plane	562
x_s, y_s	true Cartesian coordinates	563
y	north-south position on the local EPSG 3310 WDGS84 plane	564
Kalman Filter		565
α_{yk}	input: smartphone body-fixed longitudinal acceleration component	566
ν_k	measurement noise vector	567
Δt	time differential	568
\mathbf{A}	state transition matrix	569
\mathbf{B}	input matrix	570
\mathbf{C}	output matrix	571
\mathbf{D}	feed-through matrix	572
\mathbf{L}_k	gain matrix	573
\mathbf{P}_0	initial estimate covariance	574

P _k	estimate covariance	575
Q	process noise covariance matrix	576
R	measurement noise covariance matrix	577
u _k	input vector	578
w _k	process noise vector	579
x ₀	initial state vector	580
x _k	state vector	581
y _k	output vector	582
ϕ_k	state: accelerometer bias	583
a_k	input: acceleration	584
d_k	state: distance	585
v_k	state: speed	586
Other Symbols		587
$\alpha_{x,y,z}$	smartphone body-fixed acceleration components	588
a	boat mounted body-fixed smartphone acceleration vector	589
$\hat{\mathbf{x}}', \hat{\mathbf{y}}', \hat{\mathbf{z}}'$	smartphone path-fixed unit vectors	590
$\hat{\mathbf{x}}, \hat{\mathbf{y}}, \hat{\mathbf{z}}$	smartphone body-fixed unit vectors	591
a	path-fixed acceleration vector	592
θ	boat pitch angle	593
a	magnitude of the acceleration along the boat's path	594
$a_{x,y,z}$	smartphone path-fixed acceleration components	595
g	acceleration due to gravity	596
CF	abbreviation for complementary filter	597
KF	abbreviation for Kalman filter	598
SP	abbreviation for smartphone	599
Acknowledgments		600

The authors acknowledge Li Wang's contributions to the data collection and preliminary analysis and Scott Kresie's early mentorship. The authors acknowledge and thank River City Rowing Club and the University of California, Davis Rowing Club for the use of their equipment and facilities. The authors also acknowledge and thank Mark Dirrim and Seth Weil for the generous donation of their time and rowing expertise as rowing subjects in support of the project. Finally, we thank Ton van den Bogert for his assistance in developing the real time Butterworth filters.

References

1. Winter DA. Biomechanics and Motor Control of Human Movement. John Wiley & Sons; 2009. 608
609
610
2. Lee L, Jones M, Ridenour GS, Bennett SJ, Majors AC, Melito BL, et al. Comparison of Accuracy and Precision of GPS-Enabled Mobile Devices. In: 2016 IEEE International Conference on Computer and Information Technology (CIT); 2016. p. 73–82. 611
612
613
614
3. Zhizhong Ma, Yuansong Qiao, Lee B, Fallon E. Experimental Evaluation of Mobile Phone Sensors. In: 24th IET Irish Signals and Systems Conference (ISSC 2013). Letterkenny, Ireland: Institution of Engineering and Technology; 2013. p. 49–49. 615
616
617
618
4. Smith TB, Hopkins WG. Measures of Rowing Performance. Sports Medicine. 2012;42(4):343–358. doi:10.2165/11597230-000000000-00000. 619
620
5. Kleshnev V. Biomechanics of Rowing. Crowood Press; 2016. 621
6. Cejuela Anta R, Turpin P, Antonio J, Cortell-Tormo JM, Mira C, José J. An Analysis of High Performance in Long-Distance Rowing by Means of Global Positioning System Technology. In: Symposium Proceedings 6TM IACSS; 2008. p. 1–4. 622
623
624
625
7. Simões ND, Gonçalves JL, Caeiro ML, Boavida MJ, Cardoso FD. ZigBee/GPS Tracking System for Rowing Races. In: 2011 IEEE EUROCON - International Conference on Computer as a Tool; 2011. p. 1–4. 626
627
628
8. Ai K, He S. Development of a Speed Measurement System with Globle Positioning System in Rowing and Canoeing. In: ISBS-Conference Proceedings Archive. vol. 1; 2000. p. 1. 629
630
631
9. Zhang K, Deakin R, Grenfell R, Li Y, Zhang J, Cameron WN, et al. GNSS for Sports – Sailing and Rowing Perspectives. Journal of Global Positioning Systems. 2004;3(1&2):280–289. doi:10.5081/jgps.3.1.280. 632
633
634
10. Hedgecock W, Maroti M, Sallai J, Volgyesi P, Ledeczi A. High-Accuracy Differential Tracking of Low-Cost GPS Receivers. In: MobiSys 2013. ACM Press; 2013. p. 221. 635
636
637
11. Kiam JJ, Cardenas JM, Henkel P. Cost-Effective Cooperative RTK Positioning for Rowing Boats. In: Proc. of ION International Technical Meeting (ITM); 2014. p. 541–550. 638
639
640
12. Hill H, Fahrig S. The Impact of Fluctuations in Boat Velocity during the Rowing Cycle on Race Time. Scandinavian Journal of Medicine & Science in Sports. 2009;19(4):585–594. doi:10.1111/j.1600-0838.2008.00819.x. 641
642
643
13. Waegli A, Skaloud J. Optimization of Two GPS/MEMS-IMU Integration Strategies with Application to Sports. GPS Solutions. 2009;13(4):315–326. doi:10.1007/s10291-009-0124-5. 644
645
646
14. Groh BH, Reinfelder SJ, Streicher MN, Taraben A, Eskofier BM. Movement Prediction in Rowing Using a Dynamic Time Warping Based Stroke Detection. In: 2014 IEEE Ninth International Conference on Intelligent Sensors, Sensor Networks and Information Processing (ISSNIP); 2014. p. 1–6. 647
648
649
650

15. Janssen I, Sachlikidis A. Validity and Reliability of Intra-Stroke Kayak Velocity and Acceleration Using a GPS-Based Accelerometer. *Sports Biomechanics*. 2010;9(1):47–56. doi:10.1080/14763141003690229. 651
652
653
16. Mpimis A, Gikas V. Monitoring and Evaluation of Rowing Performance Using Mobile Mapping Data. *Archives of Photogrammetry, Cartography and Remote Sensing*. 2011;22:337–349. 654
655
656
17. Ruffaldi E, Peppoloni L, Filippeschi A. Sensor Fusion for Complex Articulated Body Tracking Applied in Rowing. *Proceedings of the Institution of Mechanical Engineers, Part P: Journal of Sports Engineering and Technology*. 2015;229(2):92–102. doi:10.1177/1754337115583199. 657
658
659
660
18. Anderson R, Harrison A, Lyons GM. Accelerometry-Based Feedback – Can It Improve Movement Consistency and Performance in Rowing? *Sports Biomechanics*. 2005;4(2):179–195. doi:10.1080/14763140508522862. 661
662
663
19. Tessendorf B, Gravenhorst F, Arnrich B, Tröster G. An IMU-Based Sensor Network to Continuously Monitor Rowing Technique on the Water. In: 2011 Seventh International Conference on Intelligent Sensors, Sensor Networks and Information Processing; 2011. p. 253–258. 664
665
666
667
20. Schindhelm CK, Gschwandtner F, Banholzer M. Usability of Apple iPhones for Inertial Navigation Systems. In: 2011 IEEE 22nd International Symposium on Personal, Indoor and Mobile Radio Communications; 2011. p. 1254–1258. 668
669
670
21. Hermsen H. Using GPS and Accelerometer Data for Rowing Race Tracking [Master]. University of Groningen. Groningen, Netherlands; 2013. 671
672
22. NIMA. Department of Defense World Geodetic System 1984, Its Definition and Relationships With Local Geodetic Systems. National Imagery and Mapping Agency; 2000. TR8350.2. 673
674
675
23. Anonymous JP. Peak Signal Detection in Realtime Timeseries Data; 2014. <https://stackoverflow.com/questions/22583391/peak-signal-detection-in-realtime-timeseries-data>. 676
677
678
24. van den Bogert AJ, Geijtenbeek T, Even-Zohar O, Steenbrink F, Hardin EC. A Real-Time System for Biomechanical Analysis of Human Movement and Muscle Function. *Medical & Biological Engineering & Computing*. 2013; p. 1–9. doi:10.1007/s11517-013-1076-z. 679
680
681
682
25. Kalman RE. A New Approach to Linear Filtering and Prediction Problems. *Transactions of the ASME–Journal of Basic Engineering*. 1960;82(Series D):35–45. 683
684
26. Grewal M, Andrews AP. *Kalman Filtering: Theory and Practice Using MATLAB*. 3rd ed. John Wiley & Sons, Inc; 2008. 685
686